Naval Research Laboratory
Washington, DC 20375-5320

NRL/MR/4613—92-6982

Fiber Optic Data Bus Radiation Effects Study

A. B. CAMPBELL

Radiation Effects Branch
Condensed Matter and Radiation Sciences Division

September 28, 1992

REPORT DOCUMENTATION PAGE

Form Approved
OMB No. 0704-0188

1. AGENCY USE ONLY (*Leave Blank*)	2. REPORT DATE	3. REPORT TYPE AND DATES COVERED
	September 28, 1992	1 Oct 90 - 30 Sept 91

4. TITLE AND SUBTITLE

Fiber Optic Data Bus Radiation Effects Study

5. FUNDING NUMBERS

6. AUTHOR(S)

E.J. Frieble, P.W. Marshall,* G.P. Summers, Y.J. Chen,**
A.B. Campbell, and J.B. Langworthy

7. PERFORMING ORGANIZATION NAME(S) and ADDRESS(ES)

Naval Research Laboratory
Washington, DC 20375-5320

8. PERFORMING ORGANIZATION REPORT NUMBER

NRL/MR/4613--92-6982

9. SPONSORING/MONITORING AGENCY NAME(S) AND ADDRESS(ES)

SPAWAR

10. SPONSORING/MONITORING AGENCY REPORT NUMBER

11. SUPPLEMENTARY NOTES

*Sachs Freeman Associates, Inc.
**University of Maryland, Baltimore County

12a. DISTRIBUTION/AVAILABILITY STATEMENT

Approved for public release; distribution unlimited.

12b. DISTRIBUTION CODE

13. ABSTRACT (*Maximum 200 words*)

This report summarizes a study of radiation effects in components of a proposed fiber optic data bus for space, including models of the natural radiation environment.

14. SUBJECT TERMS

Fiber optic
Space radiation

15. NUMBER OF PAGES

91

16. PRICE CODE

17. SECURITY CLASSIFICATION OF REPORT	18. SECURITY CLASSIFICATION OF THIS PAGE	19. SECURITY CLASSIFICATION OF ABSTRACT	20. LIMITATION OF ABSTRACT
UNCLASSIFIED	UNCLASSIFIED	UNCLASSIFIED	UL

NSN 7540-01-280-5500

Standard Form 298 (Rev. 2-89)
Prescribed by ANSI Std 239-18
298-102

CONTENTS

Fiber Optic Data Bus Radiation Effects Study

1. INTRODUCTION

The technology has been in place for several years to put a successful Fiber Optic Data Bus (FODB) in space, with all the benefits to Navy systems. These advantages include:

1. Increased data rate (from 25 Mbit/s to over 1500 Mbits/s).
2. Weight reduction (fewer copper wires).
3. Simplified system (one fiber-optic cable as opposed to multiple copper wires).
4. More testable system.
5. Isolated system - no ground loop or interference problems.
6. Reduced power consumption.

The FODB Program is in its definition phase and in order to ensure that the system can survive in the hostile environment in space, the components will be radiation hardened to some specified level. In order to optimize the use of resources, this study has been initiated early in the program to assess the component technology currently available with regard to radiation tolerance. The authors have analyzed and assessed the state of knowledge of the radiation tolerance and of the survivability of a wide variety of candidate components. This report will serve as a guide for making informed decisions in the procurement specification process to ensure a radiation hardened system at the lowest possible cost to the Navy.

The specification is for a system to be operated in an orbit where the approximate total dose exposure behind typical shielding is expected to be the order of 100 Krad(Si) for a 5-year mission. This report will include a detailed study the natural radiation environment for four generic orbits to provide baseline radiation specifications for devices and fibers. [The non-natural radiation environment can and should be addressed as a separate classified study. Traditionally, contributions to radiation effects damage are included (as in the example dose given above) based on incidental weapon's products that can produce significant degradation compared with that from the natural environment.]

The natural radiation environment relevant to radiation damage in a fiber-optic data bus system includes electrons and protons. The electrons can cause total dose damage and protons can cause both total dose and displacement damage. Displacement damage can also result in degradation of performance but through a totally different mechanism of crystalline structure changes. In many cases the displacement damage equivalent to the rad is the nonionizing energy loss (NIEL) which enables calculations to be made comparing performance in different orbits, and between different technologies. Also important for displacement damage calculations is the differential energy spectra of the protons.

It will be apparent as the report is read that several trade-offs will need to be considered when the final specifications are written for the FODB. In particular, the need to operate the FODB at an

Manuscript approved July 13, 1992.

ambient temperature of 60°C will have serious reliability implications for 1.3μm technology devices. Thermoelectric coolers could be used to reduce the temperature locally, but would increase the power budget of the system. Increased temperature will improve the radiation tolerance of optical fibers, but since the radiation-induced optical attenuation of many fiber types is very sensitive to temperature (see Section 3), a substantial safety margin will need to be considered in any detailed specifications.

The report concludes that almost no radiation effects data exists for the advanced technology components that are likely to be included in the FODB. Data is available for Co-60 gamma testing of optical fibers, but very little for proton environments. Recommendations are given for radiation specifications for subsystems of the FODB in Section 6. However, it is clear that it will be important to follow up this study with a comprehensive testing program in order to develop a full understanding of the main issues involved in the long term use of large scale advanced technology fiber opto-electronic systems in space.

2. Radiation Environment

This part of the Fiber Optic Data Bus (FODB) radiation study investigates the natural radiation environment for four generic orbits to provide baseline radiation specifications for devices and fibers. The calculations are based on the AP-8 and AE-8 models of the trapped radiation environment developed by NASA over many years that are accepted by the radiation effects and environment modeling community as highly accurate when averaged over time periods of the order of months. Also included in this study is a model of the protons produced as a result of a solar flare, after King. These models are included in several computer codes available at NRL. The principal code used for these calculations was Space Radiation, but another code was used also to check the results. This code was developed by one of the authors (JBL) and is based on the same NASA models mentioned above. In addition, since in practice there is always some incidental shielding in any space system, the effects of various thicknesses of aluminum shields typical of spacecraft is considered.

The four orbits chosen for this study were:

1) 63° inclination, 1,212x11,527km elliptical orbit
2) 63° inclination, 1,110 km circular orbit
3) 98.7° inclination, 806x828 km elliptical orbit
4) 63° inclination, 555 km circular orbit

The natural radiation environment relevant to radiation damage in a FODB system includes electrons and protons. The electrons can cause total dose damage and protons can cause both total dose and displacement damage. Total dose can result in degradation of performance over time through such mechanisms as trapped charge in isolation layers. The magnitude of radiation dose is expressed in rads or deposited energy density, in units of 100 ergs/gram. Displacement damage can also result in degradation of performance but through a totally different mechanism of crystalline structure changes. The magnitude of the displacement damage depends on the nonionizing energy loss (NIEL) at a given energy and is also proportional to proton fluence expressed as protons/cm^2.

Electrons and protons exist in the earth's radiation belts which vary with orbital altitude and inclination, as well as with time. Variations in the earth's magnetic field result in a region known as the South Atlantic Anomaly where the magnetic fields, and thus the radiation belts, drop to very low altitudes in a relatively large region above the South Atlantic off Brazil. Orbital traverses through this region result in large increases in dose rate compared with the rest of the orbit. Protons produced by solar flares can also interact with a spacecraft depending on the magnitude of the flare and the orbit. The calculations consider these different radiation sources and variations with time (solar cycle only).

An important consideration for digital systems where single event upset (SEU) might be important are the cosmic ray particles. These very high energy, heavy ions from the cosmos are extremely penetrating and can not be shielded against. However, they are not normally important from a radiation damage point of view because the flux is relatively low. The cosmic ray ions can produce very localized displacement damage. It is expected that only when semiconductor feature sizes become sub-micrometer will this damage become significant. Cosmic rays are shielded from the earth by the earth's magnetic fields, so their content and flux is highly dependent on geomagnetic latitude and longitude, and thus on satellite orbit. In general, for low altitude orbits, cosmic ray fluences are low and it is only for high altitude communications satellites that fluences are significant. For this study we have chosen to ignore the contribution of cosmic rays to the radiation damage problem. If the FODB system is to include digital components, however, the cosmic ray environment may be critical to reliable operation in the absence of transient upsets.

For all four orbits, the proton (trapped and solar flare) and trapped electron contribution to total dose and the proton particle fluence as a differential energy spectra (for two cases, trapped and solar flare) have been calculated. Calculations of dose and proton spectra have been performed for four different aluminum shield thicknesses, 40, 80, 150 & 300 mils, which are typical of spacecraft shielding. This allows for a realistic estimate of the radiation environment at the location of the fiber-optic components.

A major factor in the time dependence of the dose and fluence is the approximately 11-year solar cycle, which effects both the trapped electron and proton spectra in the belts. The two extremes are solar minimum (flare activity at the sun's surface at a minimum) and solar maximum (flares at maximum). For the purposes of this report we have assumed solar maximum in 1991 and 2002 and solar minimum in 1987 and 1998. [As will be seen from the calculations, solar maximum provides the largest contribution from electron dose but the smallest from proton dose.] Extra-terrestrial flare protons come directly from the sun and are random occurrences. The large flares that can have a significant influence on the total dose are not directly correlated with the solar cycle. For comparison purposes, one of these flares has been included in the total dose estimate. It should be noted, however, recently more that one flare of this size has been seen in a time period of less than one year.

The important result from this phase of the radiation study is a series of total dose and proton fluence and spectra environments that can be applied to specific cases where trade-offs can be made with respect to shielding and orbital parameters. The worst-case can be used with sufficient safety factors to provide system radiation specifications.

Table 2.1 is a listing of the results of the calculations. The main conclusions of this part of the study are:

1) Solar flare protons can be a significant contribution (up to 44% of the trapped dose) in cases where shielding reduces the trapped contribution more than the flare proton contribution. These unpredictable flare events are an important factor in the natural radiation environment.

2) Solar maximum provides the largest trapped electron dose, while solar minimum provides the largest trapped proton dose.

3) For the largest shield thickness, trapped protons provide more dose than trapped electrons. For the 150 mil shield thickness, the contributions are comparable or close. For the two thinnest shields, the trapped electrons provide more dose than the trapped protons.

4) Orbit 3 provides the largest dose due to flare protons because it passes close to the polar regions where geomagnetic shielding is smallest. Orbit 1 provides the largest doses due to trapped electrons and trapped protons because a large part of the period is spend in the heart of the belts.

5) Solar flares and transits through the South Atlantic Anomaly can result in dose rates that temporarily go from average dose rates of the order of 1 rad(Si)/hour up to rates as high as 100 rad(Si)/hour. This can have an important effect on device performance if time dependent effects such as annealing are taking place.

Figures 2.1-2.4 are plots of the data from Table 2.1 for the four orbits. Figure 2.5 is a plot of trapped proton differential spectra for all four orbits, tow solar maximum and tow solar minimum, for 40 mils of shielding. Figure 2.6 is a plot of trapped proton differential spectra for orbit 1 for the four different shield thicknesses. Figure 2.7 is a plot of differential proton spectra for solar flare protons for orbit 3 with the four different shield thicknesses.

Table 2.1: Summary of radiation environment calculations. All doses represent total dose in kRad(Si) for one year in the specified orbit. The dose from a single flare has been included in the column labeled "FLARE PROTON." The last column labeled "TOTAL" includes trapped protons and electrons and the proton contribution from a single solar flare.

ORBIT	SOLAR CONDITIONS	MILS Al SHIELD THICKNESS	TRAPPED PROTON	TRAPPED ELECTRON	TRAPPED TOTAL	FLARE PROTON	TOTAL
1	MAX	40	17.1	940.	957.	0.183	957.
1	MIN	40	17.8	342.	360.	0.183	360.
1	MAX	80	3.52	328.	332.	0.149	332.
1	MIN	80	3.87	121.	125.	0.149	125.
1	MAX	150	1.36	73.3	74.7	0.111	74.8
1	MIN	150	2.09	25.7	26.8	0.111	26.9
1	MAX	300	0.780	2.67	3.45	0.070	3.52
1	MIN	300	0.953	1.55	2.50	0.070	2.57
2	MAX	40	4.81	33.0	37.8	0.214	38.02
2	MIN	40	5.74	19.9	25.6	0.214	25.85
2	MAX	80	3.05	9.9	12.9	0.172	13.07
2	MIN	80	3.69	5.8	9.45	0.172	9.62
2	MAX	150	2.17	2.1	4.30	0.127	4.43
2	MIN	150	2.65	1.3	3.90	0.127	4.03
2	MAX	300	1.59	0.0575	1.65	0.078	1.73
2	MIN	300	1.97	0.0407	2.01	0.078	2.09
3	MAX	40	1.30	13.9	15.2	0.712	15.91
3	MIN	40	1.68	8.2	9.88	0.712	10.59
3	MAX	80	0.861	4.3	5.20	0.541	5.74
3	MIN	80	1.12	2.5	3.61	0.541	4.15
3	MAX	150	0.631	0.928	1.56	0.381	1.94
3	MIN	150	0.826	0.530	1.36	0.381	1.74
3	MAX	300	0.473	0.0266	0.50	0.221	0.720
3	MIN	300	0.630	0.0194	0.65	0.221	0.870
4	MAX	40	0.380	8.3	8.71	0.176	8.886
4	MIN	40	0.610	4.0	4.62	0.176	4.796
4	MAX	80	0.259	2.87	3.13	0.142	3.272
4	MIN	80	0.395	1.36	1.76	0.142	1.902
4	MAX	150	0.192	0.639	0.83	0.104	0.934
4	MIN	150	0.291	0.304	0.60	0.104	0.704
4	MAX	300	0.145	0.0201	0.17	0.063	0.233
4	MIN	300	0.221	0.0136	0.23	0.063	0.293

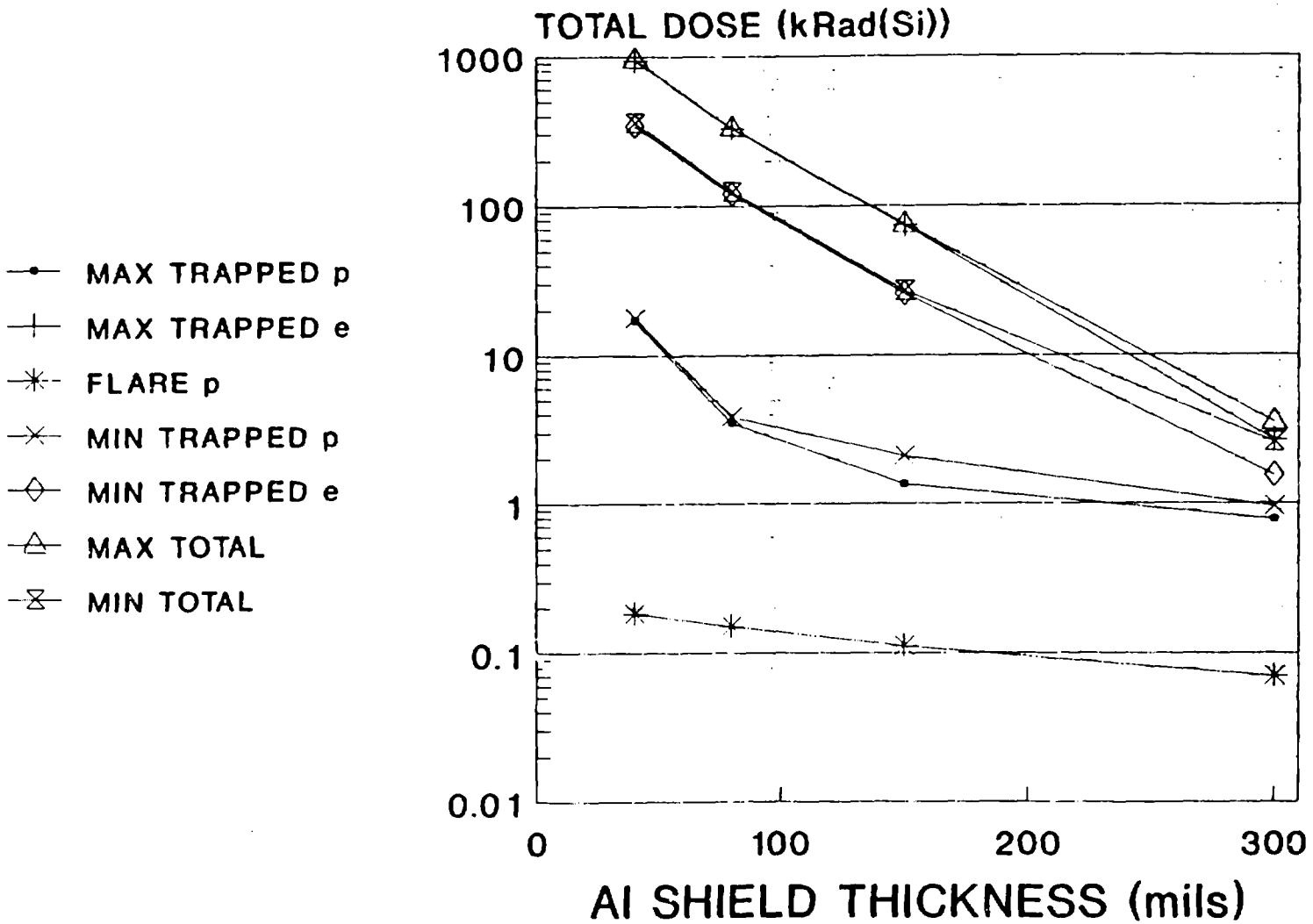

Figure 2.1: Calculated total dose for orbit 1 as a function of shield thickness.

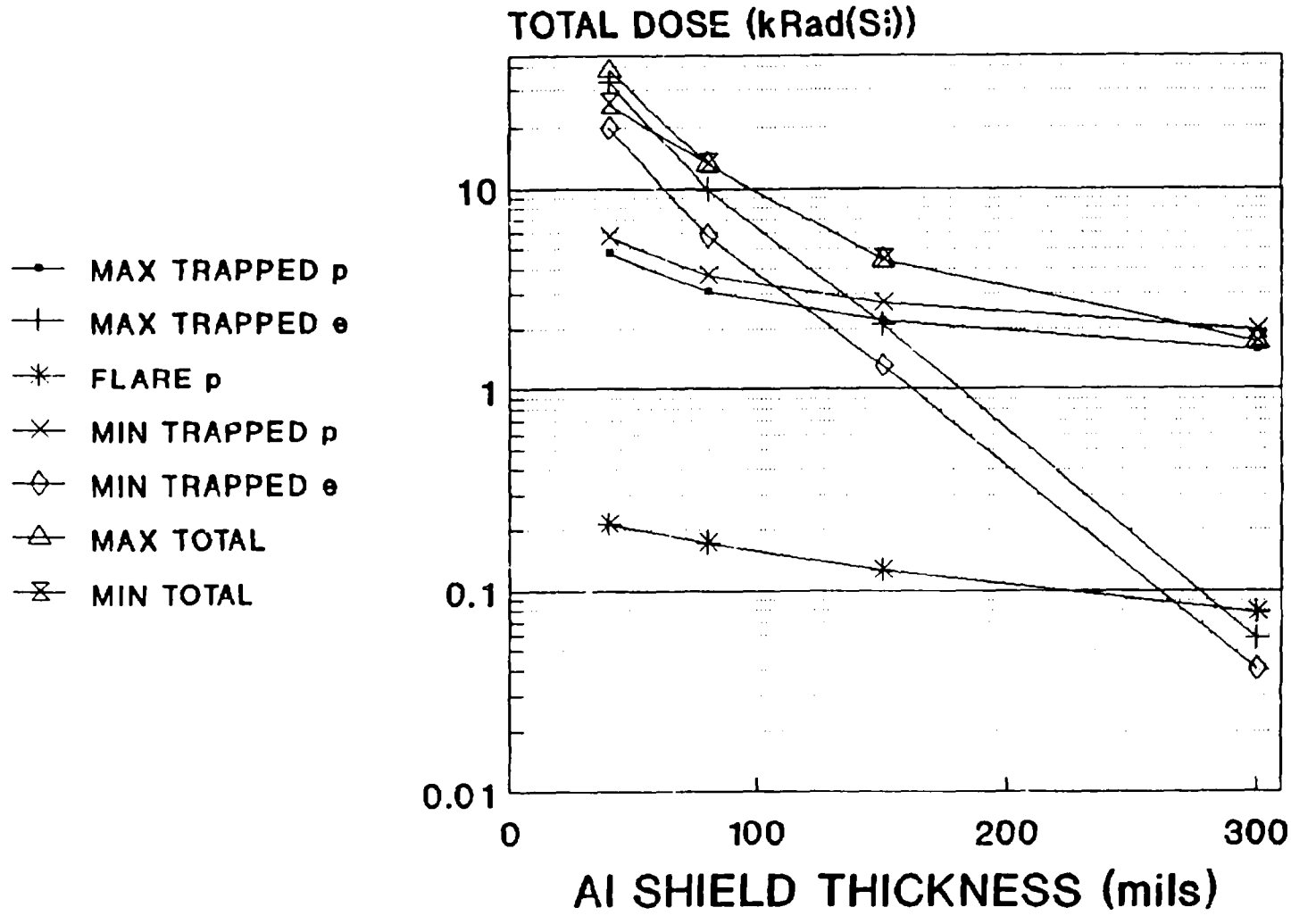

Figure 2.2: Calculated total dose for orbit 2 as a function of shield thickness.

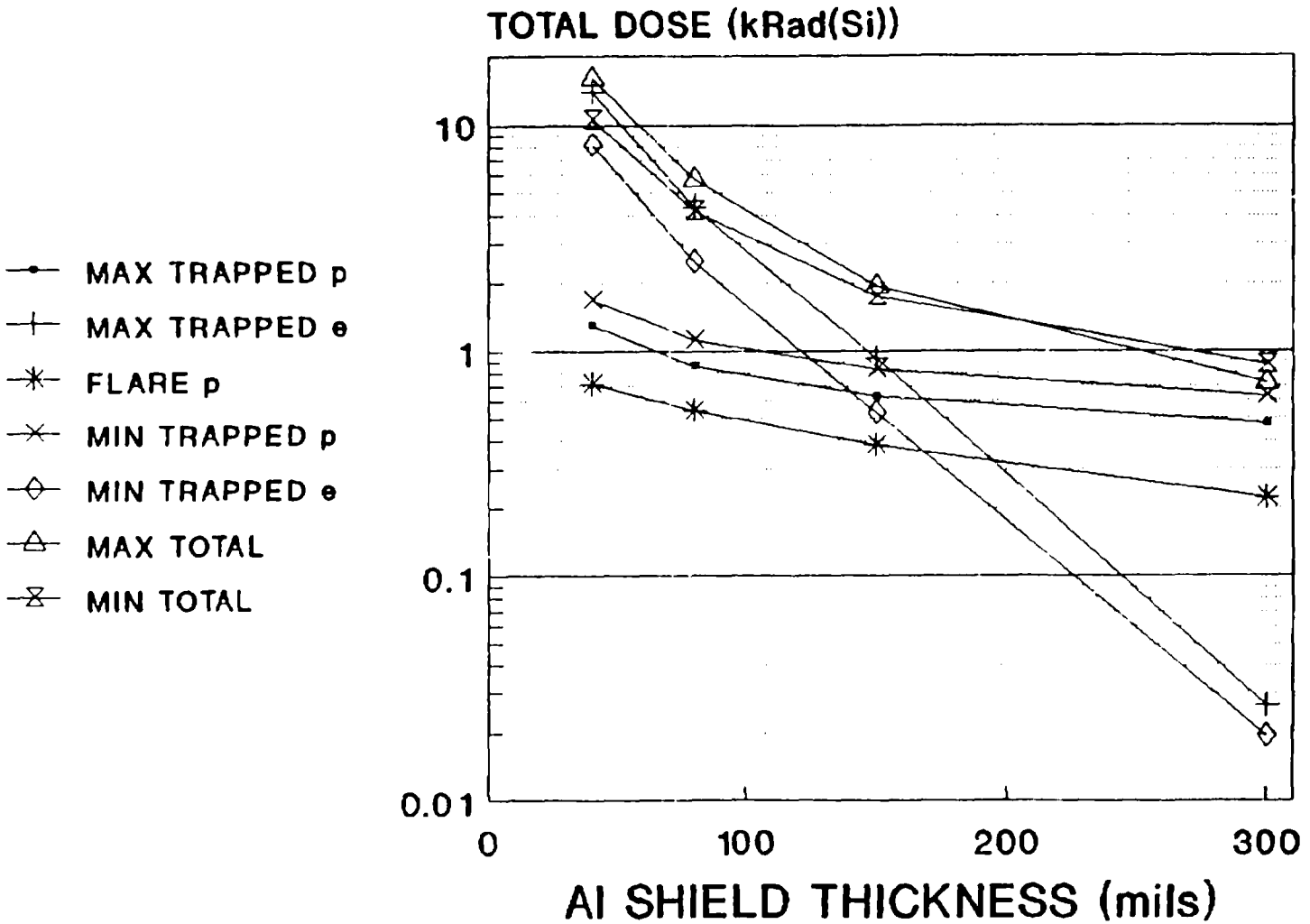

Figure 2.3: Calculated total dose for orbit 3 as a function of shield thickness.

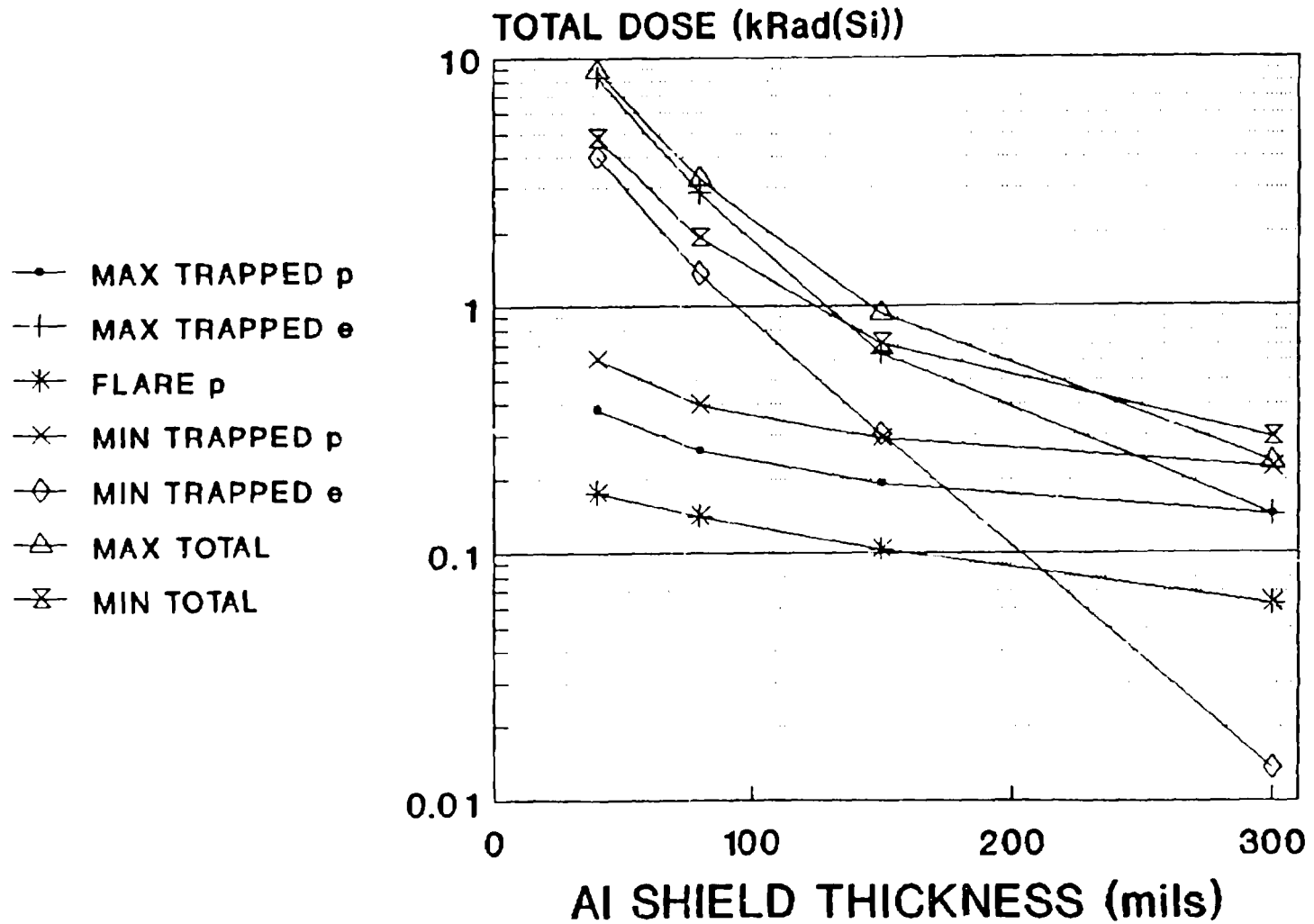

Figure 2.4: Calculated total dose for orbit 4 as a function of shield thickness.

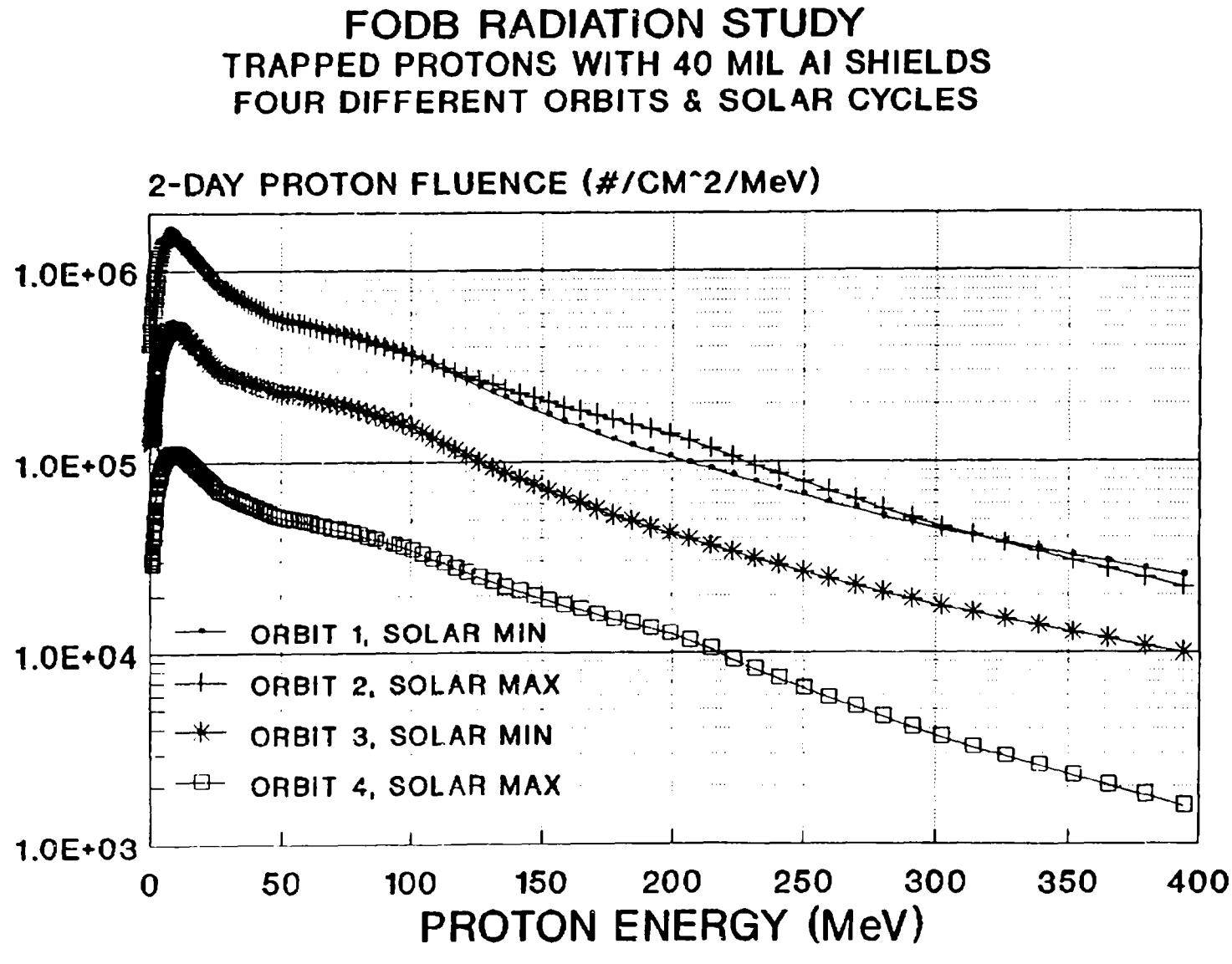

Figure 2.5: Calculated trapped proton spectra for 40 mil shielding for all four orbits, two solar max and two solar min.

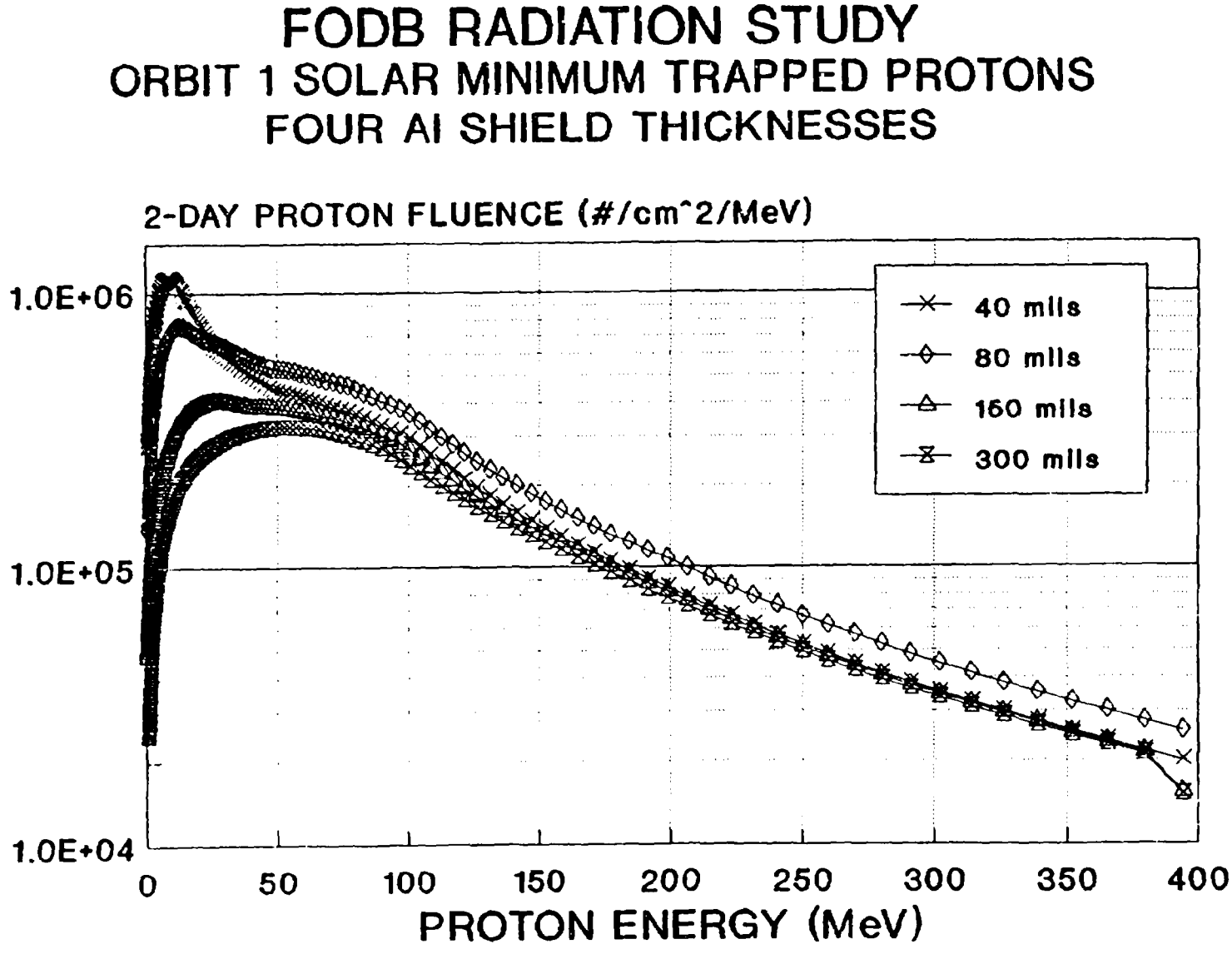

Figure 2.6: Calculated trapped proton spectra for orbit 1, four different shield thicknesses.

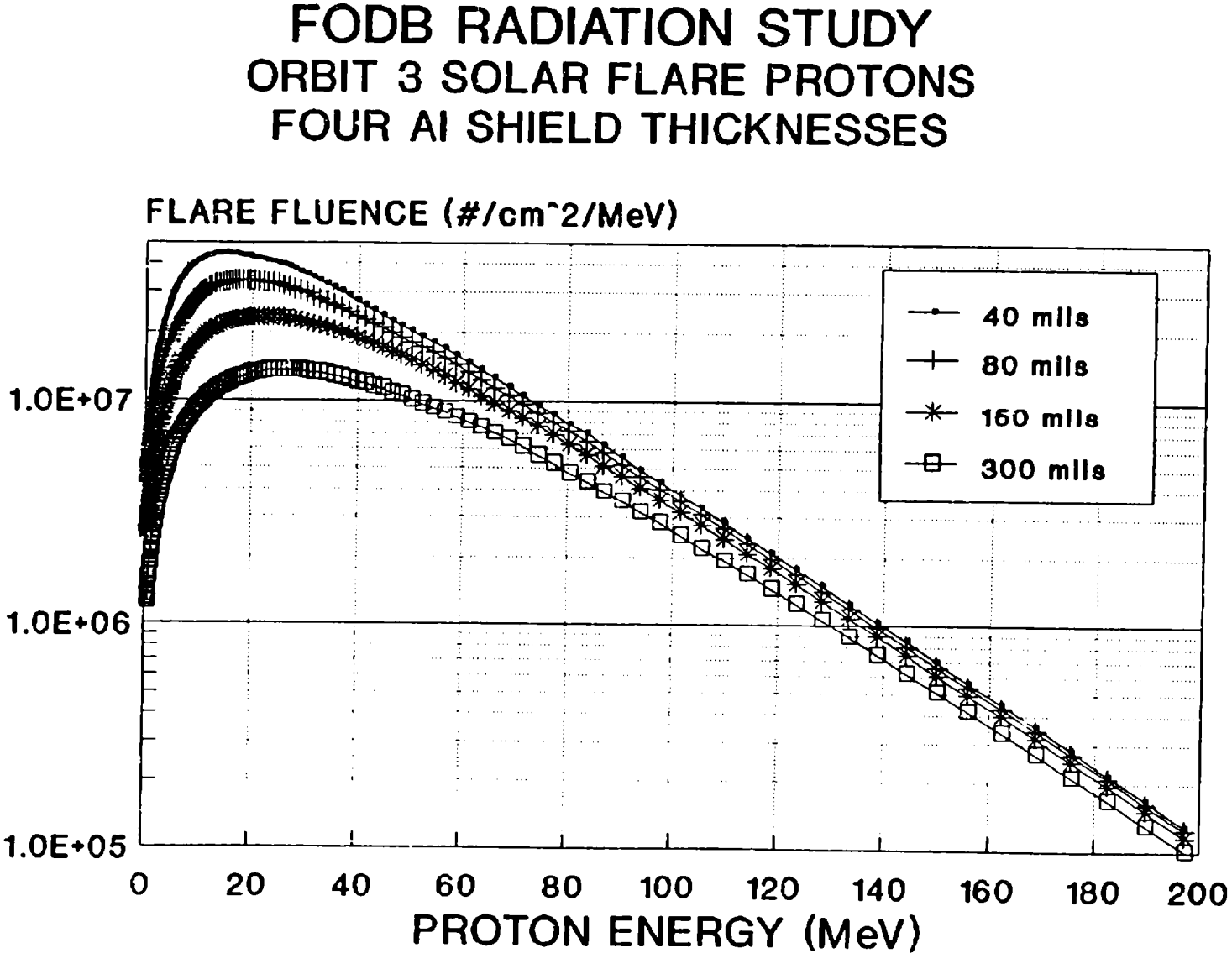

Figure 2.7: Calculated flare proton spectra for orbit 3, four different shield thicknesses.

3. Optical Fibers

3.1 CANDIDATE FIBER PROPERTIES AND TRADEOFFS

Conventional telecommunications fibers are based on silica made in an ultrapure process by chemical vapor deposition.[1] Waveguiding occurs as a result of the higher index of refraction of the core relative to the cladding. To increase the index of the core, germanium is doped into the glass, while fluorine is used to decrease the index of the cladding. Boron also decreases the index but is not routinely used because it introduces undesired attenuation of the signal (as well as increasing the sensitivity of the fiber to neutron irradiation). Phosphorus, which also raises the index, is often used because it lowers the deposition temperature and eases fabrication. To achieve the same index as the SiO_2 substrate tube, clads are deposited with the proper combination of Ge-F or P-F doping since these are easier to fabricate and provide better intrinsic optical properties than pure silica clads. Pure silica core fibers are fabricated with either F-doped or B-F-doped clads.

The diameter and NA of the fiber core determine the amount light that can be injected into the fiber, and large-core, high NA fibers are preferred for applications with many connectors. However, these core parameters also determine the pulse broadening due to modal dispersion in the waveguide. In a step index, multimode fiber the modal dispersion is quite high because of the different transit times required for different modes. In the extreme, the axial ray will transit fiber length L in $t = L/v$, where $v = c/n_1$, while a ray injected at θ_a, the maximum acceptance angle of the fiber, will require

$$t = \frac{Ln_1^2}{c\sin\theta_a} \qquad (1)$$

since the effective length for this mode has increased. Modal dispersion in a typical step index fiber with an NA of 0.35 is ~50 nsec/km, leading to relatively low bandwidth.

To decrease the modal dispersion in multimode fibers, the index is graded into a near-parabolic shape. In this case, the higher order modes (those intersecting the interface at high angle) travel in regions of lower index and therefore at greater velocity than the lower order modes. The theoretical modal attenuation of an optimized graded index fiber is ~6 ps/km. However, it is difficult to achieve this optimized profile in practice, and typical bandwidths of high-quality graded index fibers are 1-2 Gbit/sec-km. There is an additional source of dispersion due to the fact that the refractive index varies with wavelength. Since there is a slight spectral width to laser diode emission (and even broader width with LED's), this material dispersion causes the nonmonochromatic pulse to broaden and thereby decreases the bandwidth of the system.

Single mode fibers are fabricated with the proper core diameter (3-8 μm) and index to support only one guided mode and therefore eliminate modal dispersion. In this case, the bandwidth of the fiber is determined by the material and waveguide dispersion. Since the waveguide dispersion has the opposite sign from the material dispersion, proper design of the fiber structure can further minimize the overall dispersion. The matched clad design achieves maximum

bandwidth at the zero material dispersion point, near 1.3 μm for doped silica, while more complex profiles, such as the depressed clad or multiple core, introduce waveguide dispersion to shift the zero point to longer wavelength or flatten the region of near-zero dispersion to provide a wider range of operational wavelengths. The dispersion of single mode fibers is ~3 ps/nm-km at 1.3 μm and bandwidths of > 100 Gbit/sec-km can be achieved for laser diode sources.

Radiation induced loss margin. The evaluation of optical fibers for a 1.5 GHz spacecraft fiber optic data bus (FODB) will be made with respect to a lifetime total dose of 100 krad, a maximum link length of 20 m, and a margin for radiation-induced loss of 6 dB. This translates into a margin of 300 dB/km for the incremental loss, or a radiation response of 3 dB/km-krad.

Because of the natural variations in solar flux and the possibility of traversals of the South Atlantic Anomaly, the dose rate will not be a constant 45 rad/day over the anticipated 6 year lifetime of the spacecraft. Rather, dose rates as high as 100 rad/h could be experienced, as described in Section 2. Additional environmental concerns include an operating temperature range of -20 to +40 °C, a storage range of -40 to +60 °C, and a mixed environment of electrons, protons, and cosmic rays.

Step index multimode fibers. The most common fiber of this type consists of a 100 μm pure silica core clad with 120 or 140 μm of either F-doped or F-B-doped silica. Virtually all fibers with F-doped clads are pulled from Fluosil preforms with cores of Suprasil synthetic silica manufactured by Heraeus in Hanau, Germany. Fiber manufacturers include Spectran, Fiberguide, Polymicro, etc. The F-B-doped fibers are fabricated by Mitsubishi using Diasil silica as the core. Although there were numerous fibers with polymer clads available several years ago, only Ensign Bickford now fabricates them; they use a proprietary hard polymer, which has overcome most of the difficulty in connectorization which was experienced with the softer silicone claddings.

Because of differences in processing, silica core fibers can have wide extremes of OH content, from < 5 ppm to 1200 ppm. Although there have been various reports of effects of OH on radiation response, most of these have been traced to differences in other processing variables.[2,3] Nevertheless, there are significant differences in their radiation response.

Figure 3.1 compares the radiation-induced loss at 0.85 μm in several different multimode fibers whose properties are shown in Table I. (It should be pointed out that almost all reports of steady state exposures of optical fibers have used ^{60}Co γ-ray sources because of their convenience and accessibility.) It is apparent from Fig. 3.1 that the data generally divide into approximately 3 groups, and the silica core fibers suffer the least damage. The behavior of the Raychem fiber is typical for many with pure silica cores--there is an initial linear growth region at low dose followed by saturation as both thermally-induced and light-induced annealing compete with the darkening. In some fibers there may actually be a decrease in the incremental loss at high dose! By contrast, there is no measurable incremental loss in the Dainichi fiber until 10^6 rad since this fiber is extremely susceptible to light-induced annealing, or photobleaching,[4] and this experiment was carried out with relatively high optical power in the fiber. A reasonable explanation for the sudden onset of attenuation is radiation-induced cross-linking of the polymer fiber coating, which causes the material to harden and induce microbend losses.

The different behaviors of these two fibers illustrate the effects of fabrication and dopants. Although the cores of both the Raychem and Dainichi (now sold under the Mitsubishi name) fibers

are pure synthetic silica, the Raychem fiber core contains ~1200 ppm of OH impurity introduced during the flame deposition of the silica. Although the OH content of the Dainichi core, fabricated by deposition in an Ar plasma, is < 3 ppm, there is ~3000 ppm Cl. Further, the clad of the Raychem fiber is F-doped silica, while the Dainichi is F-B-doped silica. Although the radiation responses of silica core fibers are quite diverse, several general statements can be made. By contrast to earlier supposition, fibers with high OH content *are not* more radiation resistant than those with low OH content. Rather, the radiation sensitivity depends strongly on all the fabrication parameters (as well as the clad material), and for this reason, considerable effort has been expended by a number of Japanese and German companies to optimize their silica for radiation hardness.

Although pure silica core multimode fibers are definitely attractive from the standpoint of their radiation hardness, especially in applications where sufficient light power can be transmitted to effect photobleaching, the limited bandwidth makes them unusable for high data rate applications. Nevertheless, the attractive properties of these fibers are also found in pure silica core single mode fibers, described below.

Graded index multimode fibers. Fibers of this type are typically found with 50, 62.5, or 85 μm core diameters; the fiber outer diameter is either 85 or 125 μm. The grading of the refractive index to achieve higher bandwidth is accomplished by carefully increasing the Ge content as each succeeding core layer is deposited on the inside of the MCVD tube. However, this Ge doping drastically changes the fiber's radiation sensitivity.

When 10-25 mole% Ge is doped into the fiber core to increase the refractive index, the presence of this dopant dominates the radiation response. As shown in Fig. 3.1, the growth of the incremental loss in all 3 Ge-doped silica core fibers is virtually identical. The induced loss A between 10^2 - 3 x 10^5 rad can be described as a power law $A \alpha D^b$, where D is the dose and b = 0.61; saturation occurs at higher doses. Effects of fabrication are obviously more subtle, but still significant in this type of fiber, as described below.

An additional dopant that may be used to ease fiber fabrication by lowering the deposition temperature and collapse time of the preform is phosphorus. The presence of P in the core greatly increases the fiber's radiation response.[5] In general, the growth is nearly linear, and no saturation is evident. The loss in the fibers is 10 dB/m by 10^5 rad, rendering them useless in a radiation environment. The origin of this high radiation sensitivity has been carefully studied, and the numerous defect centers attributed to P have been elucidated.[6] Other interesting effects of P on the radiation response will be described below.

Certainly, the Ge-doped silica core graded index multimode fibers are attractive from an intrinsic standpoint--even a poorly graded fiber with 300 MHz-km has sufficient bandwidth for the 1.5 GHz FODB, and the attenuation is minimal in a 20 m link. However, there are several aspects of the space environment which have not been fully explored, including the response of the fibers to high total dose at low dose rate, the effect of temperature cycling, and synergistic effects of different radiations, e.g. protons, electrons, cosmic rays. There have been only a few initial studies of these effects, and the results will be discussed below.

Single mode fibers. The cores of almost all single mode telecommunications fibers are doped with Ge since it is quite difficult to fabricate pure silica core fibers, and their intrinsic losses are often

higher. In fact, many so-called "silica core" fibers are actually slightly doped with Ge to reduce the anomalous intrinsic attenuation. The two possible exceptions are the Sumitomo Z fiber (sold by AT&T as Litespec ZSM) and a fiber sold by Schott. Because of the similar natures of their cores, the discussion above regarding pure silica core multimode and Ge-doped graded index fibers pertain to the single mode fibers as well.

Because so much glass has to be deposited for the cladding of a single mode fiber and because collapsing pure silica clad fiber preforms requires an extended length of time at high temperature, the clads are often codoped with P and F. The high radiation sensitivity of P-doped optical fibers is attributable to the fact that P inhibits recovery while decreasing, or even reversing, the temperature dependence of the incremental attenuation (see below). A quantitative relationship between the incremental loss and [P] in the clad was reported by Mies and Soto.[7] In this work, a series of depressed-clad single mode fibers was fabricated with different concentrations of P in the clad. The P distributions were measured analytically, and an optical power-weighted average phosphorus level P_{eff}(wt%) was calculated using the far field beam profile. Linear regression of the Mies and Soto data (Fig. 3.2) shows a high degree of correlation between the radiation sensitivity α (dB/km-krad) induced by low dose rate (2.3 rad/h) exposure and $[P]_{eff}$:

$$\alpha_{1.3\,\mu m} = 2.98[P]_{eff} + 0.17 \qquad R^2 = 0.994 \qquad (2)$$

$$\alpha_{1.53\mu m} = 4.63[P]_{eff} - 0.09 \qquad R^2 = 0.982 \qquad (3)$$

Note that the growth of the radiation-induced attenuation was linear in these fibers so that their response could be expressed as dB/km-krad. For FODB applications with a lifetime dose of 100 krad, it would appear that doping single mode fiber clads with as little as 0.5 wt% would result in a marginal radiation hardness, at best. Nevertheless, this work was the first comprehensive study relating fiber fabrication variables to radiation response in a statistically-significant manner.

Use of single mode fibers in a FODB involves several compromises. The intrinsic properties (attenuation and bandwidth) more than satisfy the requirements of a 1.5 GHz LAN, and it is possible to use pure silica core single mode fiber to take advantage of photobleaching and the lower radiation response of silica. However, by definition, single mode fibers have small cores of 3-8 μm diameters, so connectorization and fan-out become more difficult. In particular, the use of star couplers may be precluded.

Wavelength of operation. Selection of the operational wavelength of the FODB will involve trade-offs between intrinsic and radiation-induced fiber attenuation and device reliability. Typically, there are three operational windows of 0.85, 1.3, or 1.55 μm. In the first window sources are based on GaAs, and Si or GaAs detectors can be used, while InGaAsP and other quaternaries are required for 1.3 and 1.55 μm. Because of the extremely strong overtone and combination absorptions of OH, as shown for the Polymicro fiber in Fig. 3.3a, high OH content fibers, such as those based on Fluosil preforms, can be used only at 0.85 μm. In contrast, the 0.95 μm third OH overtone is absent in low OH content fibers, and the 1.4 μm second OH overtone is much weaker (Figs. 3.3b and c); these can be used at either 0.85 or 1.3 μm. Operation at 1.55 μm requires extremely low OH contents, in the ppb range; the 1.4 μm OH band is virtually absent in fibers such as the single mode fibers (Fig. 3.3c).

Single mode fibers present an additional factor regarding the operational wavelength. It is desirable to have the cutoff wavelength λ_c for the LP_{11} mode at as long a wavelength as possible for tight confinement of the LP_{01} optical mode within the fiber core. As shown in Figs. 3.3c, λ_c is placed in the 1.15-1.27 μm range for good 1.3 μm transmission; operation at longer wavelengths results in weaker confinement and increased bending loss, especially in the case of matched clad designs. Note the intrusion of the bending edge from long wavelength, especially in the ZSM fiber where λ_c = 1.15 μm. Thus, the range of operation of single mode fibers is limited by the single mode cutoff at short wavelengths and the bending edge at long wavelengths.

The radiation-induced loss in the fiber waveguide in a FODB system will depend upon the operational wavelength because of the spectral nature of the color center absorptions. In general, the resolved color center bands reside at short wavelengths in the ultraviolet or near-uv spectral region, and the tails of these bands extend into the infrared, giving rise to the incremental loss at the operational wavelength.[8] In addition, there are weaker, unresolved radiation-induced absorptions that also contribute to the ir loss. Typical absorption spectra of irradiated fibers are shown in Figs. 3.3 and 3.4. With the exception of the fibers containing P in the core or clad (e.g. CGW 1519 in Fig. 3.3b and the Ge-P doped fibers in Fig. 3.4), the incremental loss decreases with increasing wavelength. As a general rule-of-thumb, the ratio of the radiation sensitivity of a Ge-doped silica core fiber at 1.3 to 0.85 μm is ~0.25and that at 1.55 to 1.3 μm is ~0.6. Although the ratio of the damage at 1.3 to 0.85 μm in silica core fibers is ~0.1,use of these waveguides (or any fibers for that matter) at 1.3 or 1.55 μm requires low OH content since the second overtone of the OH vibration occurs at 1.39 μm.

The spectrum of the Ge-P-doped fibers suggests the presence of a radiation-induced absorption band at long wavelengths, which causes the attenuation to rise for $\lambda > 1.05$ μm.[8,9] The spectra of irradiated P-doped silica have been resolved into Gaussian components, and a band centered at 1.57 μm was correlated with a PO_3^{2-} defect center, formed by trapping a hole on a unit consisting of a phosphorus which has a pair of electrons in a nonbonding orbital and is bonded to three bridging oxygens.[6] Fibers doped with P not only show little or no recovery of the incremental loss, they undergo an anomalous temperature dependence where less damage is induced at low temperature than at high, contrary to normal intuition concerning thermal annealing.[9] This behavior is explicable in terms of the interaction of this so-called P_1 defect center and a phosphorus oxygen hole center (POHC): Because the POHC is thermally unstable, trapped holes are released and retrapped by the P_1 precursor. Thus, the radiation-induced loss in the ir, which is primarily determined by the P_1 absorption, *increases* with time after exposure and with increasing temperature. Since the P_1 defect is stable to ~450°C, the incremental loss in fibers doped with P does not recover significantly at room temperature.[6]

For FODB applications, it would appear that 1.3 μm is the optimum wavelength. There is a significant reduction in radiation-induced attenuation on going from 0.85 to 1.3 μm,[3,10]and as described in other chapters of this report, the device technology is mature. Good reliability has been achieved in the telecommunications industry, and a 1.3 μm FODB should easily survive a 6 year mission in space. In contrast, the lower intrinsic loss and slightly lower incremental loss of fibers at 1.55 μm is not an issue for a 20 m fiber link, and the devices are not as mature. Long term reliability still remains an issue with the long wavelength sources.

3.2 RADIATION DAMAGE MECHANISMS AND EFFECTS

Color center formation. It is well accepted in the literature of radiation effects in glass that trapping of the radiolytic electrons and holes generated by the radiation photons or particles gives rise to defect centers which may absorb light. The trapping sites can exist prior to the exposure or be formed by the radiation itself. It is apparent that knock-on collisions between incident ions (or relativistic electrons) and atoms in the glass can create copious displacements and charge trapping sites. However, it is only recently that it has been recognized that displacements can also occur as a result of radiolytic (photochemical) reactions. For example, if the incident radiation creates a hole-electron pair, it can decay nonradiatively, providing sufficient energy to the glass matrix to displace an oxygen atom. [11]

Impurities in the glass provide preexisting sites on which the charges can be trapped, and for this reason, the radiation damage in silica made from fused natural quartz, which contains ppm quantities of alkali and aluminum, is significantly greater than that in synthetic silica where these impurities are virtually absent. Likewise, the chemical purification that has been undertaken to reduce the intrinsic loss of fibers has had the corollary benefit of reducing their radiation sensitivity.

It might be thought that pure silica core fibers would be the most radiation-resistant, and therefore the most desirable for use in radiation environments. However, there are a number of other factors, including ease of fabrication and the intrinsic loss and bandwidth which must be considered. In addition, the core/clad dopant type and concentrations, fabrication conditions, wavelength and intensity of the transmitted light, temperature of operation, and the total dose, dose rate, and time after exposure that have a significant but varied effect on the incremental loss. Because of the multidimensionality of the problem, predicting the radiation response of a fiber is a difficult task. The safest approach may be to test fibers under consideration for a system in a radiation environment that simulates as accurately as possible their intended application.

Recovery mechanisms. As the total dose to which a fiber is exposed increases, the net darkening that is measured is the sum of the competing effects of color center formation by charge trapping vs. recovery via thermal annealing or light-induced processes. In the absence of annealing, (or if the dose rate is low enough that the time constant of the recovery is much faster than that of the darkening) power law growth behavior $A \alpha D^b$, which may be linear in some cases, is observed, as for the P-doped fibers in Fig. 3.1. Significant saturation of the induced loss is observed in during irradiation of silica core fibers, which is attributed to photobleaching, and in Ge-doped silica core fibers, due to thermal annealing, as described below.

It has recently been recognized that the recovery data of irradiated fibers can be fit quite well to the expression for n^{th} order kinetics

$$A = (A_o - A_f)[1 + ct]^{-1/(n-1)} + A_f \qquad (4)$$

where $c = (1/\tau)[2^{n-1} - 1]$.[12] The parameters of the fit are the initial and final, or permanent, induced attenuations, A_o and A_f, the half-life of the incremental loss τ, and the kinetic order of recovery n. Examples of the recovery for different values of n are shown in Fig. 3.5. Although there is no temperature-dependent term in Eq. 4, the recovery is thermally-activated.

Values of n = 2 are typically observed for pure silica core fibers which are transmitting light during the recovery.[12,13] This case is classical, diffusion-limited bimolecular recombination, and there is considerable evidence that the diffusing species is hydrogen in pure silica. However, much larger values of n are measured for Ge-doped silica core fibers, and the interpretation is more complex. Although these cases may also be understood physically as diffusion-limited, the diffusing species is now limited to specific paths. As n increases, the dimensionality of the available diffusing space decreases from fractal surfaces to fractal dust. The physical interpretation of n = 5-7 for Ge-doped silica core single mode fibers is still under investigation. Nevertheless, it is apparent from Fig. 3.5 that recovery will be much more rapid for lower values of n.

Photobleaching. One of the most intriguing effects is light-induced annealing or photobleaching of the incremental loss either by the data signal itself or by an additional optical signal of a different wavelength.[4] Many of the variations in radiation sensitivity reported by different laboratories for nominally identical fibers can be traced to differences in optical power used to make the measurement. Photobleaching over a range of optical powers is demonstrated in Fig. 3.6 for a pure silica core multimode fiber. Here, the requisite power was maintained in the fiber during irradiation and recovery. The data labeled "Dark" were obtained using a 100 nW source which was turned off during exposure and shuttered on for ~2 s for each measurement plotted. Similar effects have been observed for Ge-doped silica core fibers, although the extent of the light-induced annealing is much less.

It is clear from Fig. 3.6 that increasing the optical power greatly enhances the recovery. What was not recognized until recently was that there is a significant change in the kinetics between the cases where the fiber is dark and where it is transmitting even the least amount of power.[13] Note from the fits that the order of the kinetics changes from 7.5 to 2 when the fiber transmits light, implying that even 300 nW of 0.85 μm light is sufficient to activate the diffusing species.

Although photobleaching is obviously effective at 23 °C, fiber cables onboard spacecraft may be routed in areas where the temperature could be much lower. At the extreme, measurements have been made of photobleaching at temperatures as low as -150 °C as a worst-case simulation of fiber cables in unheated cable trays attached to the struts connecting pods of the Space Station.[14,15] To determine whether fibers are viable in such an environment a number of multimode waveguides (Table I) were exposed to 3000 rad and the growth and recovery of the incremental loss were measured while the fibers were maintained at -150 °C. These data are shown in Figs. 3.7 and 3.8. By comparison of Figs. 3.1 and 3.7 it is apparent that the induced losses of the Ge-doped silica core fibers are 2-3 times greater at the lower temperature, while the damage in the Ge-P-doped fibers is actually *less*, as expected from the temperature dependence of the P_1 center.[6] Surprisingly, the damage in the silica core fibers is approximately the same at both temperatures, although this may be due to the difference in power levels and dose rates used for the two experiments.

By comparing the solid and open points for the Raychem and ITT Rad Hard fibers in Fig. 3.7 it is apparent that the -20 dBm signal in the fiber significantly reduces the induced loss at -150 °C and in both pure and Ge-doped silica core fibers. Further evidence that photobleaching enhances the recovery even at this low temperature is seen in Fig. 3.8 where ~80 dB/km loss remains at 10^5 sec in the Raychem silica core fiber measured without the continuous light signal

while 10 μW is sufficient to reduce this loss to 2-3 dB/km. Similarly, photobleaching hastens the recovery of the ITT Rad Hard Ge-doped silica core fiber, as seen in Fig. 3.8b.

As described in more detail below, the loss induced in fibers by a low dose rate exposure can be estimated from by fitting the recovery data to Eq. 4.[16] Alternatively, as $t \rightarrow \infty$, Eq. 4 reduces to a power law of time, so plotting the recovery data on a log-log plot allows easy extrapolation to longer time. For comparison, the loss measured in the fibers at 10^6 sec and that extrapolated to 10 years (10^8 sec) are shown in Table I. In spite of the large losses induced initially at -150 °C in the doped silica core fibers, the surprisingly good light-induced annealing in all fibers except those containing P means that there will be less than 1 dB incremental loss in a 100 m length following a 3000 rad exposure over 10 years. However, this will be the case *only if the fiber is continuously transmitting an optical signal.* Nevertheless, these data show that photobleaching can be used to good advantage in some fibers to ameliorate the effects of space radiation.

Low dose rate response. Radiation damage in fibers has an apparent dose-rate dependence because of the annealing that occurs simultaneously with the darkening. An example of this behavior is shown in Fig. 3.9. Since the time constant for recovery of the induced loss is ~1000 sec, the incremental losses for fibers irradiated at the two slower rates of 16.7 rad/min and 1 rad/day are almost identical, i.e. virtually all recovery occurs on a time scale shorter than the irradiation at these rates.

Because obtaining low dose rate data requires low activity sources and long times, few reports have appeared in the literature. A set of data for multimode fibers exposed at 1 rad/day was published several years ago and is summarized in Table II. Unfortunately, the emphasis in this study was primarily on the 0.85 μm region. Data such as those in Fig. 3.9 suggested that it might be possible to extrapolate the radiation-induced loss in a fiber irradiated at a low dose rate R for a period of time t from the recovery to time t following a high dose rate exposure to a dose Rt. Such a procedure was qualitatively verified for the multimode fibers.

Recently, polarization-maintaining 1.3 μm single mode fibers anticipated for use in fiber gyroscopes in space were irradiated at 0.5 rad/h and 3000 rad/min.[16] In addition, Corning 1521 (now Corning SMF28), a conventional 1.3 μm single mode fiber was exposed in the same manner. Typical low dose rate results are shown in Fig. 3.10. Because the growths of the induced losses are linear with dose, linear regression of the data was valid to determine the radiation response in dB/km-krad. These responses compare favorably with the values of A_f determined by fitting the recovery data following high dose rate exposure to Eq. 5, as shown in Table III. Although polarization-maintaining fiber is not required for the FODB, this study demonstrated that it is possible to quantitatively predict within 20-30% the low dose rate response of fiber waveguides without having to perform long duration experiments using low activity sources. A more precise procedure is to fit the recovery data to Eq. 4 and then calculate the anticipated attenuation after a low dose rate exposure of time t. This procedure has been used to extrapolate recovery data for the FODB.

Temperature. Because the depth of the color center traps depends intimately on their nature, and hence on the core and clad dopants, the temperature dependence of the recovery of optical fibers varies considerably.[3,10] Since the recovery is thermally activated, one would anticipate faster recovery at higher temperature. Although this is the case with pure and Ge-doped silica core fibers, as mentioned above, doping with P can actually invert this dependence.

Since the trapping sites associated with Ge in Ge-doped silica are relatively shallow, substantial recovery of the incremental loss occurs during or following exposure, giving rise to the saturation shown in Fig. 3.1 and the dose rate dependence shown in Fig. 3.9. In addition, there is a strong temperature dependence to the recovery, as shown in Figs. 3.11a and b, so that much less damage is evident in these fibers at 80 °C than at -55 °C. Typically, the incremental attenuation at -55 °C is ~20 times greater than at 23 °C, and is 3-4 times less at 80 °C than at 23 °C. In contrast, the incremental attenuation increases by factors of 10 in the Dainichi silica core multimode fiber on going from 80 to 23 to -55 °C, as shown in Fig. 3.11c.

As shown in Figs. 3.11b and 3.12a, for a Ge-doped silica core fiber, the temperature dependence is primarily expressed in the attenuation, i.e. the number of color centers, and the half-life τ (at least at the lowest temperature) with only a weak dependence on kinetic order.[18] Note also that the behavior of both A_o and τ can be reasonably fit to an Arrhenius relationship $C = C_o e^{E/kT}$, as shown by the straight lines, implying thermal activation of the initial concentration of color centers and the half-life. Similar Arrhenian behavior is noted for pure silica core fibers in Figs. 3.11c and 3.12b. A_o, A_f, and τ appear to be thermally activated, but the half-life *increases* with increasing temperature in the single mode Sumitomo Z fiber. Note that the kinetic order n is independent of temperature in both the Corning 1521 and Sumitomo Z fibers.

Although the origins of the temperature dependence of the radiation damage in these fibers bear further detailed study, it is clear that irradiation at lower temperature produces greater attenuation, and that the recovery of this damage is slower. It should be emphasized that there have been no studies of the synergistic effects of temperature cycling and radiation exposure, such as might be observed in space. Although there have been several earlier studies of the behavior of fibers over the MIL-SPEC temperature range of -55 to +80 °C,[10] the emphasis was on tactical dose levels of several krad rather than the 100 krad anticipated for the FODB. Furthermore, the measurements of these studies were made on fibers available 7-10 years ago, and there has been substantial development and improvement since that time.

Total dose. Perhaps the most significant void in applying existing fiber radiation damage data to the FODB is high total dose exposures of appropriate candidate fibers over the anticipated temperature range. Fig. 3.1 shows data of numerous multimode fibers exposed to 10^7 rad at 23 °C, and Fig. 3.13 contains data of state-of-the-art multimode and single mode fibers exposed to 10^6 rad at 50 °C. These latter fibers are described in Table IV. The behaviors of the fibers at 1.3 μm divide into 3 groups: Corning 1519 is significantly more radiation sensitive than the other fibers, while the induced losses in the two multimode Spectran fibers and the Corning and Litespec Ge-doped silica core single mode fibers are all similar and approximately an order of magnitude less than Corning 1519.

As shown in Fig. 3.13b, the incremental loss in the Mitsubishi silica core multimode fiber at 1.3 μm is minimal, and the growth is virtually saturated. This is likely due to photobleaching, which is much more effective in annealing the damage in this low OH content silica core fiber at both 0.85 and 1.3 μm. In spite of the fact that both the Fiberguide and Polymicro fibers were pulled from Fluosil preforms, their induced losses are almost an order of magnitude different, as seen in Fig. 3.13b. Nevertheless, the growths of the attenuations are almost saturated under these irradiation conditions.

Comparison of the data of Figs. 3.1 and 3.13 is instructive. Note that the response of Corning 1519 is approximately 5 times greater at 0.85 μm and 23 °C than it is at 1.3 μm and 50 °C. In contrast, the damage in the Raychem fiber is ~30 dB/km at the short wavelength vs. 10 dB/km for the Polymicro and ~3 dB/km for the Fiberguide pure silica core multimode fibers, even though all three were drawn from high OH content Fluosil preforms. What is particularly noticeable in comparing the two data sets is that there is a set of Ge-doped silica core multimode and single mode fibers that is significantly more radiation resistant at 50 °C than Corning 1519. This result may be due to the different temperatures at which the two data sets of Figs. 3.1 and 3.13 were taken, since it is suspected that Corning 1519 may be slightly doped with P, which would minimize its temperature dependence.

From the data of Fig. 3.13 it should be possible to extrapolate the attenuation after an exposure of 100 krad, and this has been done in Section 3.4. However, extrapolation to different temperatures and temperature cycling may be fraught with error. As usual, the best course of action would be to test the candidate fibers under conditions that simulate the realistic space environment.

Radiation type. Almost all reports of steady state radiation-induced attenuation in fibers have used γ-ray sources such as ^{60}Co, or to a much lesser extent, ^{137}Cs, while transient studies have used pulsed x-ray or electron machines. However, the space environment consists of electrons, protons, and cosmic rays, and a valid concern is how laboratory measurements using ^{60}Co sources simulate the damage a fiber optic waveguide would experience in space. There have been several studies of neutron-irradiated fibers, including both filtered reactor exposures to minimize the gamma ray component of the flux[19] and 14 MeV neutrons from D-T reactions.[20] Computations have shown that for ~10^{12}-10^{15} n/cm^2 neutron fluences all the kinetic energy deposited in the fiber is converted to ionizing processes, e.g. a neutron flux of 10^{12} n/cm^2 was found to be equivalent to an ionizing dose of 2000 rad. The computed ionizing dose was then used for comparing neutron and γ-ray results, and the optical absorption induced by equivalent neutron and ionizing doses were found to be quite similar. Although there seems to be an equivalence for pure silica core fibers, there has been one report of greater damage in silica with increasing neutron content in mixed field exposures[19] and greater sensitivity to neutrons in Ge-doped silica core fibers.[21]

To investigate the effects of different types of irradiation, several different pure and Ge-doped silica core fibers were exposed to ^{60}Co γ-irradiations, mixed neutron-gamma fields from a reactor, and energetic protons from a cyclotron.[22] As shown in Fig. 3.14, the damage induced by γ-rays and protons was virtually identical in pure silica core fibers, while there was greater damage for proton exposures in the Corning 1519 and ITT Rad-hard Ge-doped silica core fibers. The high loss of the proton-irradiated Corning sample in Fig. 3.14c is likely due to microbending losses in the fiber during the measurement. But the appearance of a band at 1 μm, which is not evident in the neutron-irradiated fiber, is a notable feature which cannot be attributed to microbending. An additional concern is the loss that might be added to the waveguide from protons which are captured in the fiber core and then bond with the network atoms, forming Si-OH. Such hydrogen-induced aging, which has been observed in submarine cables, can cause substantial increases in the attenuation at 1.3 μm.

Unfortunately, there have been too few studies of proton-irradiated optical fibers to fully characterize their response, and it is too early to conclude that γ-ray and proton exposures are equivalent. Rather, it appears that neither mixed γ-neutron fields nor γ-ray sources adequately

simulate the effects of proton irradiation of doped silica core fibers, although there is good correspondence in the case of pure silica core waveguides.

3.3 FIBERS IN SPACE

The Long Duration Exposure Facility (LDEF) carried two experiments to determine the effect of the space radiation environment on optical fibers. An active experiment involving data transmission at 0.85 μm through 4 different fiber coils was fielded by the Air Force Weapons Laboratory (now Philips Laboratory), and signal/noise and error statistics were measured as a function of radiation and temperature cycling. The fibers included two polymer-clad silica core fibers, a high numerical aperture Pb-silicate core fiber, and a Ge-doped silica core fiber; these were near state-of-the-art in the early 1980's when they were selected.

Although all 4 fiber links operated for the planned 1 year duration, only 3 of the 4 were operational upon LDEF recovery. It is not clear at this time whether the failure was due to micrometeorite impact or component failure. There were significant modulations in the transmitted signal level, which could be qualitatively correlated with variations in temperature and radiation flux.[23] In some cases, the fibers were completely attenuating for extended periods of time. It is possible that the origin of this effect is the change in index of refraction that occurs with some silicone polymer optical claddings at low temperature, leading to a condition where the fiber no longer guides light. However, it appeared that the temperature was not sufficiently low for this to occur. It was hoped that the LDEF data and a detailed analysis would be available for this report, but PL personnel were unable to complete the analysis in time and would not release the raw data. Nevertheless, it is clear that there are synergistic effects of temperature cycling and variations in radiation flux on the radiation-induced attenuation in optical fibers.

A second, passive experiment was fielded by the Jet Propulsion Laboratory, which comprised 10 different fiber optic cables with both pure and Ge-doped silica cores from 7 manufacturers. However, to date the data obtained from these fibers has not been released although Dr. Alan Johnston has contacted NRL concerning the possibility of a cooperative effort to determine the low dose rate response of the fibers.

LDEF is the only known case where a number of fibers were flown in space for an extended period with the purpose of determining their radiation-induced degradation. However, the fibers used on LDEF are in general not representative of those available from fiber manufacturers today, and the data were obtained at 0.85 μm. Thus, rather than being directly applicable to the FODB, the LDEF data, when available, should serve as a guide to potential problems and synergistic effects of temperature cycling and radiation on the fiber attenuation.

3.4 ANTICIPATED DEGRADATION

Fiber optic waveguides. The various factors affecting the response of optical fibers to radiation environments have been described in detail in the preceding sections.[3,9] Although there are no data currently available which were obtained under conditions which precisely (or even adequately) simulate the environment to which fibers will be exposed in the FODB, it is useful to extrapolate their behavior from existing measurements. The most appropriate data appear to be those recently obtained for state-of-the-art single mode and multimode fibers exposed to 10^6 rad at 50 °C and shown in Figs. 3.13 and 3.15.

The losses induced at 10^5 rad will obviously be less than those at 10^6 rad, but a linear extrapolation to the lower dose will underestimate the damage if there is any saturation. Thus, the extrapolation has been made using the ratio of the incremental losses at 10^5 and 10^6 rad taken from the growth data of Fig. 3.13. These ratios are shown in Table V. A second assumption is that the recovery process is independent of dose rate, so the attenuation A calculated at t = 6 years from the parameters obtained from fitting the recovery data in Fig. 3.15 to Eq. 4 is a measure of the loss that would be induced by a low (or variable) dose rate exposure to 10^5 rad over 6 years. Finally, it is assumed that the recovery process is independent of dose, so A_f obtained from the recovery data following the exposure to 10^6 rad can be scaled to 10^5 rad using the loss ratios in Table V.

The results of the extrapolations of high dose rate recovery data to low dose rate response are contained in Table V. It is apparent that both the multimode and single mode silica core fibers (Table IV) show virtually no induced loss at this temperature. In contrast, there would be measurable losses induced by low dose rate exposures in the Ge-doped silica core fibers; the magnitude varies among the fibers. Clearly, Corning 1519 shows the highest attenuation, but interestingly, the recovery of Spectran 320R is sufficiently greater than that of the two Ge-doped single mode fibers (SMF-28 and GSM12) that its low dose rate response is anticipated to be less.

One can additionally extrapolate the response from 1.3 to 0.85 μm using a factor of approximately 5 for the ratio of the incremental losses at the two wavelengths.[3,8,11] Any of the Ge-doped or pure silica core fibers would perform adequately in the FODB at either 0.85 or 1.3 μm with the exception of Corning 1519, whose response now becomes somewhat marginal at 175 dB/km. However, it should be emphasized that these data and extrapolations pertain to *fibers exposed to ionizing radiation and maintained at 50 °C.*

Extrapolating the data of Figs. 3.13 and 3.15 and Table V to different temperatures is much less straightforward, since varying the temperature may affect not only the color center concentration, i.e. A_o and A_f, but also the recovery kinetics, i.e. n and τ of Eq. 4. Using the data of Fig. 11b for Ge-doped silica core fibers, it is possible to extrapolate from +50 to -60 °C assume a worst-case ratio of the induced losses of approximately 50.[10] Obviously, the extrapolated low dose rate responses of the Ge-doped silica core fibers of Table V become quite marginal under this assumption that only the color center concentration changes. If the recovery kinetics are also altered on going to -60 °C, as is the case for the Corning 1521 and Sumitomo Z fibers, as shown in Fig. 3.12, the situation is much more grim.

It would be desirable to extrapolate the degradation of fibers from the available set of data obtained with γ-ray sources to the space environment. However, this can only be done under the assumption that exposure to protons and electrons results only in ionization damage processes. It is reasonable to assume that this is not the case based on the data to date,[22] and it is therefore prudent not to extend these extrapolations too far.

Passive components. In addition to optical fibers, a realistic data bus will include various couplers, splitters, and taps to achieve the desired network architecture and topology. In spite of the fact that the path length of these components is relatively short, the optical signal will be transmitted through them, and their potential degradation in a radiation environment must be taken into consideration.

To our knowledge, there are no recent data on the radiation response of any of these devices. To the extent that they are made from the same core and clad glass compositions as the fibers, it is anticipated that there radiation responses will be similar. However, this may not always be the case. As an example, consider the fused taper fiber coupler where two fibers are twisted, fused together and drawn down to a much smaller diameter. The coupler works on the principle that light can no longer be propagated in the core since it is so small, and the wave is no guided by the whole fused fiber structure, which consists of the minuscule cores of both fibers, their clads, and the support tubes used during preform deposition. Whereas the radiation response of the fiber was primarily determined by the core composition and processing, since the signal now extends through the whole fiber structure, the response of the clad and the tube now become dominant. Any P doping in the clad now becomes a much greater concern as does the quality of the substrate tube, which is likely to consist of silica made from impure fused natural quartz, whose radiation sensitivity is considerably higher than that of synthetic silica.

One component which was has been evaluated is the Selfoc microlens,[10,24] which may be used in some applications to couple light from a laser diode into the fiber or in couplers between fibers. This study established that a dose of 10^5 rad induced a loss at 1.3 μm of approximately 2 dB at 23 °C, and that there was only slight recovery. No measurements were made at other temperatures or under low dose rate conditions. Certainly, if these lenses, or other components from similar glass compositions, are used to any extent in the FODB, they could easily consume the loss margin for radiation effects.

Other types of splitters or taps may involve dielectric coatings, holographic filters, or fiber grating reflective filters. None of these have been evaluated for radiation hardness, especially in environments appropriate for space. However, it is well known that the intrinsic stability of holographic filters is a concern, so it can be anticipated that they will not fare well in a radiation environment.

CHAPTER 3 REFERENCES

1. Optical Fiber Telecommunications, S.E. Miller and A.G. Chynoweth, Ed. (Academic Press, New York, 1979).

2. E.J. Friebele, M.E. Gingerich, K.J. Long, P.S. Levin, and D.A. Pinnow, "Radiation-resistant low OH content silica core fibers," IEEE J. Lightwave Tech. LT-1 (1983) 462-465.

3. E.J. Friebele, K.J. Long, C.G. Askins, M.E. Gingerich, M.J. Marrone, and D.L. Griscom, "Overview of radiation effects in fiber optics," Crit. Rev. Tech.: Opt. Materials in Radiation Environments (SPIE Vol. 541), P. Levy and E.J. Friebele, Ed. (SPIE, Bellingham, WA, 1985), pp. 70-88.

4. E.J. Friebele and M.E. Gingerich, "Photobleaching effects in optical fiber waveguides," Appl. Opt. 20 (1981) 3448-3452.

5. E.J. Friebele, P.C. Schultz and M.E. Gingerich, "Compositional effects on the radiation response of Ge-doped silica-core optical fiber waveguides," Appl. Opt. 19 (1980) 2910-2916.

6. D.L. Griscom, E.J. Friebele, K.J. Long and J.W. Fleming, "Fundamental defect centers in glass: Electron spin resonance and optical absorption studies of irradiated phosphorus-doped silica glass and optical fibers," J. Appl. Phys. 54 (1983) 3743-3762.

7. E.W. Mies and L. Soto, "Characterization of the radiation sensitivity of single-mode optical fibers," Proc. ECOC '85 (Venice), 1985.

8. E.J. Friebele, M.E. Gingerich and K.J. Long, "Radiation damage of optical fiber waveguides at long wavelengths," Appl. Opt. 21 (1982) 547-553.

9. E.J. Friebele, C.G. Askins, M.E. Gingerich, and K.J. Long, "Optical fiber waveguides in radiation environments, II," Nucl. Inst. Meth. in Phys. Res. B1 (1984) 355-369.

10. E.J. Friebele, K.J. Long, C.G. Askins, and M.E. Gingerich, "Radiation response of optical fibers and Selfoc Microlenses at 1.3 um," Fiber Optics in Adverse Environments, II (SPIE Volume 506), R.A. Greenwell, Ed. (SPIE, Bellingham, WA, 1984), pp. 202-208.

11. D.L. Griscom, "Nature of defects and defect generation in optical glasses," Radiation Effects in Optical Materials (SPIE Volume 541), P.W. Levy, Ed. (SPIE, Bellingham, WA, 1986), pp. 38-59.

12. E.J. Friebele, C.G. Askins, C.M. Shaw, M.E. Gingerich, C.C. Harrington, D.L. Griscom, T.E. Tsai, U.C. Paek and W.H. Schmidt, "Correlation of single mode fiber radiation response and fabrication parameters," Appl. Opt. 30 (1991) 1944-1957.

13. D.L. Griscom, "Radiation induced color centers in bulk silicas and fibers," Am. Ceram. Soc. Bull. 70 (1991) 483.

14. E.J. Friebele, K.L. Dorsey and M.E. Gingerich, "Optical fiber waveguides for spacecraft applications," Fiber Optics in Adverse Environments III (SPIE Volume 721), R.A. Greenwell, Ed. (SPIE, Bellingham, WA, 1986), pp. 98-103.

15. R.A. Greenwell, D.M. Scott, D.R. Biswas and R.E. Jaeger, "Radiation testing of optical fiber for the space station," Proc. Eur. Conf. on Radiations Effects on Devices and Systems, 1991.

16. E.J. Friebele, L.A. Brambani, M.E. Gingerich, S.J. Hickey and J.R. Onstott, "Radiation-induced attenuation in polarization-maintaining fibers: Low dose rate response, stress and materials effects," Appl. Opt. 28 (1989) 5130-5143.

17. E.J. Friebele, C.G. Askins and M.E. Gingerich, "Effect of low dose rate irradiation on doped silica core optical fibers," Appl. Opt. 23 (1984) 4202-4208.

18. E.J. Friebele, Radiation Response Prediction of Single Mode Fibers (NCS Tech. Bull. 88-1) (National Communications System, Arlington, VA, 1988).

19. W. Schneider, "Radiation sensitivity of thick core all-glass fibers in reactor radiation fields," Appl. Phys. A 28 (1982) 45-51.

20. P.L. Mattern, L.M. Watkins, C.D. Skoog and E.H. Barsis, "Absorption induced in optical waveguides by pulsed electrons as a function of temperature, low dose rate gamma and beta rays, and 14 MeV neutrons," IEEE Trans. Nuc. Sci. NS-22 (1975) 2468-2474.
21. W. Schneider and U. Babst, "Induced attenuation in optical fibers during steady state and pulsed irradiation," Optical Fibers in Adverse Environments (SPIE Volume 404), D. Boucher, Ed. (SPIE, Bellingham, WA, 1984), pp. 33-39.
22. M.E. Gingerich, K.L. Dorsey, C.G. Askins and E.J. Friebele, "A comparison of gamma, neutron and proton irradiations of multimode fibers," Optical Techniques for Sensing and Meas. in Hostile Env. (SPIE Vol. 787), C.H. Gillespie and R.H. Greenwell, Ed. (SPIE, Bellingham, WA, 1987), pp. 77-83.
23. E.W. Taylor, private communication.
24. E.J. Friebele, "Effect of nuclear radiation on Selfoc microlenses," Elect.Lett. 19 (1983) 972-974.

Table I

Multimode fibers irradiated to 2 x 10^7 rad at 23 °C (Fig. 3.1), incremental losses at 0.85 μm after 10^6 sec recovery following a 3000 rad exposure at -150 °C (Fig. 3.7), and maximum induced losses anticipated for a 10 year exposure at 1 rad/day at -150 °C. Optical power -20 dBm

		Induced Loss (dB/km)	
Fiber	Core Material	10^6 sec	10 year
Corning 1517	Ge-P-doped silica	---	---
Corning 1519 85/125 LAN	Ge-doped silica	9.2	5.3
Dainichi ST-R100B	Pure silica, low OH	---	---
Heraeus Fluosil SS1.2	Pure silica, high OH	3.0	< 2.0
ITT "Rad Hard" MM	Ge-doped silica	8.5	5.3
Dark measurement*		< 700.0	< 300.0
ITT Standard MM	Ge-P-doped silica	70.0	55.0
ITT Large Core MM	Ge-(P)-doped silica	16.5	14.5
Raychem VSC 100/140	Pure silica, high OH	2.1	< 1.8
Dark measurement*		< 50.0	< 20.0
Spectran 200R 50/125	Ge-doped silica	11.0	4.5

*Measured with an intermittent 100 nW optical signal.

Table II
Radiation response (dB/km-10^2 rad) of multimode fibers exposed at 1 rad/day

Fiber	0.85 μm	1.3 μm	1.55 μm
Ge-P-Doped Silica Core			
Corning 104	3.52	1.52	2.36
Corning 1516	3.89	4.02	6.48
Corning 1517	4.17	1.70	2.75
Corning 1518	1.68	0.84	1.37
Valtec MG05-850	2.23	0.45	0.84
Valtec MG05-1300	1.91	0.98	0.97
Ge-Doped Silica Core			
Corning 1508*	0.17	0.026	0.024
Valtec Prototype	0.34	< 0.012	0.02
Silica Core			
Raychem RSC 100/140 high OH	-0.39**		
Dainichi SM100	-0.25**	-0.13**	-0.14**
Heraeus Fluosil SW	0.09	0.03	0.09

*Slight P doping on the fiber centerline
**These fibers actually became more transparent following a 100 rad exposure. Presumably, increased attenuation would be induced at higher doses

Table III

Low Dose Rate Radiation Response (dB/km-krad), 10 Year Extrapolated Total Loss (dB/km), and High Dose Rate Recovery Parameters A_o and A_f (dB/km) n, and τ (sec).

Fiber	Response	10 Yr	A_o	A_f	n	τ
Corning 0.85 μm	5.78	61.4	7.3	3.7	3.2	22
Corning 1.3 μm	0.47	5.8	0.7	0.4	3.3	82
Hitachi 0.85 μm	2.19	23.8	14.6	1.7	3.6	64
Hitachi 1.3 μm	0.38	4.6	1.5	0.5	3.4	68
Fujikura 0.85 μM			7.3	0.7	12.1	43200
Fujikura 1.3 μm STD			1.1	0.2	5.5	100
Fujikura 1.3 μm RH			7.2	0.0	3.7	2
Corning 1521 1.3 μm (Std. Single Mode)	0.11	1.3	2.5	0.1	4.1	20

Table IV.
Fibers for Radiation Environment Testing (Fig. 3.13)

Fiber	Part No.	Wavelength	Core	Buffer
Large Core Step Index				
Fiberguide Industries	SFS100/140Y	0.85	S	A
Polymicro Technology	FHP10014017	0.85	S	P
Spectran	SG420R	0.85	G	A
Mitsubishi	ST-100B-SY	0.85/1.3*	S	A
Graded Index Multimode				
Corning	1519	0.85/1.3*	G	A
Spectran	SG320R	1.3	G	A
Single Mode				
Corning	SMF28	1.3	G	A
Litespec	ZSM-13-A	1.3	S	A
Litespec	GSM-12	1.3	G	A
Spectran	SG100	1.3	G	A

Notes: Wavelengths in μm; Core material: S - pure silica; G - germanium-doped silica; Buffer material: A - epoxy acrylate; P - polyimide. Fibers marked with an asterisk were measured only at 1.3 μm.

Table V
Extrapolated Low Dose Rate Induced Loss A (dB/km) After a 6 Year Exposure

Fiber	Loss Ratio ($10^5/10^6$)	A(10^6 rad)	A(10^5 rad)
Corning 1519	0.496	70.3	34.9
Corning SMF28	0.445	9.2	4.1
Litespec GSM12	0.449	9.2	4.1
Litespec ZSM13A	0.065	0.1	0.0
Spectran 320R	0.318	10.3	3.3
Spectran 420R	0.337	21.7	7.3
Mitsubishi ST-R100B	0.331	0.1	0.0
Fiberguide SFS100/140	0.429	0.6	0.2
Polymicro FHP100140170	0.618	1.6	1.0

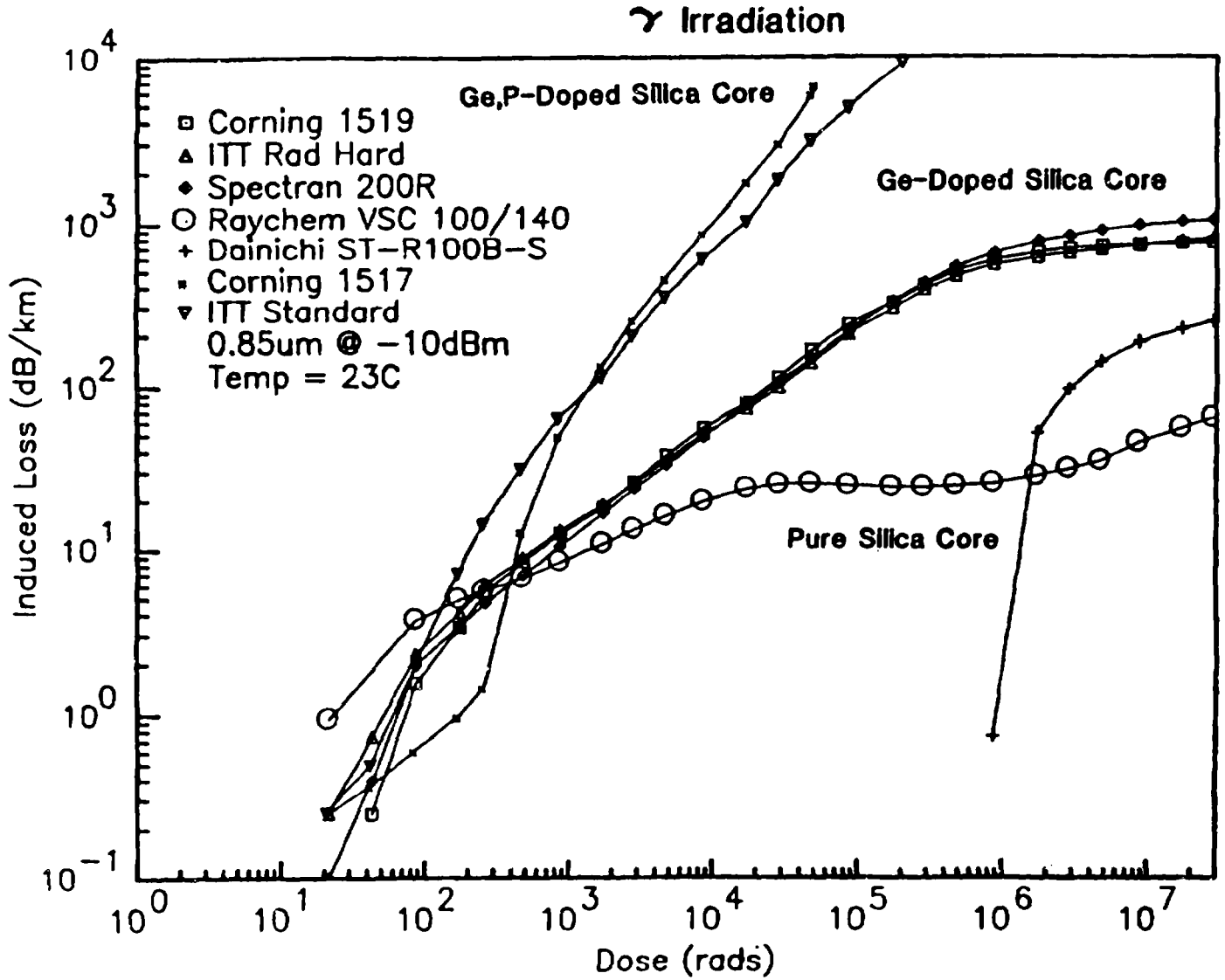

3.1 Radiation-induced loss at 0.85 μm vs. dose in multimode fibers measured *in-situ* during ^{60}Co γ-ray irradiations at ~4000 rad/min. The light power in the fiber was 100 μW (-10 dBm). The silica core fibers are step index while the Ge-doped silica are graded index.

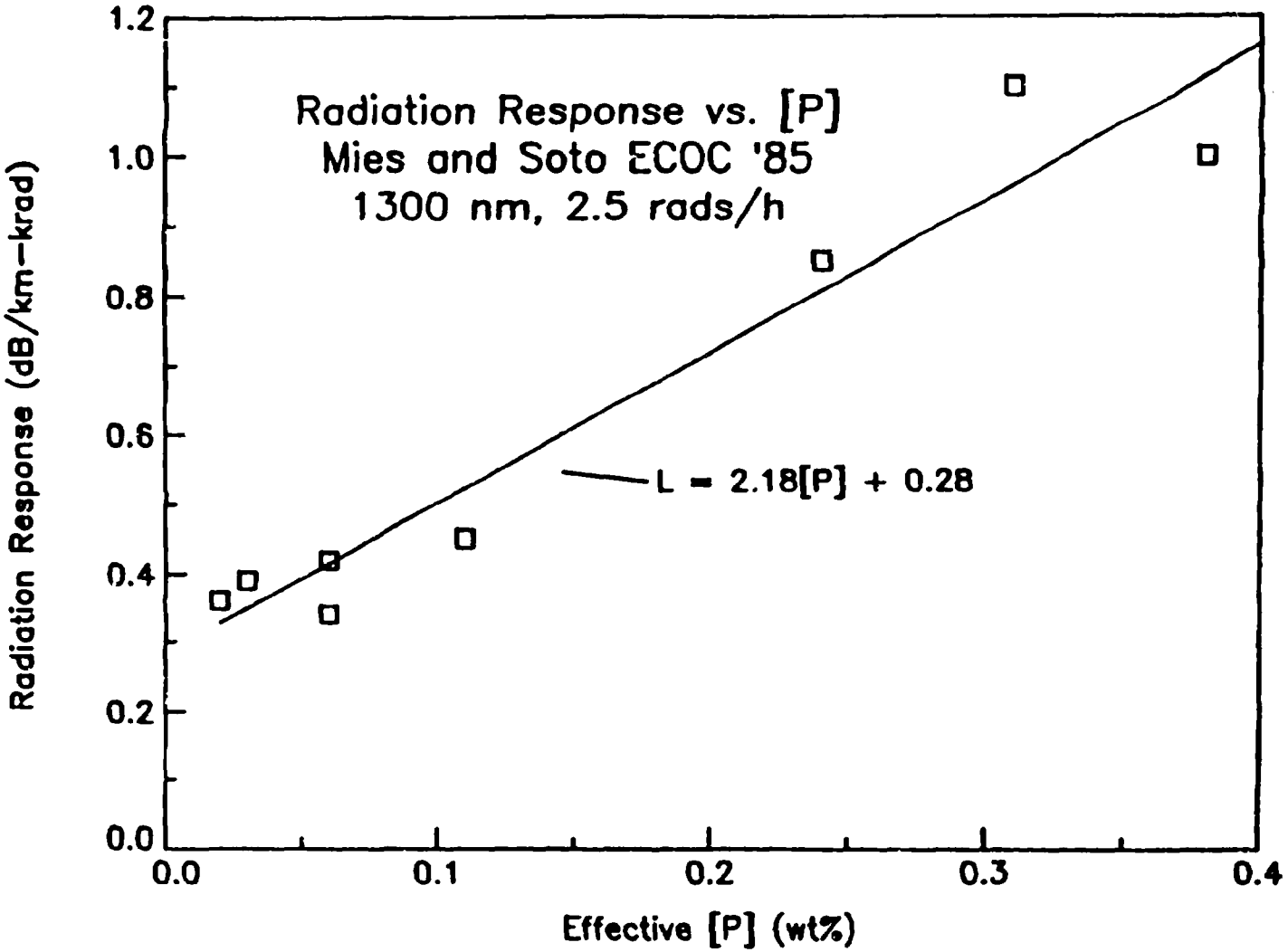

3.2 Correlation of incremental loss at 1.3 and 1.53 μm with [P] in the clad of depressed-clad single mode fibers irradiated at 2.3 rad/h.

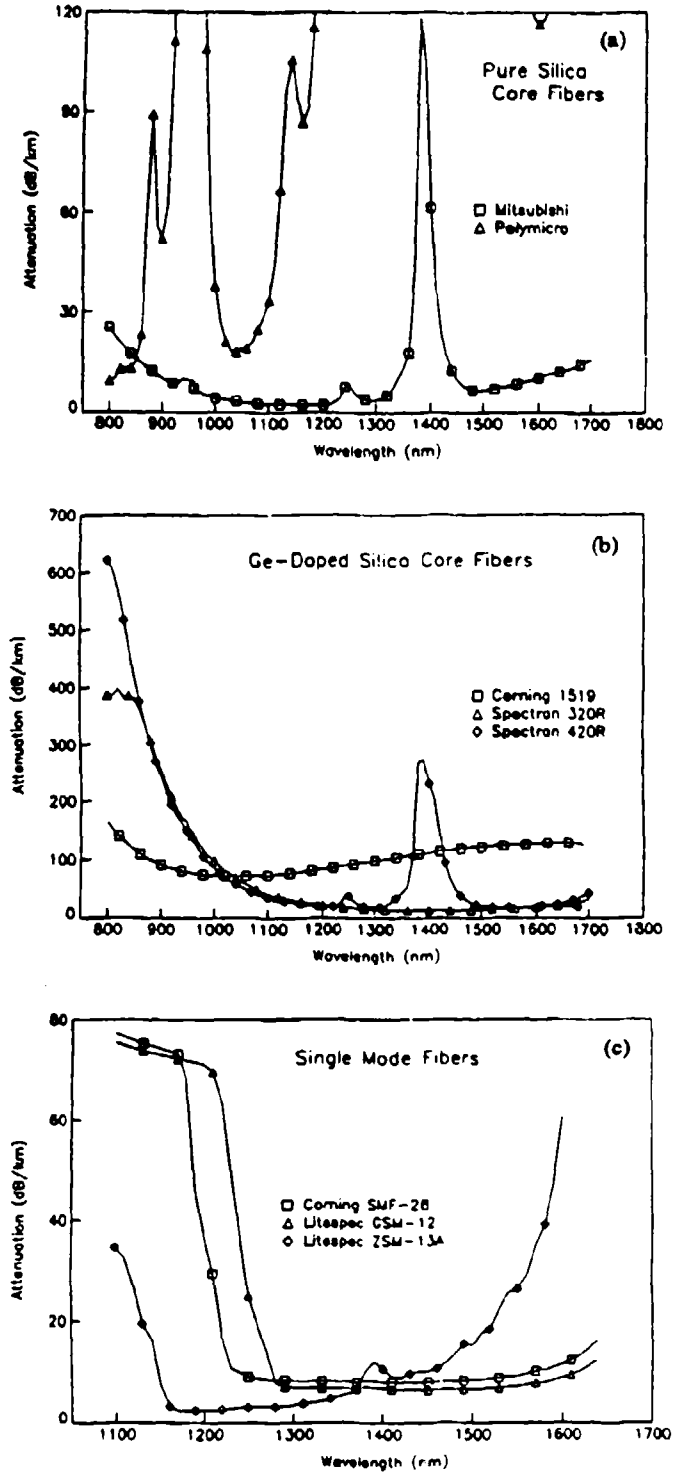

3.3 Total attenuation (intrinsic + radiation-induced) of fibers irradiated to 10^6 rad at a dose rate of 1300 rad/min. The fibers were maintained at 50 °C and were measured approximately 1 day after termination of the exposure. (a) Polymicro 100/140 high OH and Mitsubishi 100/140 low OH pure silica core multimode; (b) Corning 1519, Spectran SG320R, and Spectran SG420R Ge-doped silica core multimode; and (c) Corning SMF28 and AT&T GSM-12 Ge-doped silica core and AT&T ZSM-13 pure silica core single mode fibers. Corning 1519 Ge-doped silica core apparently has some P doping as well.

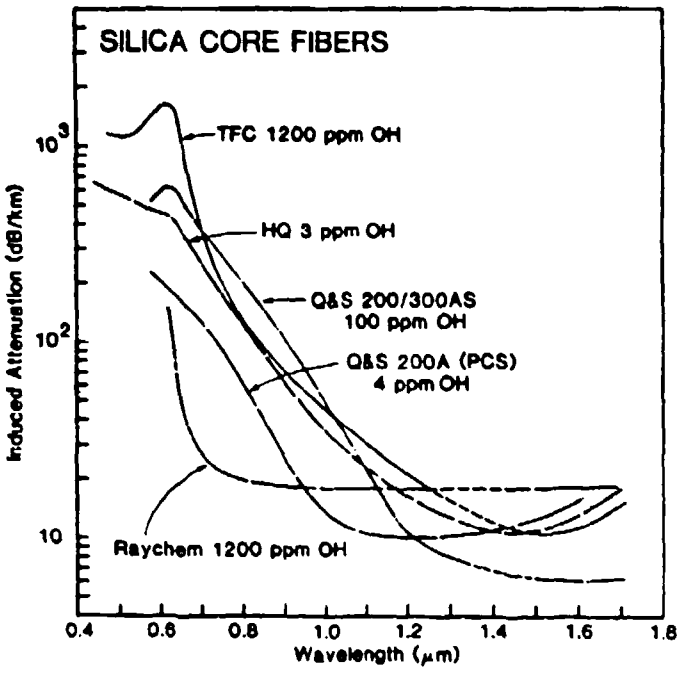

(a)

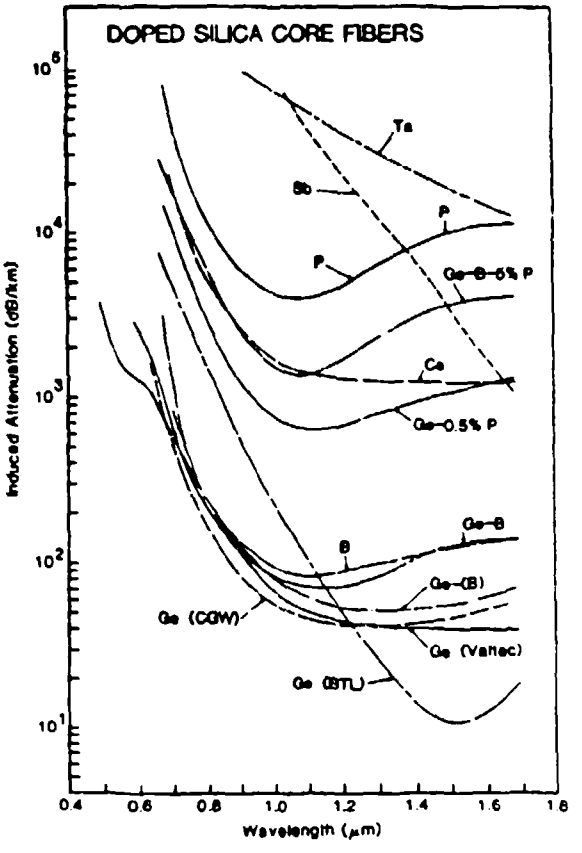

(b)

3.4 Radiation-induced absorption spectra of (a) pure silica core and (b) doped silica core multimode fiber waveguides measured 1 h after an exposure of 10^5 rad.

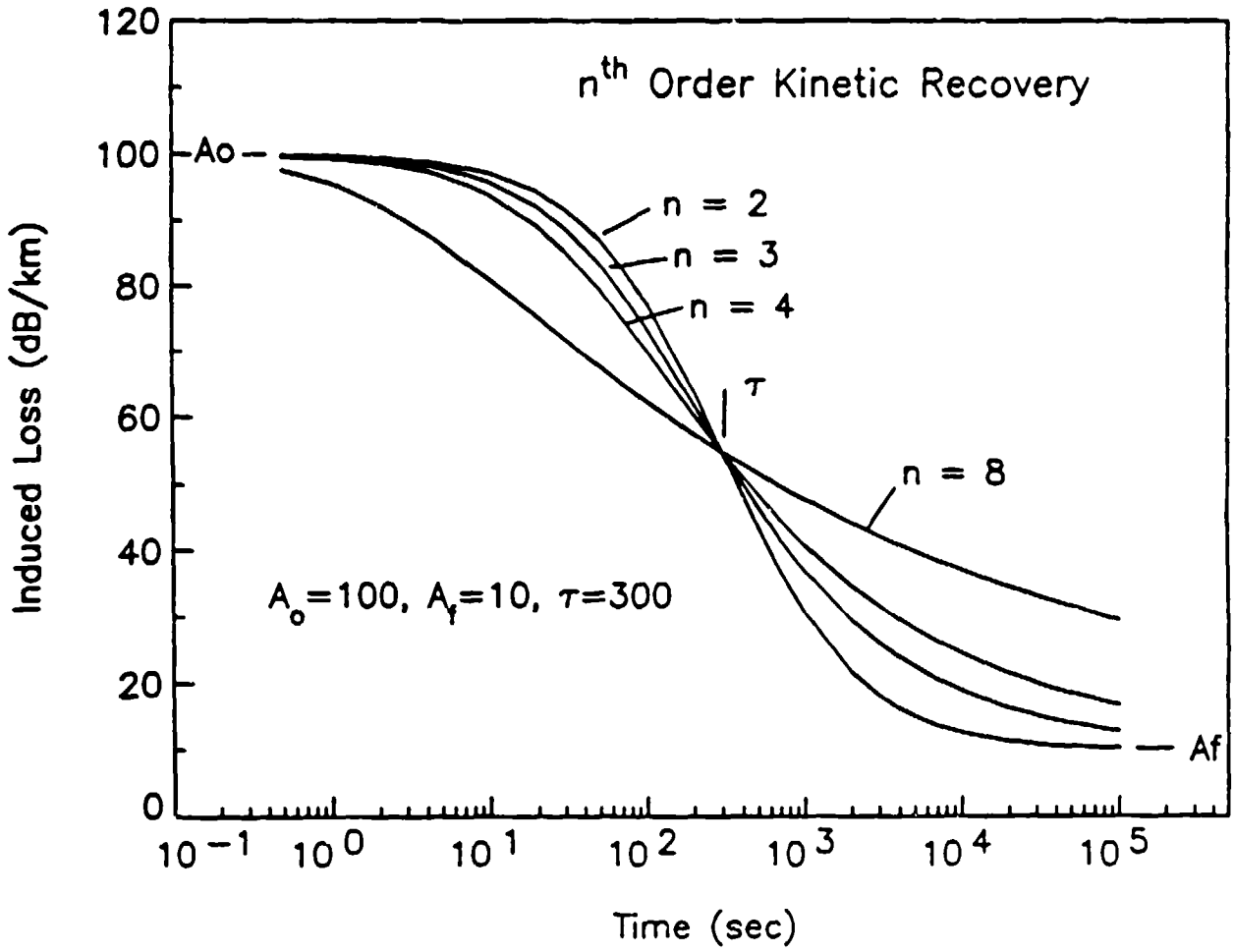

3.5 Plots of n^{th}-order kinetic recovery behavior (Eq. 4) for various values of kinetic order n.

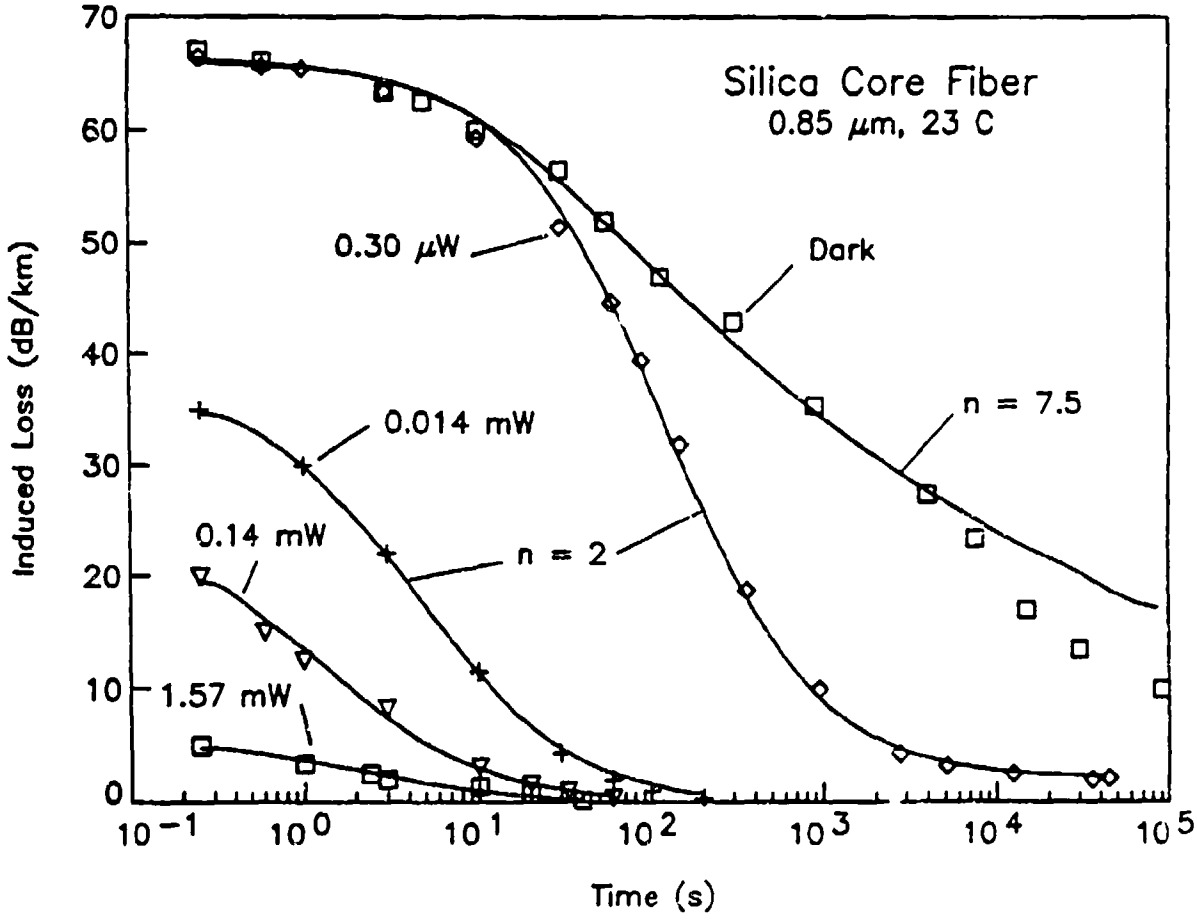

3.6 Recovery of the radiation-induced attenuation in a multimode pure silica core-polymer clad fiber vs. light power. The data (points) have been fit to n^{th}-order kinetic recovery using Eq. 4, shown as the lines.

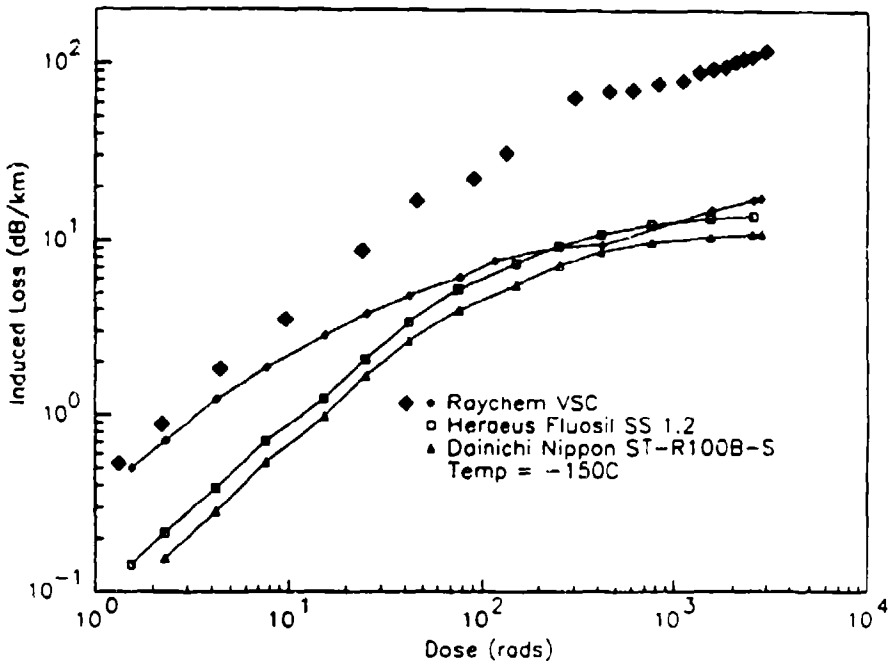

(a)

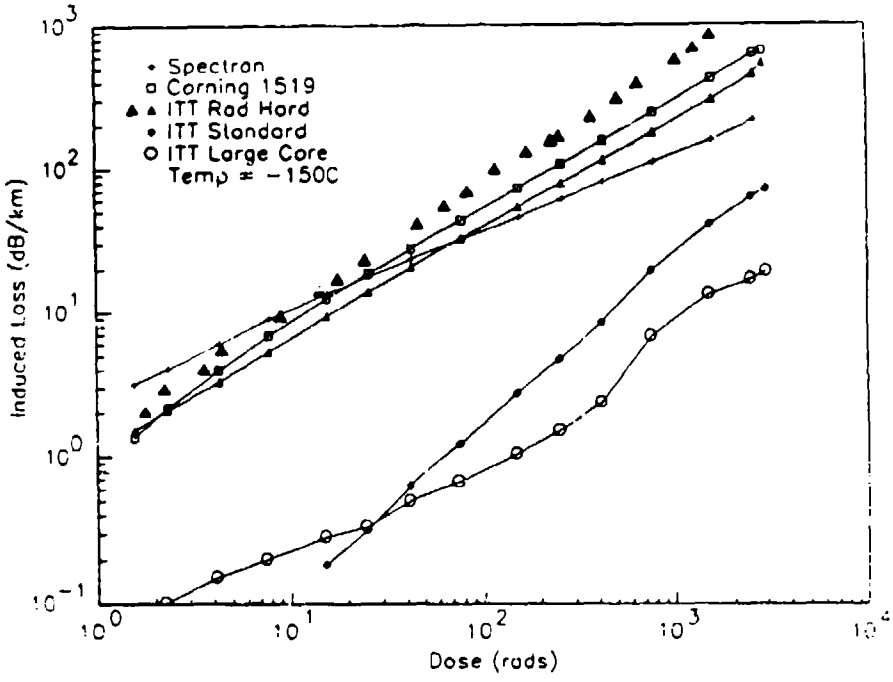

(b)

3.7 Incremental loss at 0.85 μm induced during low temperature exposure of optical fibers at 50 rad/min. Data for points with lines were obtained with continuous -20 dBm optical power in the fiber. Dark solid points for the Raychem (a) and ITT Rad Hard (b) fibers were measured with intermittent 2 sec measurements with 100 nW.

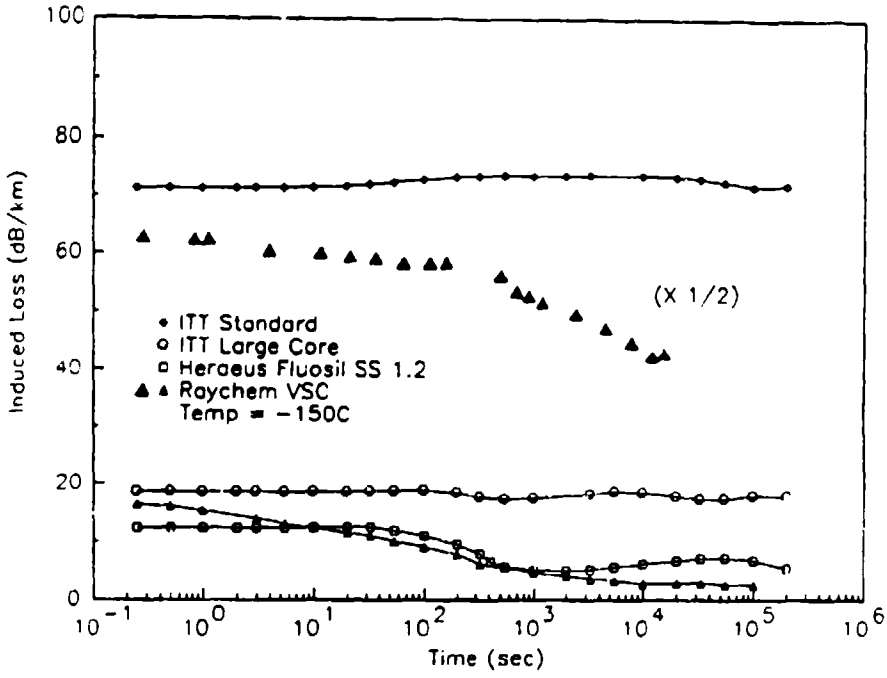

(a)

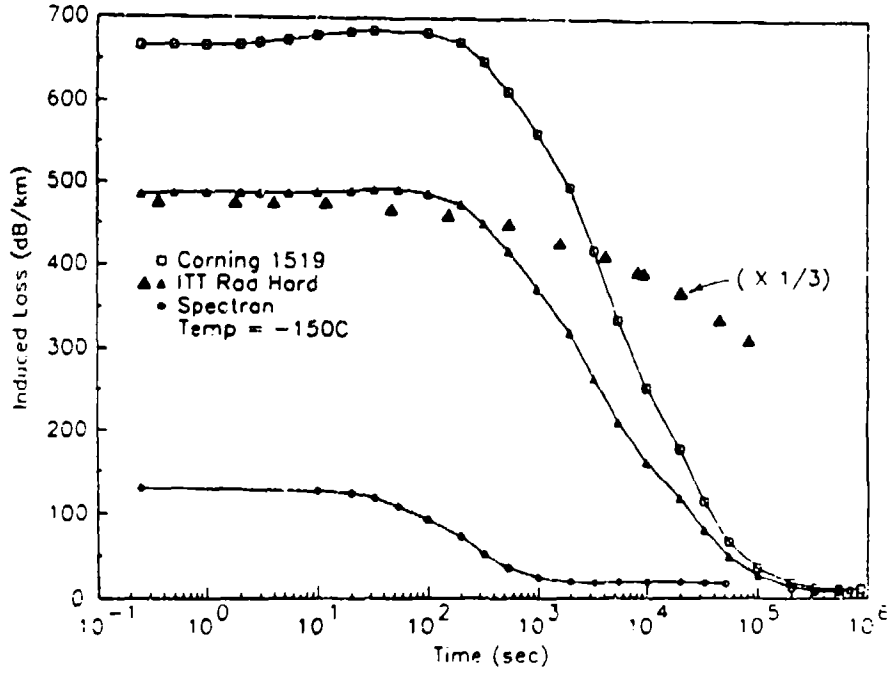

(b)

3.8 Recovery of the incremental loss induced during the exposures shown in Fig. 11.

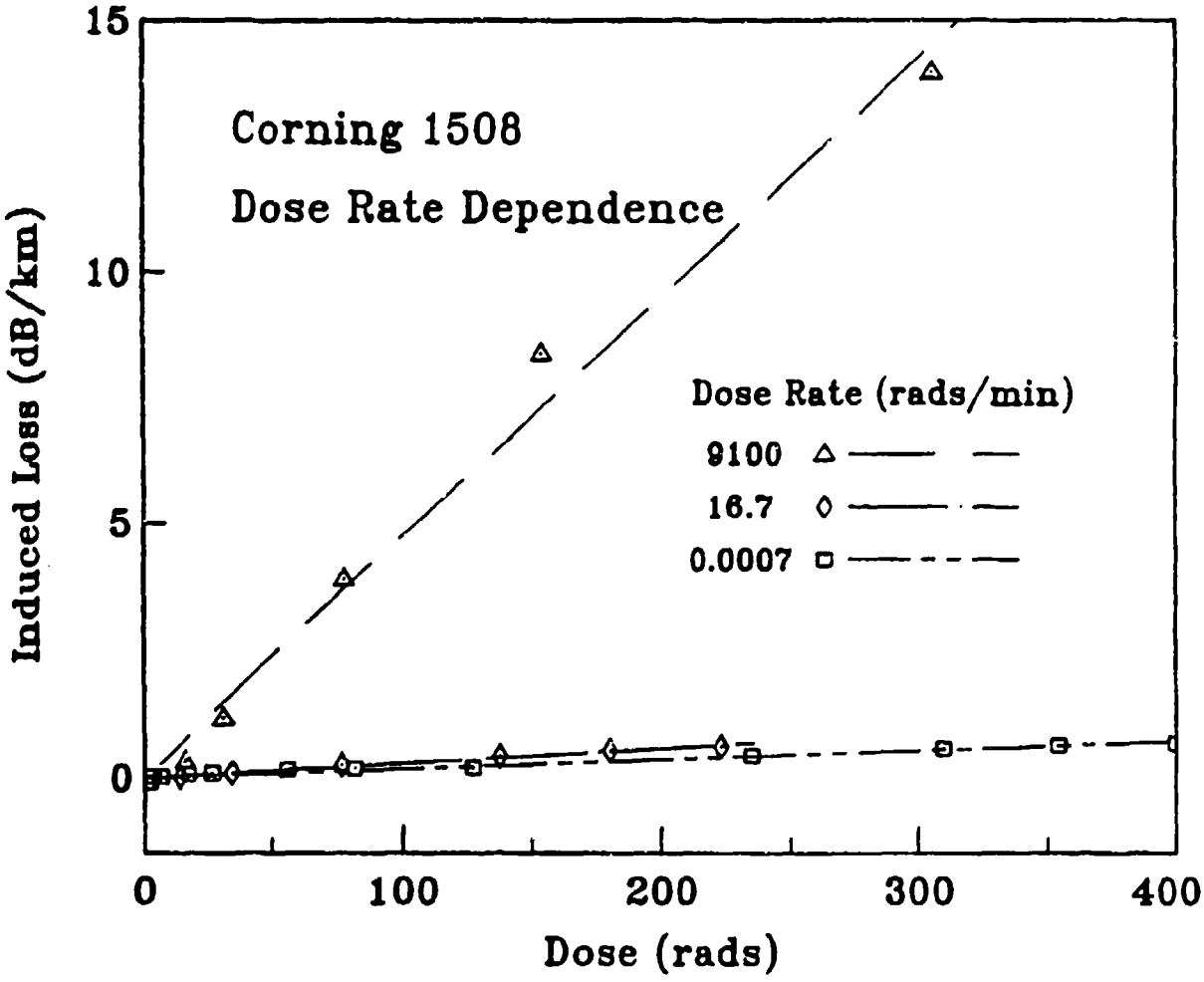

3.9 Apparent dose rate dependence of the incremental attenuation at 0.85 μm in a 85/125 Ge-doped silica core fiber.

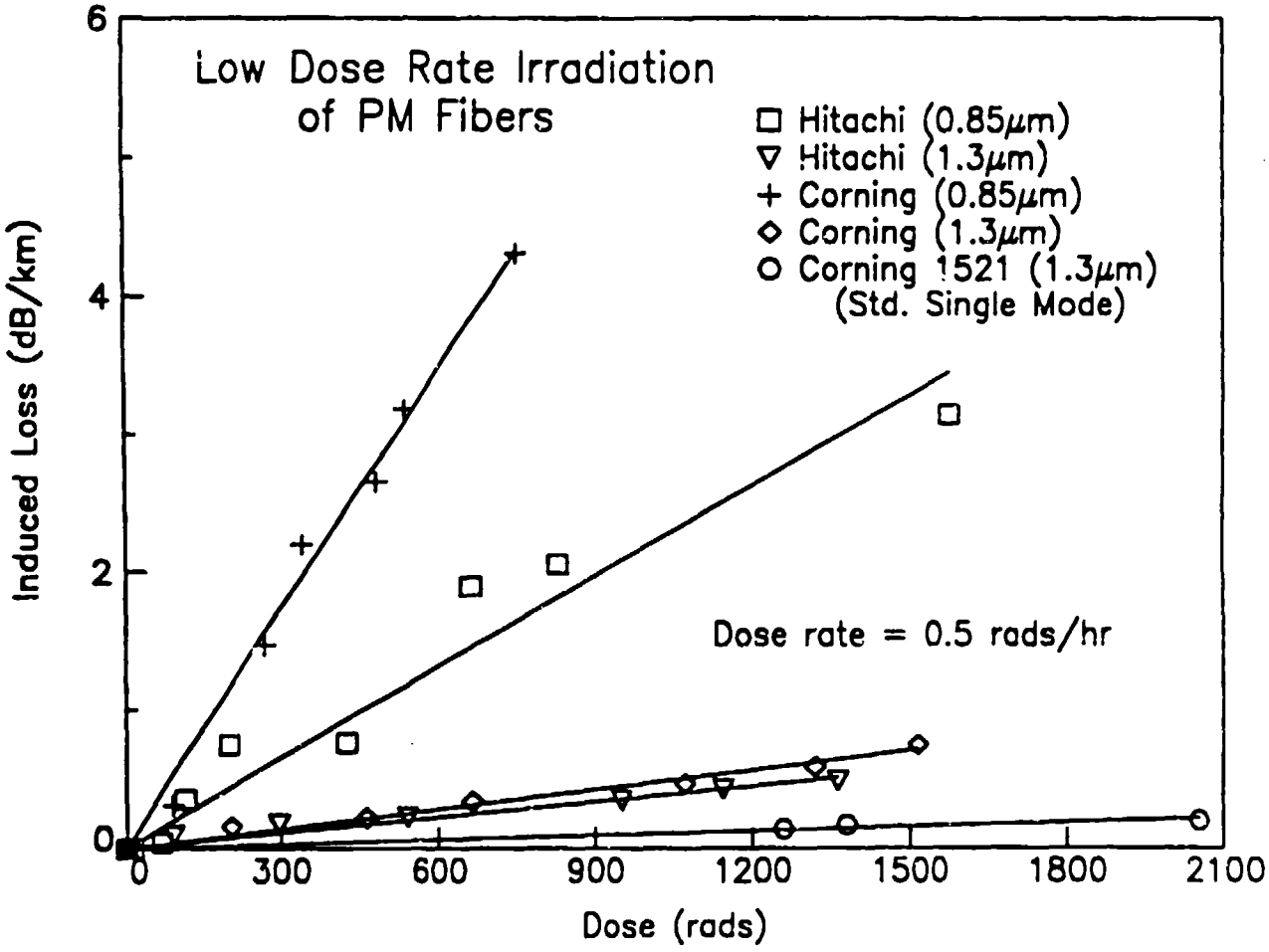

3.10 Growth of the radiation-induced loss at 1.3 μm in polarization-maintaining and conventional single mode fibers during low dose rate (5 rad/h) exposure.

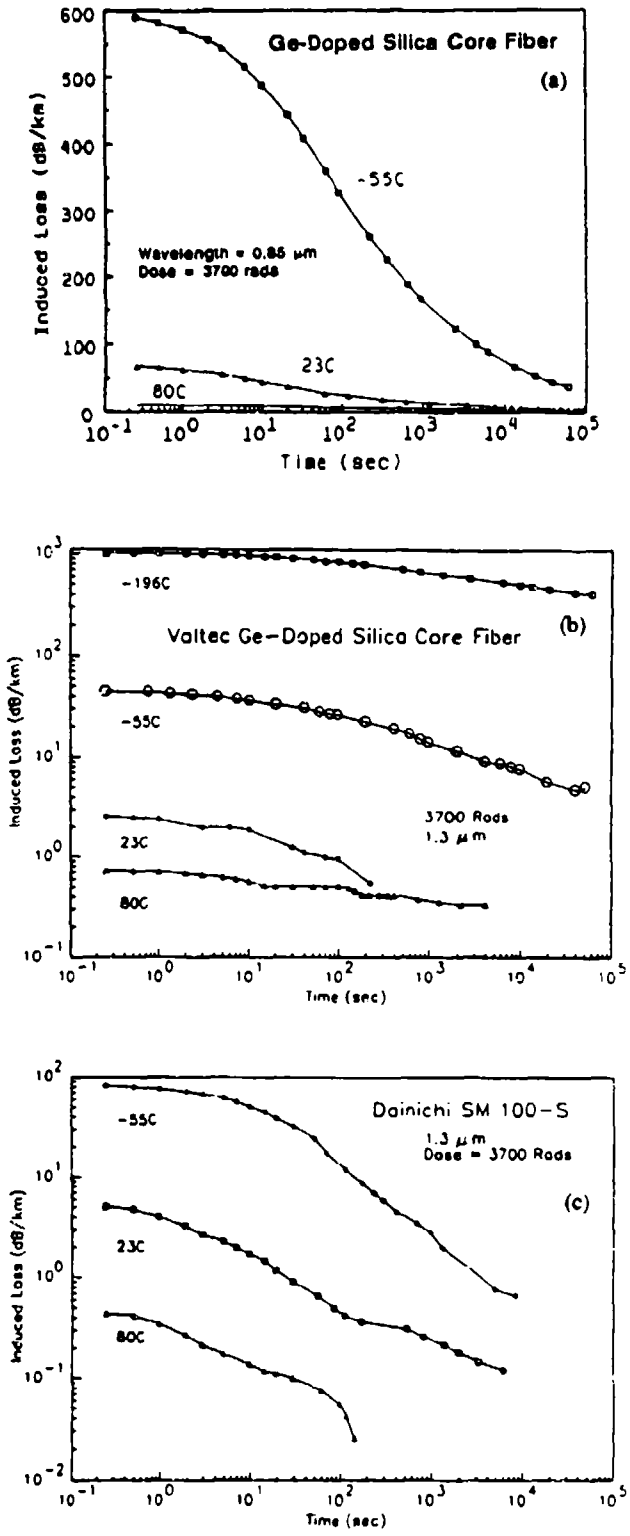

3.11 Temperature dependence of the recovery of the incremental attenuation in (a,b) Ge-doped silica core multimode and (c) pure silica core multimode fibers. The data in (a) and (b) are representative of Ge-doped silica core fibers; the 100/140 fiber in (c) is similar to the Mitsubishi fiber of Fig. 3. The waveguides were maintained at temperature during exposure and recovery.

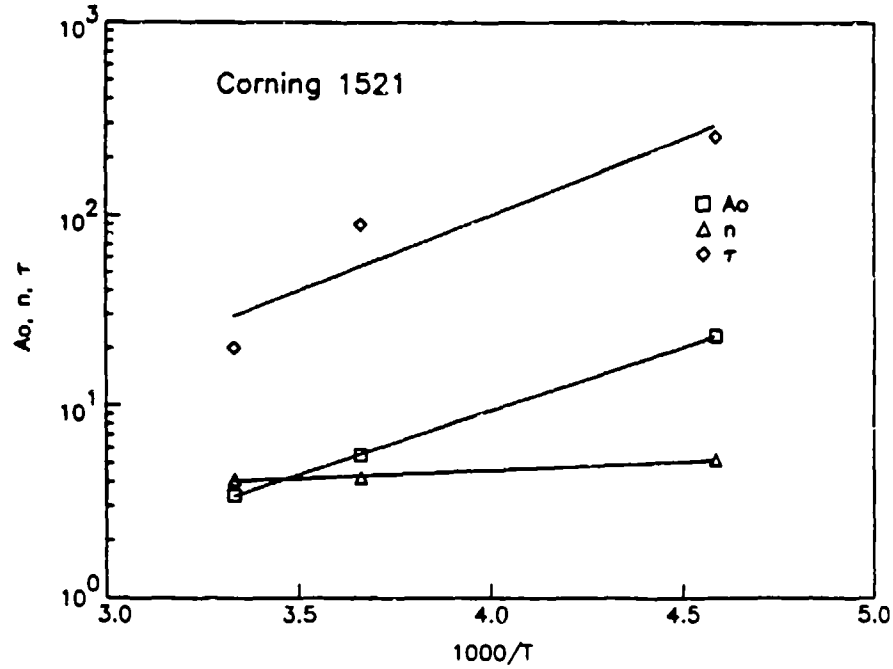

(a)

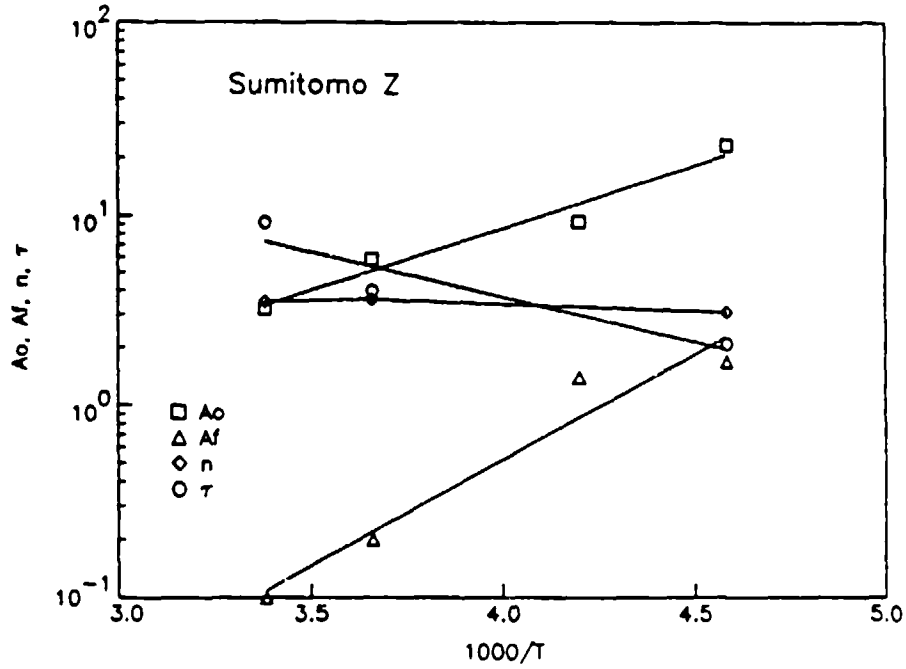

(b)

3.12 Temperature dependence of the 1.3 μm recovery parameters (Eq. 4) of (a) Corning Ge-doped single mode silica core fiber (now Corning SMF28) and (b) Sumitomo Z pure silica core single mode fiber (now AT&T Litespec ZSM) irradiated to 2000 rad. The lines are fits to the Arrhenius equation.

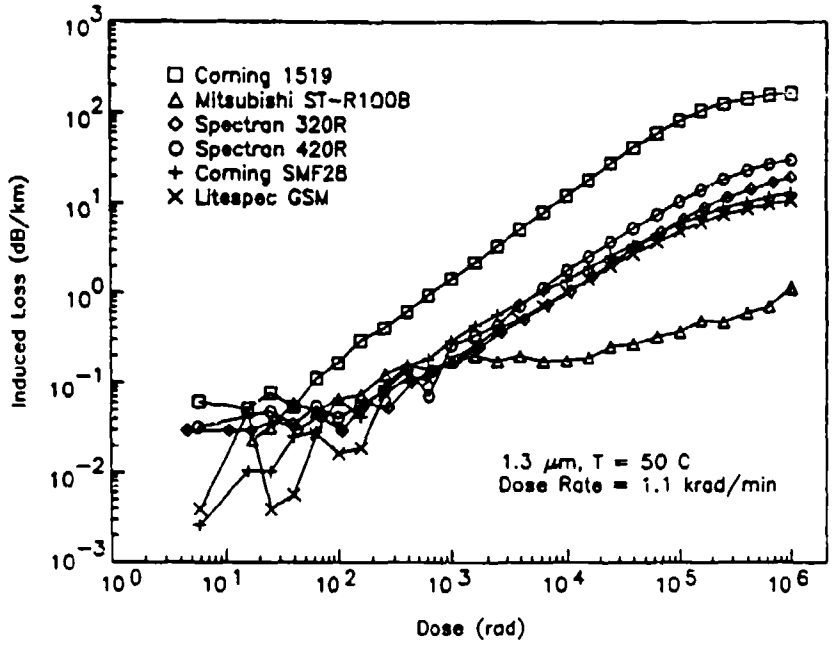

(a)

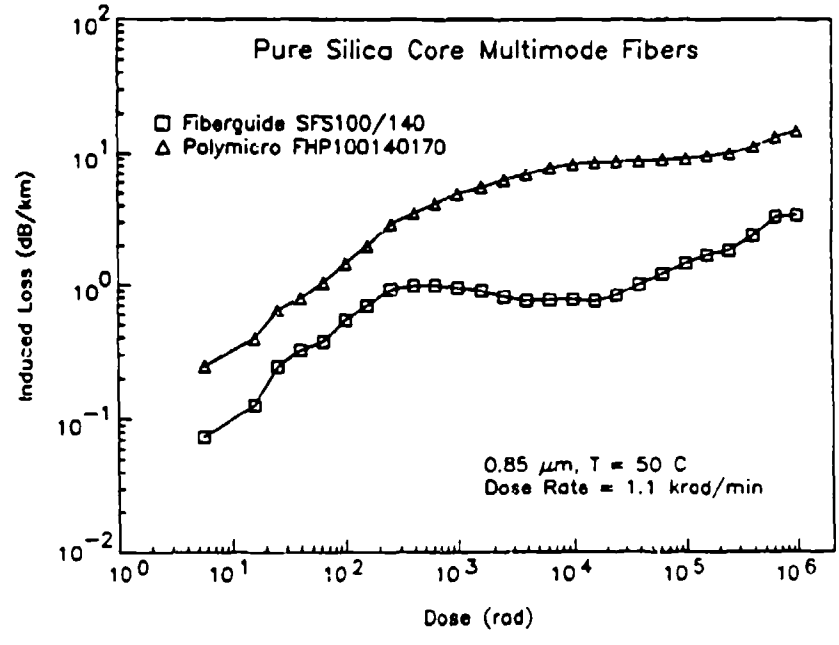

(b)

3.13 Growth of the radiation-induced attenuation at (a) 1.3 μm and (b) 0.85 μm in Ge-doped and pure silica core optical fibers irradiated at 1.1 krad/min at 50 °C.

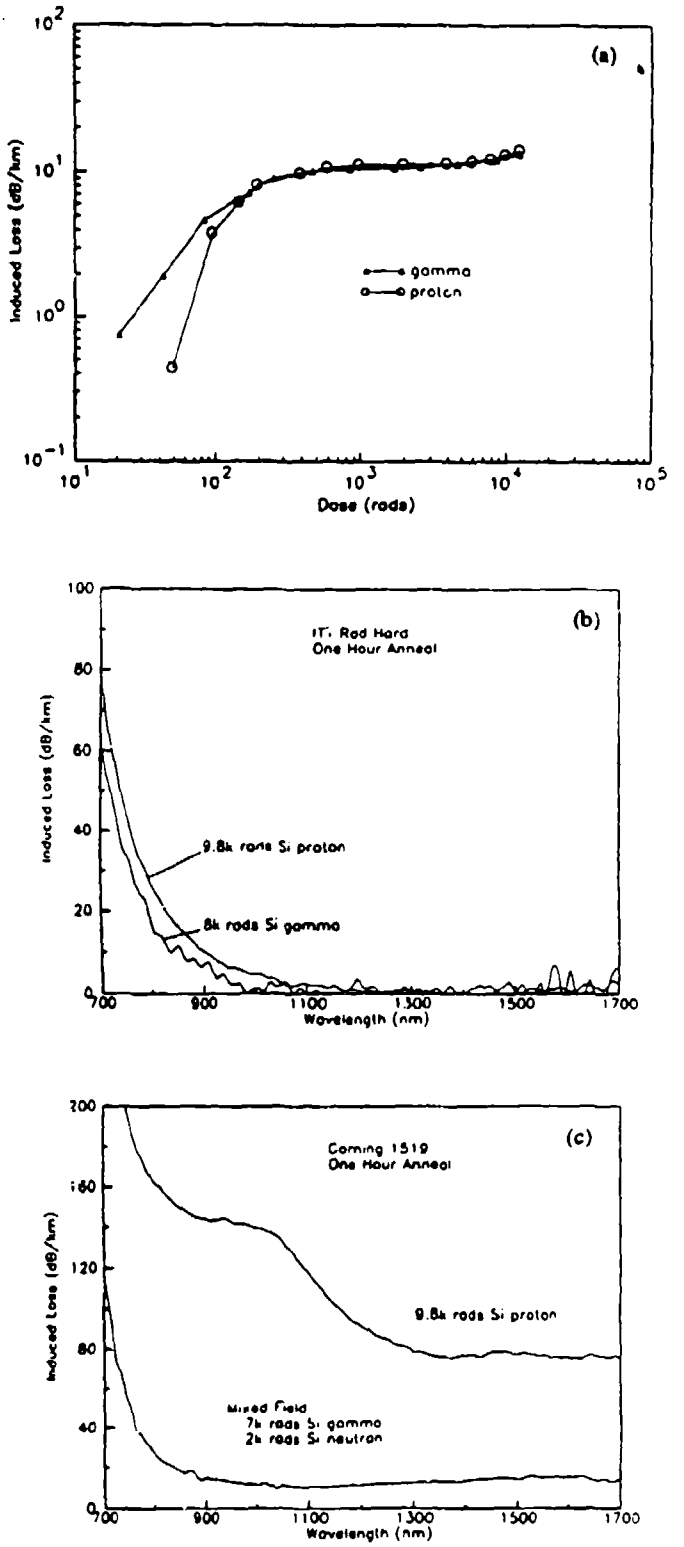

3.14 Effect of different radiation types on optical fibers: (a) Heraeus SS1.2 pure silica core fiber similar to the Raychem and Fiberguide 100/140 fibers in Figs. 1 and 13; (b) ITT "Rad-hard" Ge-doped silica core fiber; and (c) Corning 1519 Ge-doped silica core fiber. All fibers were irradiated with -30 dBm of 0.85 μm optical signal propagating during the radiation exposure. Spectral measurements in (b) and (c) were taken one hour after exposure. T = 23 °C.

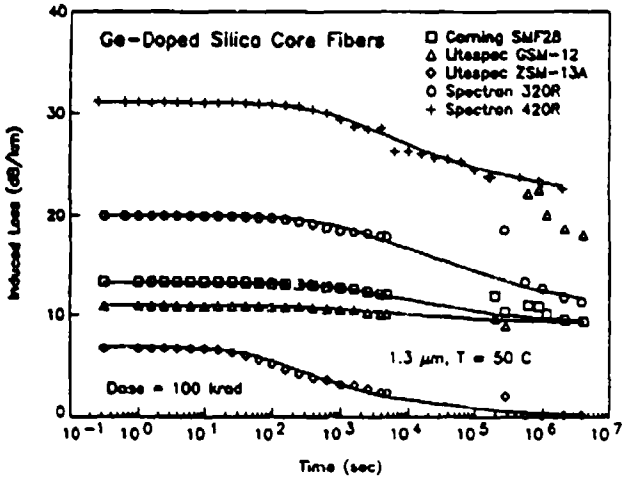

(a)

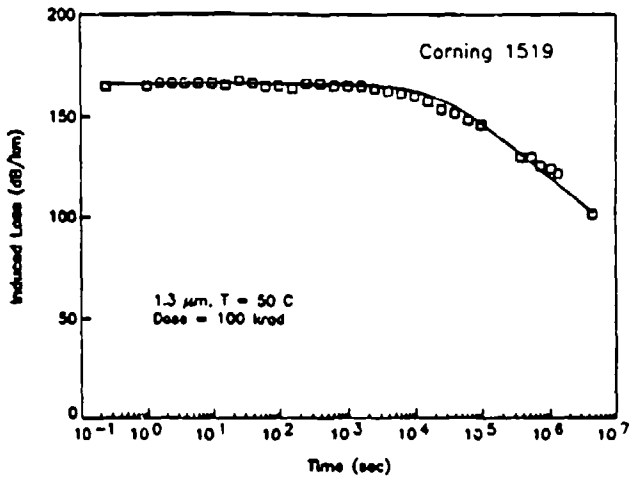

(b)

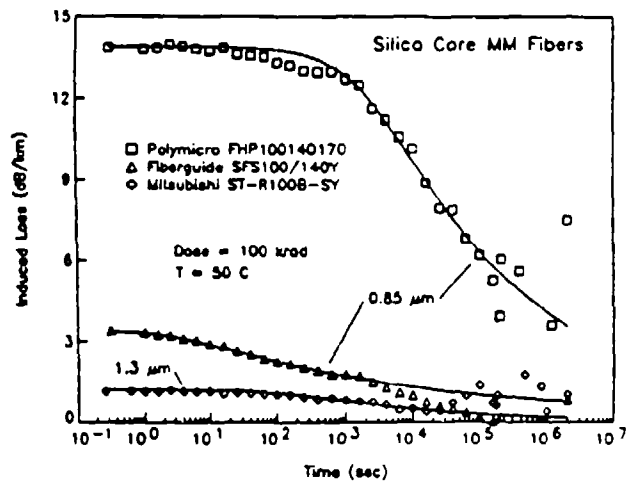

(c)

3.15 Recovery of the radiation-induced attenuation in (a,b) Ge-doped and (c) pure silica core optical fibers irradiated to 10^6 rad at 1.1 krad/min. The fibers were maintained at 50 °C during the exposure and recovery periods except for the brief times when they were measured by the cutback method at times $> 10^5$ sec. The scatter in the long time data is due to the fact that the cutback measurement is made on only 50 m of irradiated fiber.

4. Photonic Communication Technology and Issues

4.1 General Photonic Communication Technology Survey

Optical performances of fibers, light sources (LED and laser diode), and receivers are three important areas of consideration for planning a fiber communication system. Since the electrical performances of light sources and receivers at the three commonly used wavelength regions (850 nm, 1300 nm and 1550 nm) are comparable, a system of choice is determined mainly by the properties of fibers. For long distance communication applications, fiber attenuation is a key limiting factor, thus a 1300 nm and/or 1500 nm system is preferred as has been discussed in Section 3. For short haul communication at a data rate no more than a few GHz, which fits the FODB system requirements of this study, systems operating at all three wavelength regions are applicable. It should be noted that the 850 nm technology is well developed, and thus is most economical. However it also has the most limitations in both fiber attenuation and bandwidth. Of importance for this study, it should be noted that most of the radiation-harden studies were done in this wavelength region. Considerable light sources and receivers for the 1300 nm region are also now available commercially. The fiber attenuation and, more importantly, the fiber bandwidth at this wavelength are superior to those at the 850 nm. It is an interesting technology to consider, in particular, for a system "expandable" in the future to multi-GHz and beyond. However, considerable radiation effects study needs to be done to fully qualify the 1300 μm technology for space born operation. However, based on the current limited knowledge, no major new radiation issue in the optoelectronic device areas is expected (see Section 5). The receiver-amplifier end, which is similar to a compound semiconductor microelectronic circuit, there could be some SEU issues to be addressed because of high energy cosmic rays (see Section 2). The 1500 nm technology, which is the backbone of the long distance telecommunication systems, is the newest of the three technologies available. Therefore, light sources and receivers are least available commercially. However, that problem should disappear rapidly as the technology matures. Furthermore, a recent breakthrough in erbium-doped fiber amplifier greatly enhances its potential to applications which requires amplification of optical signal (e.g. fan out to large number of channels in a star coupled system). The fiber amplifier offers an convenient, economic, reliable and high performance means to amplify the optical signal, as many times as needed, in a fiber communication system. A recent Japanese study demonstrated a 10 GHz system fan out to 1000 channels through star coupler and fiber amplifier! However, radiation issues in doped fiber use could be significant.

A survey of photonic technologies is summarized below where LED=light-emitting-diode, DL=diode laser, PIN=p-type/insulator/n-type, PD=photo-diode, and MSM=metal/semiconductor/metal:

	OPERATING WAVELENGTH		
	850 nm	1300 nm	1550 nm
LIGHT SOURCES			
Optoelectronic material	AlGaAs/GaAs	InGaAsP/InP	InGaAsP/InP
LED power (dBm)	.7	0	0
LED bandwidth (GHz)	.1	.2	.2
Multimode DL power (dBm)	.8	>-4	>-4
Multimode DL bandwidth (GHz)	1	1	2
Single mode DL power (dBm)	.8	>-4	>-4
Single mode DL bandwidth (GHz)	10+	15+	15+
DETECTORS			
Materials	Si,GaAs	Ge,InGaAs	Ge,InGaAs
PIN PD bandwidth (GHz)	10+	10+	10+
Avalanche PD bandwidth (GHz)	1+	1+	1
MSM bandwidth (GHz)	5+	10+	10+

High performance systems requires high performance devices. The following two sections will cover the current state-of-the-art technologies of light sources and photo detectors.

4.2 Light Sources

The desirable characteristics of a diode laser are low current threshold, narrow optical linewidth, stability and tunable wavelength. Quantum well structures, through bandgap engineering can form a graded index optical waveguide, are ideal materials for low threshold Lasers. However the quantum well lasers exhibit large linewidth broadening (chirping) under (current) modulation which leads to large mode partition noise. To avoid the frequency chirping problem, the quantum well lasers are typically operated under DC bias and information is encoded to the optical beam via an external modulator. Little is known about the use of these modulators in a space environment. To achieve single and stable mode, distributed feedback (DFB) structures are commonly incorporated in the laser structure. More recently, multiple section DFB laser structures, with additional wavelength tuning and stabilization section (via current injection), are employed to achieve a constant output wavelength, which can even be controllably tuned via current injection. The strain layer materials, typically in a quantum well structure, is another new technology in the diode laser

area. Laser devices made by strain layer materials have demonstrated low threshold current, high output power, stable and reliable performance.

Another development in diode laser field is the vertical cavity surface emitting laser which utilizes Bragg reflectors to form a high Q cavity with large laser beam cross section. The vertical cavity lasers can be made at extremely high density (each laser is only 20 to 50 micron in diameter and one can, in principle, make millions on a wafer), low threshold and with highly a collimated output beam. However the optical power per laser is small due to size limitations.

All high performance diode lasers, with narrow linewidth and stable output wavelength, tend to have limited output power. Although there are ways to amplify the optical power via another diode laser amplifier, injection locking. The process is somewhat complicated, which is why the current advancement in erbium-doped fiber amplifier attracts so much attention. By inserting a diode laser pumped erbium-doped fiber amplifier, into a fiber system, the optical signal can be amplified by more than 16 dBm with no loss of bandwidth! The fiber amplifier has extremely high bandwidth and can be used in a wavelength division multiplexed system as well. Since the erbium-doped fiber amplifier must operate at 1550 nm, it underscores the importance of utilizing 1550 nm system in large data distribution systems.

4.3 Photo Detectors

Considable progress has been made in PIN and metal-semiconductor-metal (MSM) detectors (which are most suited for space-born systems). Currently PIN detectors have been integrated to junction field effect transistor JFET), heterojunction bipolar transistor (HBT) and high electron mobility transistor (HEMT) for an integrated high sensitivity and high speed receiver system. The MSM detector has also been integrated to HEMT to achieve multi-Gbit/s operation. However, MSM devices are potentially noisy because of the low Schottky barriers employed.

4.4 Reliability issues

After operating for a long period of time (khrs), a diode laser "ages". There are two basic aging effects:

(1) Average power drift due to mistracking: the development of asymmetry between the two facets in a laser cavity. This causes false-adjustment of the feedback circuit which regulates the laser output by monitoring the light output from the back facet. To avoid the mistracking problem, one needs to tap a portion of the output beam as reference for feedback control. This will add to the power budget of the laser output.

(2) Extinction ratio degradation: the increase in spontaneous light emission and drift (decrease) in the average power for a given bias current leads to a degradation of the extinction ratio.

Both effects will accelerate as the operation temperature of the diode laser increases. Therefore operating the diode laser with proper heat sinking is not only a performance issue (lower threshold current, more stable output and modal property) but also a reliability issue. Furthermore, the radiation damage effect to the diode laser device also increases with operating temperature. Since the ambient temperature of 60 - 70 °C is too low to anneal out the radiation damage, proper heat sink (use a TE cooler, if possible) is especially desirable under the radiation environment.

5. Radiation Issues for Lasers and Detectors

5.1 CANDIDATE TECHNOLOGIES

Technology for light sources and detectors needed for the FODB has reached a relatively mature stage. Several manufactures offer distributed feedback (DFB) injection laser diodes (ILDs) which can be directly modulated at 1.5 GHz and higher, and accelerated life testing studies indicate MTTFs of greater than 10^5 hours within the -20 to 60 °C operating range. Furthermore, the option of operating lower bandwidth sources in the CW mode and externally modulating the signal increases the inventory of candidate sources.

Components are available for operation at the 850 nm, 1300 nm and 1550 nm optical fiber transmission windows. GaAs technology covers the 850 nm option, and the narrower bandgap InGaAsP quaternary alloys latticed matched to InP substrates are favored for the 1100 to 1600 nm range. Because of lower dispersion within the transmission fibers, the industry seems to be selecting the 1300 nm option as is evident from the larger selection of devices for this wavelength. This benefit, coupled with the lower radiation induced losses in fibers at the longer wavelengths, makes the 1300 nm choice especially attractive for the FODB.

Two examples of currently available InGaAsP laser diodes for 1300 nm operation are the distributed feedback Mitsubishi FU-42SDF and the QCW-1301 from Laser Diodes Inc. Each of these can be operated CW or directly modulated to 1.5 GHz, and each is coupled to a single mode fiber pigtail. Both include connections to a monitor InGaAs photodiode on the back facet. This monitor can be incorporated in a feedback circuit to maintain constant optical power output in CW operation. Similar devices are available with multi-mode pigtails and for each of the indicated wavelength ranges. Thermoelectric and Pellitier cooler options are also available.

5.2 DEGRADATION MECHANISMS AND RADIATION HARDNESS

While long term changes from total ionizing dose seem to dominate the radiation damage to optical fibers, laser diodes and photodiodes are relatively immune to these effects. However, permanent displacement damage from incident particle collisions attenuates laser diode output power by introducing nonradiative recombination centers, and reduces noise margins through dark current increases in photodetectors.

Much attention has been given to the neutron induced degradation mechanisms in LEDs, laser diodes, and various photodiodes, and a limited number of proton studies are reported as well. Unfortunately, such evaluations of the most recently available technology have not yet appeared in the literature. Even so, the trends reported in the 800 nm GaAs technologies can also be identified in the more limited studies at longer wavelengths. The preliminary assessment is encouraging for the radiation response of current laser diode and detector technology.

For LEDs and laser diodes, damage induced nonradiative recombination centers compete with radiative recombination to reduce the output power. Innovations which reduce the carrier lifetime have therefore reduced the susceptibility to displacement damage. For this reason, laser diodes are more resistant than LEDs as their carrier lifetimes during laseing are in the picosecond range,

and highly doped ILDs offer improved efficiency and even shorter carrier lifetimes. The 1300 nm ILD options being considered here fall into the desired category of high efficiency lasers with low threshold currents and reasonably high maximum operating currents. These characteristics correspond to short carrier lifetimes and minimal losses to radiation induced nonradiative recombination centers. For this technology, radiation induced shifts in laseing threshold to higher currents is the most important damage issue.

Similarly, photodetectors have evolved through various stages, and certain characteristics leading to radiation hardness have been identified. For example, devices which rely on charge collection by diffusion should be avoided due to the reduction in minority carrier lifetime. Also, avalanche photodiode and large volume p-i-n structures are to be avoided because of excessive leakage levels following particle induced damage. For small volume p-i-n and double heterojunction photodiodes the most important damage effect is the increase in dark current, and noise margins must be able to accommodate the anticipated degradation. It appears that careful selection of the device should lead to successful operation of the FODB in the orbital environment

The more recently developed MSM detector technology should also be considered, but neither proton damage nor total ionizing dose studies have been reported These devices inherently operate with high leakage levels due to a very low Shottkey barrier, and proton induced damage would introduce additional leakage. Experimental input will be necessary to evaluate the level of concern for this effect.

It does not appear likely that short term ionization transients within photodiodes will be a problem in the trapped proton environment. Even if an ionizing particle traversing the depleted photodiode liberates enough charge to register a false signal, the error rates in the natural environment would be extremely low. Since rates of 10^{-10} errors per bit are normally tolerated within optical data links, any charged particle related contributions should be insignificant. A possible exception to this may occur during solar flare proton events. In high inclination orbits, the dose rates during the particle event may reach several hundred rads per hour, and the corresponding proton flux within the detector could approach several thousand per second. If proton traversals could cause data "upsets", this situation could easily lead to unacceptable error rates. Additional shielding surrounding the detector could minimize these concerns. A more careful assessment of this possibility should follow if low error rates are deemed necessary for the FODB.

5.3 DISPLACEMENT DAMAGE IN THE ORBITAL ENVIRONMENT

Trapped electrons and trapped protons are sources of both ionization and displacement damage in each of the orbits discussed in Chapter 2. As in Table 2.1, the ionization effects, based on the particle's linear energy transfer (LET), can be evaluated separately and combined for protons and electrons. However, the ionizing dose in not a valid indicator for displacement effects. Just as the LET quantifies the amount of ionization associated with a given particle and energy, the nonionizing energy loss (NIEL) describes the energy lost in producing displacement damage. NIEL is plotted in figure 5.1 for electrons and protons as a function of energy in GaAs. In general, protons are much more damaging than electrons and the lower energy protons are by far the more damaging.

The amount of displacement damage sustained in trapped proton orbits depends strongly on the amount of shielding. At the spacecraft surface, electrons contribute most of the ionizing dose, but even there the more damaging protons cause most of the displacement damage. Shielding effectively attenuates the more damaging lower energy protons, and for a given shield thickness the amount of damage can be quantified by considering the differential proton spectrum incident on the device in question. Differential proton spectra from trapped protons and solar flare particle events are plotted in figures 2.5 through 2.7. Note from figures 2.6 and 2.7 that while the thicker shielding does reduce the lower energy proton flux, the higher energy proton flux is not significantly reduced by increasing shield thickness.

Combining the damage versus proton energy shown in figure 5.1 with the number of protons at a given energy within a given time as in figure 2.5 leads to the total amount of damage expected as a function of time in orbit. For example, the 63 degree circular orbit at 1110 kilometers (orbit 2) corresponds to the top curve of figure 2.5. The product of this differential spectrum and proton NIEL in GaAs of figure 5.1 can be integrated over proton energies indicating that the damage rate will be 1.4×10^8 MeV/g(GaAs)/year. Since it is not possible to exactly replicate the natural radiation environment in the laboratory, this is a necessary step towards interpreting test data to estimate expected degradation in orbit. Laboratory simulation of damage expected over a 5-year mission could be made by characterizing components subjected to a single exposure of monoenergetic protons. For example, if testing were conducted using 63 MeV protons, the integrated 5-year damage level divided by NIEL for 63 MeV protons leads to an equivalent fluence of 2.0×10^{11} 63 MeV protons/cm^2. Here the example of GaAs is used to illustrate the calculation, and this does not indicate the performance of a 1300 nm ILD in the InGaAsP system. Even so, the evaluation of test data based on NIEL calculated for an InGaAsP alloy would proceed similarly.

It is important to note that it is not possible to predict the amount of displacement damage degradation based on total ionizing dose. Rather it is necessary to evaluate damage based on the differential particle spectra in the orbit of interest and behind the shielding of interest. Using this approach, it is then possible to conduct relevant laboratory tests to evaluate the performance in orbit.

5.4 APPLICATION ISSUES

The degree to which the FODB is compromised by damage to the laser depends to some degree on how the LD is operated. Two options are available for controlling the output power. One is to select an operating current to yield the desired output power and to maintain that current while also maintaining constant temperature with an external cooler. In the event of radiation induced ILD output power loss, the control circuitry would not compensate, and the source attenuation might contribute significantly to the overall signal loss.

If the FODB requires constant optical power but not constant wavelength operation, a second possible approach exists where the LD is allowed to drift within the ambient temperature range. A tapped signal from the output beam is fed back to the power supply circuitry and the current is adjusted to maintain constant output power. C. Barnes has demonstrated how temperature drifts and displacement damage have equivalent effects on the shift in laseing threshold and LD output power versus operating current. He reports that the displacement damage effects of 2.0×10^{14} 1 MeV neutrons are the same as an increase in operating temperature from 27 to 62 °C. Thus

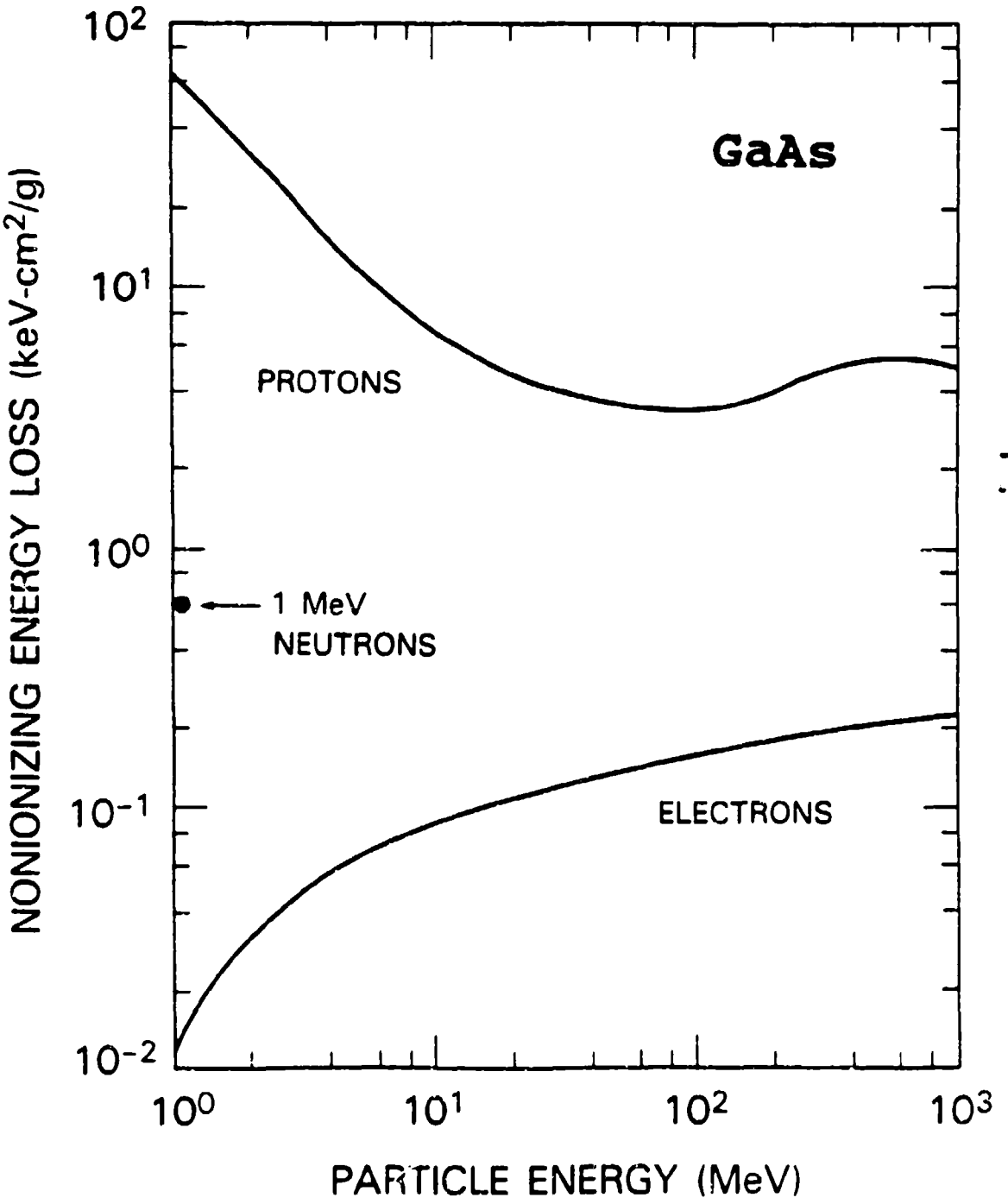

Figure 5.1 Calculated nonionizing energy loss (NIEL) in GaAs due to incident protons, electrons and 1 MeV neutrons.

current control which is based on monitor diode feedback would also adjust for radiation induced losses in the ILD. To the extent that radiation damage equates to elevated temperatures and elevated temperatures mean shorter lifetimes, the impact of radiation damage for reliability with ambient operation should be considered.

CHAPTER 5 REFERENCES

1. C. E. Barnes, "Radiation-hardened optoelectronic components: Sources," Proc. SPIE Optical Technologies for Communication Satellite Applications, Vol. 616, pp. 248-253, (1986).

2. C. E. Barnes, "Radiation effects on light sources and detectors," Proc. SPIE Radiation Effects in Optical Materials, Vol. 541, pp. 138-149, (1985).

3. C. E. Barnes and J. J. Wiczer, "Radiation Effects in Optoelectronic Devices," Sandia Report, SAND84-0771, (1984).

4. C. E. Barnes, "The effects of neutron irradiation on the high temperature operation of injection laser diodes," Proc. SPIE Fiber Optics in Adverse Environments II, Vol. 506, pp.218-223, (1984).

5. D. L. Begley, D. K. Wagner, and D. S. Hill, "Advanced laser diode structures for space communications systems,"Proc. SPIE Optical Technologies for Space Communication Systems, Vol. 756, pp.19-24 (1987).

6. R. F. Carson, "Radiation Effects in Semiconductor Laser Diode Arrays," Proc. SPIE Optoelectronic Materials, Devices, Packaging, and Interconnects, Vol. 994, pp.188-194, (1988).

7. R. F. Carson and W. W. Chow, "Neutron Effects in High-Power GaAs Laser Diodes," IEEE Trans. on Nucl. Sci. Vol. NS-36, pp. 2076-2082, (1989).

8. R. J. Chaffin, "Strained-Layer-Superlattice Optoelectronic Devices," Proc. SPIE Southwest Conference on Optics, pp. 160-167, (1985).

9. L. R. Dawson, T. E. Zipperian, C. E. Barnes, J. J. Wiczer, and G. C. Osbourn "Strained-layer superlattice emitter and detector structures using modulation-doped active regions," Inst. Phys. Conf. Ser. No. 74, pp. 415-420, (1984).

10. T. A. Fischer and J. J. Wiczer, "Radiation response of a radiation-hardened Si photodiode incorporating a sinker diffusion," Proc. SPIE Fiber Optics in Adverse Environments II, Vol. 506, pp.231-236, (1984).

11. P. B. Lyons, "Review of high bandwidth fiber optics radiation sensors," Proc. SPIE Fiber Optic and Laser Sensors III, Vol. 566, pg. 166 (1985).

12. S. J. Martin and M. A. Butler, "Wideband optical fiber magnetic field sensor," Proc. SPIE Fiber Optic and Laser Sensors III, Vol. 566, pg. 197 (1985).

13. R. J. Michal, "Radiation effects in optical fiber," Proc. SPIE Optical Technologies for Communication Satellite Applications, Vol. 616, pp. 292-298, (1986).

14. K. W. Mitchell, "Optimizing Photodetectors for Digital Communication in Radiation Environments," IEEE Trans. on Nucl. Sci., Vol. NS-25, pp. 1545-1549, (1978).

15. D. R. Myers, S. T. Picraux, B. L. Doyle, G. W. Arnold, and R. M. Biefeld, " Characterization of ion-implantation doping of strained-layer superlattices. I. Structural properties," J. Appl. Phys., Vol. 60, pp. 3631-3640, (1986).

16. D. R. Myers, R. M. Biefeld, P. L. Gourley, J. J. Wiczer, T. E. Zipperian, I. J. Fritz, C. E. Barnes, and G. C. Osbourn, " Characterization of ion-implantation doping of strained-layer superlattices. II. Optical and electrical properties," J. Appl. Phys., Vol. 60, pp. 361-3650, (1986).

17. D. R. Myers, J. J. Wiczer, T. E. Zipperian, and R. M. Biefeld, "An Ion-Implanted Ga(AsP)/GaP Strained-Layer Superlattice Photodetector," IEEE Elect. Dev. Let., Vol. EDL-5, pp.326-328, 1984.

18. B. T. Neyer, J. Chang, and L. E. Ruggles, "Calibrated Faraday current and magnetic field sensor, Proc. SPIE Fiber Optic and Laser Sensors III, Vol. 566, pg. 201 (1985).

19. T. Nishibe, M. Funamizu, H. Okuda, H. Furuyama, Y. Hirayama, and M. Iwamoto,"VPE-grown 1.3 umGaInAsp/InP DFB laser diodes with good controllability of lasing wavelength", Inst. Phys. Conf. Ser. No. 79, pp. 715-720, (1985).

20. Y. Ohmori, Y. Suzuki, and H. Okamoto, "Romm temperature CW operation of GaSb-AlGaSb MQW laser diodes," Inst. Phys. Conf. Ser. No. 79, pp. 721-726, (1985).

21. P. Poulain, M. A. Di Forte-Poisson, K. Kazmierski, B. de Cremoux, J. P. Moy, and P. Radisson, "$In_xGa_{1-x}As$ photodiodes for the 1.0 to 2.4 micron spectral region prepared by low-pressure MOCVD," Inst. Phys. Conf. Ser. No. 74, pp. 421-425, (1984).

22. B. L. Pruett, F. Roeske, R. A. Jones, K. G. Hagans, T. J. Davies, M. A. Nelson, and G. C. Gong, "A High-Bandwidth Fiber-Optic System Using Laser-Doide Transmitters," Proc. SPIE Fiber Optic and Laser Sensors III, Vol. 566, pg. 193 (1985).

23. Y. Sasai, N. Hase, M. Ogura, and T. Kajiwara, "Fundamental characteristics of 1.3 um InGaAsP MQW lasers fabricated by LPE," Inst. Phys. Conf. Ser. No. 79, pp. 709-714, (1985).

24. O Wada, T. Sanada, N. Nobuhara, M. Kuno, M. Makiuchi, and T. Fujii, "Very low threshold current AlGaAs/GaAs quantum well lasers suitable for optoelectronic integration," Inst. Phys. Conf. Ser. No. 79, pp. 685-690, (1985).

25. J. J. Wiczer, L. R. Dawson, G. C. Osbourn, and C. E, Barnes, "Permanent Damage Effects in Si and AlGaAs/GaAs Photodiodes," IEEE Trans. Nucl. Sci., Vol. NS-29, pp. 1539-1544, (1982).

26. J. J. Wiczer, C. E. Barnes, T. A. Fischer, L. R. Dawson, and T. E. Zipperian, "AlGaAs/GaAs radiation hardened photodiodes," Proc. SPIE Fiber Optics in Adverse Environments II, Vol. 506, pp.224-230, (1984).

27 J. J. Wiczer, "Radiation-hardened optoelectronic components: detectors," Proc. SPIE Optical Technologies for Communication Satellite Applications, Vol. 616, pp. 254-266, (1986).

28. J. J. Wiczer and C. E. Barnes, "Optoelectronic Data Link Designed for Applications in a Radiation Environment," IEEE Trans. on Nucl. Sci. Vol. NS-32, pp. 4046-4049, (1985).

29. J. J. Wiczer, "Summary of recent studies on AlGaAs/GaAs radiation hardened photodiodes," Proc. SPIE Southwest Conference on Optics, pp. 168-170, (1985).

6. Component Recommendations and Test Procedures

6.1 FIBER SELECTION

The selection of a fiber for the FODB must take into account the various factors described in sections 3.2-3.4, as well as the anticipated radiation environment, operating conditions, and system margin. Because of their higher radiation sensitivity and lack of recovery, it is obvious that fibers doped with phosphorus, either in the core or cladding, must be excluded. It seems reasonable to specify an operating wavelength of 1.3 μm vs. 0.85 μm to take advantage of the 3-6 times lower radiation-induced attenuation.

In view of the potential bandwidth requirements of the FODB, the large silica core multimode fibers must be eliminated from consideration in spite of the fact that the low dose rate radiation response of these fibers would be less than that of Ge-doped silica waveguides because of photobleaching in the former. The choice between graded index multimode and single mode fiber rests on a trade-off between such intrinsic system requirements as coupling loss and fanout and the somewhat better (factor of 2) anticipated radiation resistance of the single mode fibers (at least at 50 °C; see Section 3, Fig. 3.13 and Table V). However, it is clear that Corning 1519 should not be chosen, and if single mode fibers are selected, one should use the Litespec ZSM (or Sumitomo Z, its equivalent), where the radiation hardness is clearly superior.

6.2 FIBER TEST PROCEDURE

To date, FOTP49 has been approved as a test procedure for determining the radiation response of fiber optic waveguides, but it has several serious flaws. The NATO Panel IV Research Study Group 12 Nuclear Effects Task Group (NETG) has written a test procedure, which is an extensive revision of FOTP-49A, based on their collective experience in over 5 years of effort to develop reliable and consistent techniques to measure radiation-induced attenuation in optical fibers. The NETG "Procedure for measuring radiation-induced attenuation in optical fibers and optical cables" has been submitted to EIA as FOTP-64, which will supercede FOTP-49A on approval. Recently, the NETG procedure has been used by several DOD agencies as a basis for radiation tests of specific fiber optic systems, such as the Non-Line-of-Sight Missile System. It is recommended that the NETG test procedure (attached as Appendix) be the basis of testing and qualifying fiber for the FODB with the changes described in the following paragraphs.

6.2.1 Low dose rate

Because of the difficulty in obtaining low activity sources and the time involved in low dose rate exposures, we assume that the annealing is independent of damage and dose rate. In this case the fibers and devices can be exposed at a relatively high dose rate (1,300 rad/min per Table I of the NETG TP) to a total dose of 10^5 rad, and the recovery of the radiation-induced loss should be monitored *in-situ* for at least 10^4 sec following exposure. The fiber attenuation should then be measured by the cut-back technique for an extended period, $\sim 10^6$-10^7 sec. Qualification of the fiber for the FODB would occur if the incremental attenuation became < 100 dB/km. It is recommend that a factor of 3 cushion be added to the 6 dB in 20 m specification to account for various unknowns such as the details of the low dose rate radiation response to mixed proton-electron environments and temperature cycling. Alternatively, the fiber could be qualified if the recovery data are fit to Eq. 4 and the predicted loss at 2×10^8 sec (6 years) is < 100 dB/km. These same general procedures can be applied to devices as well. This latter procedure entails more risk and requires some specification of the quality of the fit to the data.

6.2.2 Radiation Types

Because of the nature of the space radiation environment, two types of exposures must be performed. It is reasonable to assume that ^{60}Co γ-ray irradiations can adequately simulate the ionizing damage produced by space electrons, and screening exposures of a number of fibers and devices can be made with this source. However, because of the large proton flux and the dearth of data describing fiber and device response to proton irradiations, these exposures must be carried out on candidate fibers and devices as well. It is suggested that two proton energies of ~ 40 MeV and > 100 MeV be used in order to ascertain that there are no energy-dependent effects. The appropriate dose rate (1300 rad/min equivalent) and energies can be readily obtained from various cyclotrons used in radiation effects studies.

6.2.3 Temperature

The optimum set of irradiations would include exposures to both ^{60}Co and protons at both the extremes of the anticipated temperature range, i.e. -60 and +40 °C and at room temperature ambient. In all cases, the fiber or device would be maintained at the irradiation temperature during the recovery period, both *in-situ* and subsequent cut-back measurements. At a minimum, the ^{60}Co irradiations should be performed at all 3 temperatures, and the proton irradiation carried out at 23 °C. However, because the incremental loss is anticipated to be greatest at the lower temperature, all effort should be made to obtain both proton and γ-ray data at -60 °C.

6.3 PHOTONIC DEVICE SELECTION

The following is a listing of device specifications and estimates of chances of meeting them.

Modulation speed

200 - 500 Mbits/sec	no problem without TE cooler
2+ Gbits/sec	possible with TE cooler

Ambient temperature

-20 to 70 °C	possible with/without TE cooler

Device lifetime

with TE cooler	100,000 to 1M hours MTBF
without TE cooler	estimated 10,000 hours MTBF

Power consumption (with T_c = 20°C TE cooler)

I_{th}	20 - 30 mA
differential quantum efficiency	.02 - .1 mW/mA
operating voltage	1.2 - 1.5 V

Power consumption (T_c = 60 - 70 °C without TE cooler)

I_{th}	40 - 50 mA
differential quantum efficiency	not available
operating voltage	1.5 - 1.7 V

TE cooler current (T_{chip} = 20 °C)

T_c = - 40 °C	< 850 mA
T_c = 70 °C	< 1100 mA

From the data above, it is obvious that the power budget is dominated by the TE cooler, if it is used. A TE cooler, in a standard diode laser package, can consume as much as ten times the current of a diode laser device, i.e. currents of the order of amps.. It is important to notice that the current consumption does not change proportionally with increasing ambient temperature. Therefore, if TE coolers are used in the system, one should design the system so that many lasers are cooled by a single TE cooler to optimize the power consumption efficiency.

As the laser ages, its output intensity will decrease. Therefore, it is important to have feedback control of the laser output. As mentioned in Section 4.4, the most effective feedback scheme is to tap a small portion of the output beam rather than using the "free" beam from the back facet. Notice that improper feedback control can lead to thermal runaway problem and accelerates the failure of the whole communication system.

For low end applications, low laser power output (100 uW) and low data rate (100 Mbits/sec), it is possible to use lasers without TE cooler. However, device reliability is an unknown issue. For high performance applications, high laser power output (> mW) and high data rate (> Gbits/sec) the heat sinking is a more critical issue. This is the case whether the high data rate is achieved by direct RF modulation of the diode laser or by modulating a cw laser output externally. In either case it is important that laser output is stable and its aging effect is minimized.

Since the data rate requirement of the FODB program can be met by lasers and photodetectors operating at any of the 800nm, 1300 nm and 1550 nm regions. The choice of a laser system (wavelength) for the FODB program depends on the *reliability issue*, which is not well known, and the *preference of optical fibers* for the applications. However it is important that good performance diode lasers, with a low threshold current (10 - 20 mA), good differential quantum efficiency (.1 mW/mA) and stable modal and spectral characteristics, are used in the system. Furthermore, it is important to emphasize the engineering issue of heat sinking. For good power management of a FODB system, it is essential that the diode lasers generates very little heat. It is even more critical that little, if any, energy is used to remove that heat from the laser devices.

6.4 PHOTONIC DEVICE RADIATION TESTING

There are no apparent radiation related constraints on the wavelength options for lasers and detectors. The better performance of optical fibers at longer wavelengths and the availability of components makes the 1300 nm wavelength particularity attractive. However, the narrower bandgap materials might be more susceptible to leakage and nonradiative recombination from displacement damage, and radiation test results on candidate components must be evaluated with this in mind.

Since the radiation response of candidate components must be viewed as an unknown, a test program should be designed to evaluate the permanent performance degradation from both ionization and displacement damage. Co-60 gamma ray tests might reasonably be used to assess total dose effects, but displacement damage must be evaluated through proton testing designed to simulate the effects of the natural environment. The procedure recommended for fibers in Section 6.2 is also recommended for the lasers and detectors. In addition, if error rate increases from cosmic ray heavy ions strikes or proton ionization transients are a concern, in situ tests on a breadboard FODB system should be conducted with heavy ions and during proton exposures at a rate comparable to solar flare conditions.

A recommended course of action would be to proceed with proton and Co-60 gamma testing of candidate components and the calculation of NIEL for protons in the alloy in question. The approach outlined previously using GaAs damage from one proton energy would be extended to InGaAsP LDs and photodiodes in a straightforward manner to predict their performance in orbit. As the orbit and spacecraft shielding information becomes available, the information would then be in hand to appraise the situation more accurately. Proton testing to assess damage susceptibility of the candidate component will be a necessary part of this evaluation, and more thorough studies to better understand damage mechanisms and effects in new technologies are strongly recommended. Also the effect of dose rate and temperature must be considered for the same reasons as mention for fibers.

7. Further Considerations and Conclusions

In order to be able to assure the on-orbit survivability of optical fibers and components in a FODB, there are significant gaps in the data available to date which must be filled. It appears that the most relevant fiber data are those being measured on the nine fibers of Chapter 3, Tables IV and V. The fibers are current, state-of-the-art products, and the measurements entail both recovery following high dose rate and low dose rate exposures. The same is true for the other components.

Virtually no data exist on the attenuation induced in state-of-the-art fibers and components exposed to proton environments, and it is therefore impossible to extrapolate from existing data to the space environment. Their behavior when exposed to protons of various energies appropriate to the natural space environment must be evaluated. It must be determined to what extent the radiation damage is due to ionizing and displacement processes, and if there is an equivalent ionizing dose for protons. Additionally, the synergistic effects of electron and proton irradiations of the appropriate energies must be evaluated.

Although the data of the nine fibers in Chapter 3, Tables IV and V are a significant first step in determining the low dose rate response of state-of-the-art fibers and correlating low and high dose rate behavior, they were obtained only at 50 °C. The radiation-induced attenuation of both fibers and other components must be evaluated over the full range of anticipated operation and storage temperatures, including simultaneous radiation exposure and temperature cycling.

Correlations have been demonstrated between low dose rate response and the recovery following high dose rate exposure for various fibers at 23 and 50 °C. This study should be extended to other components and to low temperatures. Attempts should be made to develop a model of the low dose rate response at any temperature and under thermal cycling from the recovery following high dose rate exposure.

The potential utility of ameliorating the radiation-induced attenuation in fibers with light-induced annealing should be evaluated. Previously, this has been demonstrated only during high dose rate exposures, and the experiment should be extended to low dose rates. Photobleaching may prove to be the only mechanism by which the low temperature radiation damage in the fibers can be minimized.

Similarly, laser diode and detector technology for the proposed FODB has reached a level of maturity well beyond the understanding of radiation effects in the candidate materials and structures. Significant gaps exist in radiation response data, radiation effects induced by proton exposures or synergistic electron-proton irradiations, low dose rate data obtained over the full temperature range or under temperature cycling, and modelling the low dose rate response at any temperature from high dose rate data. Preliminary evaluation suggests that the double heterojunction strip diodes and quantum well structures have been developed with characteristic radiation immunity, though this has apparently not been a conscious effort. Unfortunately, studies available in the literature focus on older technology than that being considered for the FODB. Even so, extrapolation of the existing studies suggests that the sources and detectors under consideration could probably be operated in a manner to tolerate the natural radiation environment.

Even though there are no anticipated susceptibilities to permanent ionization effects in the natural environment, it is strongly advised that both the laser diode and the detector be tested after exposure to the expected total mission dose from both electrons and protons. Availability of relatively inexpensive Co-60 gamma test facilities makes this the most reasonable ionization source though electron exposure would be an acceptable alternative.

In view of the known displacement damage effects in older technologies, preferences in candidate laser diodes and detectors should be evaluated after proton exposure to the mission equivalent damage level. The study should include thermal properties of the diode laser under various heat sinking conditions, radiation effects of diode lasers at different operating temperatures, and the aging effect under radiation and high operation temperature. Decreases in the laser output and increases in detector noise from leakage current could combine to increase error rates, and this degradation would be in addition to signal losses in fibers and couplers.

In order to conduct relevant displacement damage testing with protons, it is first necessary to determine how much damage occurs in orbit and then determine a monoenergetic proton fluence to produce the same damage. This procedure was described in Section 5 using the concept of nonionizing energy loss for protons in GaAs. Similar evaluation of damage in 1300 or 1550 nm InGaAsP components will first require the calculation of NIEL for protons in those alloys.

In situ testing is needed to determine the sensitivity of detectors to proton ionization transients. If soft errors are possible, the worst case situation would occur during a solar particle event, and this situation could be evaluated from proton test data. Also heavy ion induced single-event-upset must be considered as a possible source of reliability problems. In addition, if any complementary metal-oxid-semiconductor (CMOS) technologies are considered, one must consider screening for the possibility of catastrophic heavy ion induced single-event-latchup.

8. Appendix

Procedure for Measuring Radiation-Induced Attenuation in Optical Fibers and Optical Cables

NRL/MR/6505--92-6963

Naval Research Laboratory
Washington, DC 20375-5000

NRL/MR/6505—92-6963

Procedure for Measuring Radiation-Induced Attenuation in Optical Fibers and Optical Cables

NATO Nuclear Effects Task Group A/C 243, Panel IV (RSG.12)

E. J. FRIEBELE, Chairman

Optical Materials Research Group
Optical Sciences Division

March 27, 1992

REPORT DOCUMENTATION PAGE

Form Approved
OMB No 0704-0188

1. AGENCY USE ONLY (Leave blank)	2. REPORT DATE	3. REPORT TYPE AND DATES COVERED
	March 27, 1992	

4. TITLE AND SUBTITLE
Procedure for Measuring Radiation-Induced Attenuation in Optical Fibers and Optical Cables

5. FUNDING NUMBERS

6. AUTHOR(S)
E. J. Friebele,* Chairman

7. PERFORMING ORGANIZATION NAME(S) AND ADDRESS(ES)
Naval Research Laboratory
Washington, DC 20375-5000

8. PERFORMING ORGANIZATION REPORT NUMBER
NRL/MR/6505—92-6963

9. SPONSORING/MONITORING AGENCY NAME(S) AND ADDRESS(ES)

10. SPONSORING/MONITORING AGENCY REPORT NUMBER

11. SUPPLEMENTARY NOTES
*NATO Panel IV, Research Study Group 12
Nuclear Effects Task Group

12a. DISTRIBUTION/AVAILABILITY STATEMENT
Approved for public release; distribution is unlimited.

12b. DISTRIBUTION CODE

13. ABSTRACT (Maximum 200 words)

This test procedure outlines methods for measuring both the steady state response of optical fibers and cables exposed to continuous radiation and the transient response of optical fibers and cables exposed to a pulse of radiation. It can be used to determine the level of radiation-induced attenuation produced in single-mode or multimode optical fibers, in either cabled or uncabled form.

14. SUBJECT TERMS
Fiber optics
Nuclear radiation effects

15. NUMBER OF PAGES

16. PRICE CODE

17. SECURITY CLASSIFICATION OF REPORT	18. SECURITY CLASSIFICATION OF THIS PAGE	19. SECURITY CLASSIFICATION OF ABSTRACT	20. LIMITATION OF ABSTRACT
UNCLASSIFIED	UNCLASSIFIED	UNCLASSIFIED	UL

NSN 7540-01-280-5500

Standard Form 298 (Rev. 2-89)
Prescribed by ANSI Std. 239-18
298-102

CONTENTS

PROCEDURE FOR MEASURING RADIATION-INDUCED ATTENUATION IN OPTICAL FIBERS AND OPTICAL CABLES

1.0 INTENT

This test procedure outlines methods for measuring both the steady state response of optical fibers and cables exposed to continuous radiation and the transient response of optical fibers and cables exposed to a pulse of radiation. It can be used to determine the level of radiation-induced attenuation produced in single-mode or multimode optical fibers, in either cabled or uncabled form. This test procedure is not intended to test the non-optical components of a fiber-optic cable. Other test methods may be required to evaluate the degradation of cable materials resulting from radiation exposure. [The procedure specifically addresses steady state gamma-ray, and transient gamma-ray, X ray, or electron pulsed exposures, but it would be applicable to other radiation sources (e.g., protons, neutrons) as well, with appropriate changes in dosimetry and shielding considerations.]

1.1 Background

The attenuation of optical fibers generally increases when exposed to radiation. This is primarily due to the trapping of radiolytic electrons and holes at defect sites in the glass, i.e., the formation of color centers. The depopulation of color centers by thermal or optical (photobleaching) processes causes recovery, usually resulting in a decrease of radiation-induced attenuation. Recovery occurs simultaneously with darkening during exposure and is evident immediately after irradiation. Recovery of the attenuation after an irradiation depends on many variables, including the temperature of the test sample, the configuration of the sample, the spectrum and type of radiation used, the total dose applied to the test sample, and the light level used to measure attenuation. Under some conditions, recovery is never complete. The attenuation of an optical fiber can vary as a function of time following pulsed exposure by four or more decades during the recovery process.

This test procedure addresses both the steady state and pulsed radiation environment. Steady state measurements generally use radioactive isotope sources for which the turn-on and turn-off times are typically comparable to 1 s. This corresponds to the times required to move the source itself, shields, or test samples in and out of the source. The instrumentation used for steady state measurements typically has a time response of -0.1 s. There are two extremes of steady state exposure: the low dose rate regime for estimating the effect of environmental background radiation, and the high dose rate regime for estimating the effects of adverse nuclear environments, e.g., nuclear weapons detonation, specific areas of nuclear power plants, and accelerators. The effects of environmental background radiation are tested by a two-point attenuation measurement approach similar to FOTP-46 or FOTP-78. Alternatively, an optical time domain reflectometer (OTDR) may provide a more convenient measurement capability in some circumstances. The effects of adverse nuclear environments are tested by measuring the attenuation of the optical power (by monitoring either the transmitted or reflected light; the latter are tested by OTDR) before, during, and after exposure of the

The Nuclear Effects Task Group of NATO AC 243, Panel IV (RSG 12) modified the FOTP-49A procedure based on their collective experience in over five years of effort to develop reliable technique to measure radiation-induced attenuation in optical fibers. This procedures has been submitted to EIA as FOTP-64.

Manuscript approved January 29, 1992.

test sample to gamma radiation. The Detail Specification should specify the times at which measurements are to be made, based on the intended application.

The response of fibers to the pulsed environment addresses the time-varying (transient) behavior of an optical fiber after exposure to a single pulsed dose of radiation. This pulsed dose, with durations of < 1 s, is typically generated by various types of accelerators. The transient protocol is applicable where the radiation is not only delivered in a short pulse, but where fiber performance is to be determined on a time scale ≤ 1 s. For measurements at times after irradiation that are long compared to 1 s or measurements of the *average* response ($\tau > 1$ s) of fibers to a series of short pulses, the steady state protocol is applicable. The transient radiation-induced attenuation is tested by monitoring transmitted light power before, during, and after exposure of the test sample to the radiation pulse.

The transient procedure can be used to document transient attenuation from gamma rays, X rays, or electrons. (Interaction of gamma and X rays involves processes that generate electrons or positrons having energies comparable to the gamma ray energy.) Since few pulsed gamma/X-ray laboratory sources exist that can deliver large (>500 rad) radiation doses over significant volumes, most testing of such phenomena has involved pulsed electron sources. These irradiations yield the same results because the interaction of gamma rays and X rays with matter produces energetic electrons by the Compton process. Different applications of optical fibers may require drastically different recovery capabilities after a single pulse of radiation. For some applications near accelerators, for example, data may be transmitted through the fibers in coincidence with the radiation pulse. For some military applications involving control systems or telecommunications, system "down times" of milliseconds may be tolerable; other applications may be able to accommodate down times of minutes. For these reasons, this procedure does not specify times at which measurements are to be made. That information must appear in the Detail Specification based on the intended application.

Radiation exposures may result in luminescence phenomena that generate light in the fiber. Light will be generated during the pulsed radiation with gamma rays, X rays, or electrons through the Čerenkov process. Although the described procedure discusses only measurements of attenuation, the presence of transient Čerenkov or other luminescent light must be anticipated by users. These sources of light could overload recording instrumentation and compromise system accuracy. In this procedure, output filters limit the fraction of the out-of-band luminescent or Čerenkov light reaching the detector. A short wavelength cutoff filter to eliminate all light just below the test wavelength of interest could be sufficient for Čerenkov light because the spectral intensity is proportional to $1/\lambda^3$.

The transient procedure primarily focuses on measurements conducted at short times, generally less than a few minutes. For time scales comparable to one minute or longer, the steady state procedure may be readily applied. Photobleaching (light-induced

annealing) has not been observed at times < 10 μs, even at high optical power levels (500 μW). At longer times, as well as in the steady state procedure, light power levels must be precisely specified to minimize photobleaching in some types of fibers.

1.2 Caution

Carefully trained and qualified personnel must be used to perform this test since radiation (both ionizing and optical) and electrical hazards will be present.

2.0 REFERENCED DOCUMENTS

Test or inspection requirements include the following references:

FOTP-46 (EIA-455-46) "Spectral Attenuation Measurement for Long-Length, Graded-Index Optical Fibers"
FOTP-50 (EIA-455-50) "Light Launch Conditions for Long-Length Graded-Index Optical Fiber Spectral Attenuation Measurements"
FOTP-57 (EIA-455-57) "Optical Fiber End Preparation and Examination"
FOTP-78 (EIA-455-78) "Spectral Attenuation Cutback Measurement for Single-Mode Optical Fibers"
FOTP-80 (EIA-455-80) "Cutoff Wavelength of Uncabled Single-Mode Fiber by Transmitted Power"

3.0 TEST EQUIPMENT

Figures 1a and 1b show schematic diagrams of test equipment.

3.1 Radiation Source

The source should provide a variation in dose across the fiber sample not exceeding ±10%. Average total dose should be expressed in gray [1 Gy = 100 rad] to a precision of ±5% (steady state) or ±10% (transient), traceable to national standards. For typical doped silica core fibers, dose should be expressed in Gy calculated for SiO_2, i.e., Gy(SiO_2); if a non-silica-based light guiding material is used, dose should then be expressed in Gy calculated for that material composition.

3.1.1 Steady State Measurements

Caution: The energy of the gamma rays emitted by the source should be above 500 keV to avoid serious complications with rapid variations in total dose as a function of depth within the fiber and/or cable sample.

Dose rate must be constant for at least 95% of the shortest irradiation time of interest.

3.1.1.i Testing of Environmental Background Radiation

A Co^{60} or other gamma ray source shall be used to deliver radiation at a dose rate of 0.20 Gy/hour (or as specified in the Detail Specification).

3.1.1.ii Testing of Adverse Steady State Nuclear Environments

A Co^{60} or other gamma ray source shall be used to deliver radiation at dose rates ranging from 3 to 100 Gy/minute (or as specified in the Detail Specification).

3.1.2 Transient Measurements

Many types of pulsed electron accelerators are available and may be used for testing. Either the electron beam may be used to directly irradiate samples, or the electron beam may be converted (via the bremsstrahlung process) to deliver an X-ray radiation pulse to the samples.

Note: Theoretical analyses and some data suggest that use of electron/gamma ray sources with energies above about 10 MeV may not duplicate irradiations with lower energy sources. The relative importance of ionizing events vs displacement events in the fiber material will be decreased with the higher energy sources, potentially leading to different recovery processes. Note that if application of a fiber requires exposure to radiations that can produce significant atomic displacements in the fiber material [neutrons, energetic electrons (above a few MeV), or protons, for example], then care must be taken to use a radiation source that will duplicate the relative fractions of displacement vs ionization interactions. This is also true if the intended application involves a pulsed environment with a complex pulse structure; in such cases the test conditions should duplicate this pulse structure as closely as possible. Specific applications would, therefore, benefit from specification of the desired source characteristics to be used for attenuation testing.

If t_1 represents the earliest time specified in the Detail Specification for measuring transient attenuation, the radiation source pulse width (full width at half-maximum, FWHM) should be less than $0.1t_1$, unless otherwise specified, to avoid competition between recovery and damage mechanisms.

The source should be capable of delivering absorbed radiation doses to the optical fibers of 5 or 100 Gy (or as required in the Detail Specification). In the case of low-energy photon or electron irradiations, corrections to the absorbed dose may be required to compensate for fiber buffer or cable materials that attenuate the beam before interacting with the optical fiber. If a low-energy X-ray

source (< 100 keV) is used, the variation of dose through the fiber dimensions may be so extreme that detailed transport calculations must be used to relate measured dose to the dose actually deposited in the fiber core. X-ray sources should be filtered to > 100 keV unless confidence in dose profiles in the different materials comprising the fiber, buffer coating, jacket, and cable has been demonstrated.

3.2 Light Source

A light source such as a tungsten-halogen lamp, set of lasers, or LEDs shall be used to produce light at wavelengths of 850 ± 25, 1310 ± 20, and 1550 ± 20 nm, or at wavelengths specified in the Detail Specification. Only one wavelength should be used during any single test, unless specified in the Detail Specification.

3.2.1 Steady State Measurements

The optical power coupled from the source into the test sample shall average -30 dBm (1 μW), or as listed in the Detail Specification, determined by an optical power meter or calibrated detector/preamplifier/recorder system accurate to within ±8%. The light source may be modulated at a 50% duty cycle to enable phase-locked detection techniques.

3.2.2 Transient Measurements

For measurements specified for times less than 10 μs, the optical power is not limited, and increased power may be required to achieve adequate detection/recording signal and to avoid complications arising from the level of Čerenkov light generated by the radiation pulse. For longer times, the optical power coupled from the source into the test sample shall average -30 dBm (1 μW), measured as in Section 3.2.1, or as listed in the Detail Specification. A modulated light source may be used, subject to the average power limitations expressed above.

Depending on the details of the detection and recording system, it may be necessary to pulse the light source (see Section 3.8).

Note: Even at 1 μW power level, photobleaching may occur at times beyond 10 μs, depending on the fiber type and test temperature.

Note: Use of long fiber lengths can lead to a significant variation in the light power available for photobleaching at different positions in the fiber. Calculating attenuation in dB/km by multiplying the measured induced loss (dB) by $1000/L$, where L is the test length in m, is allowed only when fibers show no significant photobleaching.

3.3 Optical Filters/Monochromators

A filter or monochromator at the input end of the fiber may be required to restrict wavelengths to the limits of Section 3.2. During a transient test, a filter and/or monochromator or short wavelength cutoff filters (see Section 1.1) should be used at the output end of the fiber to avoid saturation or nonlinearities of the detector and recording instrumentation by transient light sources (Čerenkov or other luminescence phenomena).

3.4 Cladding Mode Stripper

A device that extracts cladding modes shall be used at the input end of the test sample unless it has been demonstrated that the fiber coating materials completely strip the cladding modes.

3.5 Optical Interconnections

The input and output ends of the test sample shall have a stabilized optical interconnection, such as a clamp, connector, splice, or weld. During an attenuation measurement, the interconnection shall not be changed or adjusted except as necessary to perform a two-point cutback measurement. (See Section 5.3.4.)

3.6 Optical Splitter

An optical splitter or fiber-optic coupler may divert some portion of the input light to a reference detector (Figure 1). The reference path may then be used to monitor system fluctuations for the duration of a measurement. (If the reference detector is used, all requirements for the detector/recorder bandwidth discussed in Section 3.8, apply to it as well.) Note that if a polarized light source, like a laser, is used, a polarization-insensitive coupler should be used.

3.7 Input Launch Conditions

3.7.1 Class Ia Fibers - (Graded Index Multimode Fiber). A means to establish an equilibrium mode distribution must be developed to establish a steady-state mode condition in the irradiated region of the fiber. Refer to FOTP-50.

3.7.2 Class IV Fibers - (Single-Mode Fiber). An optical lens system or fiber pigtail may be used to excite the test fiber. If an optical lens system is used, a method of making the positioning of the fiber less sensitive is to overfill the fiber core spatially and angularly. A mode filter shall be used to remove high-order modes whose cutoff is in the wavelength range less than or equal to the fundamental mode cutoff wavelength of the test fiber. The test condition specified in Section 4.1 of FOTP-80 satisfies this requirement. When testing polarization-maintaining fiber, particular care must be given to understanding and

documenting the polarization state of light, both injected into the test fiber (and any reference detector) and detected after exiting the test fiber.

3.7.3 Class Ib/Ic Fibers - (Quasi-graded and Step Index Fibers). The minimal requirement shall be for the input light to fill the numerical aperture of the test fiber. Launch conditions shall be specified in the Detail Specification.

3.8 Optical Detection

An optical detector that is linear and stable over the range of intensities that are encountered shall be used. A typical system might include a PIN photodiode amplified by a current input preamplifier. Although the stability of avalanche photodiodes is not sufficient for steady state measurements, they may be used for transient measurements, provided their stability meets the requirements of Sections 3.13 and 3.14. For steady state measurements, synchronous detection by a lock-in amplifier can be used.

For transient measurements, the time response of the overall detection system, including the data recording system, must be carefully evaluated. Limited high frequency or low frequency response of the system may distort measurements unless the following conditions are documented.

3.8.1 High-Frequency Response

The impulse response width (in seconds) of the total detection and recording system shall be 10× less than the earliest time at which measurements are to be recorded or as specified in the Detail Specification. This impulse response is most easily verified by injecting an optical pulse, whose pulse width is 10× less than the detection/recording system impulse response, into the detector and measuring the full width at half maximum (FWHM) as displayed with the data recorder. Alternatively, a modulated light source can be used in conjunction with a network analyzer. The high and low bandwidth limits (3 dB points) are determined by changing the modulation frequency from low values (>50 Hz) to the highest value of interest (e.g. 500 MHz).

Note: If capabilities exist to unfold or deconvolve the system time response from all observed data (using, for example, Fourier transforms), the 10× requirement specified above can be relaxed. However, even in that case, detailed knowledge of the actual system response will be essential in the unfolding process.

3.8.2 Low Frequency Response

The low-frequency response of the entire detector/recording system should extend to zero frequency, with a flat gain curve from dc to the high frequency cutoff, i.e., a completely dc-coupled system should be used. If such a dc-coupled

system is used, the light source may be run in a continuous mode, and complications involving operation of the source in a pulsed mode, and timing the light source pulse to the radiation pulse are avoided. The cw mode of light source operation also simplifies all absolute optical power measurements. [However, for measurements at extremely short times, it may be advantageous to use a pulsed source to obtain adequate light levels that simplify detection and recording considerations since most light sources can deliver higher outputs in a short pulse than in a cw mode.]

If the detector/recorder system is not dc-coupled, the light source must be used in a pulsed mode. A single, flat-topped light pulse may be used for measurements to times $< < 1/f_L$, where f_L is the low frequency 3 dB point of the recorder. Such a single pulse must be appropriately timed relative to the radiation pulse. The low frequency limit of the system will introduce distortion in the observed pulse at times comparable to $1/f_L$. In an ac-coupled system, repetitive pulses or a modulated signal can also be used (and *must* be used for measurements to times $\geq 1/f_L$), but the modulation frequency f of the pulse train must be $> 10\, f_L$, and $1/f$, i.e. the time between pulses or cycles, must be considerably shorter (by at least 10×) than t_1.

3.9 Elements of the Recorder System

A suitable data recording system must be incorporated. For steady state measurements, a chart recorder or computer can be used; for transient measurements, the recording system must provide a bandwidth commensurate with the tests specified in Section 3.8. Examples include: a transient digitizer or storage oscilloscope, an analog oscilloscope with either a film or digital camera, a digital sampling oscilloscope coupled to a data display unit, coherent demodulation of the modulated light signal by a lock-in amplifier (for times $> > 1\ \mu s$), or incoherent demodulation with a high frequency amplifier and demodulator.

3.10 Radiation Dosimeter

Dosimetry traceable to National Standards shall be used. Dose should be measured in the same geometry as the actual fiber core material to ensure that dose-build-up effects are comparable in the fiber core and the dosimeter. The dose must be expressed in Gy calculated for the core material.

3.11 Temperature Controlled Container

Unless otherwise specified, the temperature-controlled container shall have the capability of maintaining the specified temperature to within ± 2°C or as specified in the Detail Specification. The influence of the temperature-controlled container on the dose within the test object must be taken into consideration.

3.12 Test Reel

The test reel shall not act as a shield for the radiation used in this test or, alternatively, dose must be measured in a geometry that duplicates the effects of reel attenuation. The diameter of the test reel and the winding tension of the fiber can influence the observed radiation performance. If reel diameter and fiber tension are not specified in the Detail Specification, the fiber should be loosely wound on a reel diameter exceeding 10 cm. (Some radiation sources will require a much more compact fiber geometry, which should be noted in the report discussed in Section 7.)

3.13 System Stability

Stability of the total system under illumination conditions, including the light source, light injection conditions, variations in fiber microbend conditions, light coupling to a detector, the detector, and the recording device, must be verified prior to any measurement for a time exceeding that required for determination of the output power prior to irradiation P_b and the output power during the duration of the attenuation measurement P_t (see Section 6). During that time, the maximum fluctuation in observed system output shall be converted into an apparent change in optical attenuation due to system noise ($\Delta\alpha_n$) in dB/km by using either Equation 6.1.A (if no optical splitter and reference detector is used) or 6.2.A (if an optical splitter and reference detector are used). Any subsequent measurement must be rejected if the observed ΔA (defined in Section 6) does not exceed $10 \times \Delta\alpha_n$.

3.14 Baseline Stability

Baseline stability shall also be verified for a time comparable to the attenuation measurement with the light source turned off. The maximum fluctuation in output power P_n shall be recorded. Any subsequent measurement must be rejected if the transmitted power out of the irradiated fiber is not greater than $10 \times P_n$.

4.0 TEST SAMPLE

Either a fiber or cable specimen may be tested. An unirradiated sample shall be used in each test unless otherwise specified in the Detail Specification.

4.1 Fiber Specimen

The test specimen shall be a representative sample of the fiber specified in the Detail Specification.

4.2 Cable Specimen

The test specimen shall be a representative sample of the cable described in the Detail Specification and shall contain at least one of the specified fibers.

4.3 Test Specimens

A length at the ends of the test sample shall reside outside of the irradiation chamber and shall be used to connect the fiber into the optical measurement system. In addition, the fiber length must be adjusted to meet the system stability limits of Section 3.13 and the baseline stability limits of Section 3.14. (If a system is seriously unstable, no fiber length may meet the requirements of Section 3.13 and 3.14. In such a case, the measurement cannot proceed until the measurement apparatus is improved.) The irradiated length of the test sample shall be reported.

4.3.1 Environmental Background Radiation Test

Unless otherwise specified in the Detail Specification, the irradiated length of the test sample shall be 500 ± 10 m. The length outside the test chamber shall be sufficient for a minimum of two cutback measurements (refer to Section 5.3).

4.3.2 Adverse Nuclear Environments Test

Unless otherwise specified in the Detail Specification, the irradiated length of the test sample shall be 100 ± 5 m.

4.3.3 Transient Test

The length of the test sample is dependent on the total dose, the time regime for which measurements are required in the Detail Specification, and the beam size/uniformity of the irradiation source. The irradiated fiber length shall be such that the transit time of light through the irradiated region is at least 10× shorter than t_1 specified for attenuation measurements. For measurements only at times beyond 1 ms, 100 m length of fiber is recommended for direct comparison to the steady state specification. This recommendation cannot be followed if the radiation source is not capable of uniformly exposing an irradiation volume large enough to hold the fiber coil or if the induced attenuation in that length of fiber results in power throughputs violating the baseline stability test of Sec. 3.14.

4.4 Test Reel

The test sample shall be spooled onto a reel per Section 3.12. Allowance shall be made for the unspooling of a measured length of the test sample from each end of the reel for attachment to the optical measurement equipment.

4.5 Ambient Light Shielding

The irradiated fiber length shall be shielded from ambient light to prevent photobleaching by any external light sources and to avoid apparent baseline shifts in the zero light level. An absorbing fiber coating or jacket can be used as the light shield provided it has been demonstrated to block ambient light and its influence on the dose within the fiber core has been taken into consideration.

5.0 TEST PROCEDURE

5.1 Calibration of Radiation Source

Calibration of the radiation source for dose uniformity (at a minimum of four locations) and dose level shall be made prior to introduction of fiber test samples. Regardless of dosimeter used, per Section 3.1, the variation in dose across the fiber reel volume shall not exceed ±10%.

If thermoluminescent detectors (TLDs) are used for the measurements, four TLDs shall be used to sample dose distribution at each location. The readings from the multiple TLDs at each location shall be averaged to minimize dose uncertainties. To maintain the highest possible accuracy in dose measurement, the TLDs shall not be used more than once. TLDs should be used only in the dose region where they maintain a linear response.

5.1.1 Steady State Sources

Total dose shall be measured with an irradiation time equal to subsequent fiber measurements. Alternatively, the dose rate may be measured, and the total dose calculated from the product of the dose rate and irradiation time. Source transit time (from off-to-on and on-to-off positions) shall be less than 5% of the irradiation time.

5.1.2 Transient Sources

Various types of dosimetry may be used for source calibration, such as thermoluminescent dosimeters (TLDs), microcalorimeter, radiachromic film, or Faraday cup (for electron beam measurements). Of these alternatives, the TLD, microcalorimeter, and radiachromic film can potentially provide a response calibrated directly in absorbed dose. Depending on the composition of the TLD, microcalorimeter, or radiachromic film and the energy spectrum and type (electron beam or bremsstrahlung) of radiation source used, it may be necessary to correct the observations to obtain the dose actually deposited in the optical fiber material. Such corrections should include dose build-up and/or attenuation factors that may occur due to materials (such as fiber cable material, fiber buffer

material, reel composition, or self-shielding of a fiber coil) and differing electron stopping powers in the detector and fiber materials. Similar materials (such as thin aluminum foils, for example) may be placed in front of the dosimeter to simulate these phenomena.

A Faraday cup shall be used only as a transfer standard for electron beams, not as the primary dose-measuring instrument, and it shall be calibrated against one of the absorbed dose instruments (TLD, microcalorimeter, or radiachromic film) prior to its use. The Faraday cup will measure only total charge, and this quantity may be complicated by a variety of charge loss or gain mechanisms. It does not measure any quantity directly related to absorbed dose. If radiachromic film is used, multiple pulses may be required to obtain adequate darkening of the film. In this case, a Faraday cup provides a convenient pulse-to-pulse normalization method.

Total dose shall be measured on each pulse of the radiation source, unless stated otherwise in the Detail Specification.

5.2 Fiber End Preparation

The test sample shall be prepared such that its endfaces are smooth and perpendicular to the fiber axis, in accordance with FOTP-57.

5.3 Data Acquisition Process

5.3.1 The reel of fiber or cable shall be placed in the attenuation test setup shown in Figure 1. Sufficient fiber should be available on the input end of the fiber to allow an attenuation measurement using the two-point cutback method to be performed.

5.3.2 The light source shall be coupled into the input end of the fiber, as described in Section 3.7. The output end of the fiber shall be positioned such that all light exiting the fiber impinges on the active surface of the detector.

5.3.3 The test sample shall be stabilized in the temperature chamber at 23 ± 2°C prior to proceeding (or at the test temperature specified in the Detail Specification).

5.3.4 For all steady state tests and for those transient tests requiring precise power injection level (i.e., tests requiring attenuation measurements at times longer than 10 μs), a two-point attenuation measurement shall be completed without disturbing the fiber on the test reel in the temperature chamber. The procedure of FOTP-46 shall be used for Class Ia fibers. The procedure of FOTP-78 shall be used for Class IV fibers. (If the OTDR procedure of 5.3.10.i.b.3

is being used, the fiber attenuation can be directly measured.) The attenuation A_f, in dB/km, of the fiber sample on the reel shall be calculated and recorded. Note that the length of the fiber used in this measurement must necessarily be longer than the length on the test reel because of the leads and the length used for the cut-back measurement, if performed.

5.3.5 The system baseline test of Section 3.14 shall be completed and the results recorded, unless the OTDR procedure in 5.3.10.i.b.3 is being used. For the steady state adverse environment test, a continuous measurement device shall be connected to the detection system so that a continuous power measurement can be made. The measurement equipment shall be set up such that the detection signal does not exceed the limits of the equipment.

5.3.6 If a two-point attenuation measurement was done in Section 5.3.4, the test sample input end shall again be prepared in accordance with Section 5.2. The light source shall be coupled to the input end of the fiber, as described in Section 3. The output end of the fiber shall again be positioned such that all light exiting the fiber impinges on the active surface of the power meter or detector. The light power exiting the test sample shall be measured with the power meter or the detector/recorder system (see Sec. 3.9) and recorded. If A_f was determined using Section 5.3.4, the power level at the input end of the test sample (Point A in Figure 1) shall be determined by using the known length of the fiber (in km) from Point A to the exit end and A_f (in dB/km) determined in Section 5.3.4 to scale the measured exit power to that in the fiber at Point A. For measurements at times longer than 10 μs, the input power should be adjusted to be in compliance with the value specified in Section 3.2.

5.3.7 The complete detector/recording system shall be placed in operation.

5.3.8 Prior to irradiation, the system stability and baseline stability tests specified in Sections 3.13 and 3.14 shall be performed unless the OTDR procedure in 5.3.10.i.b.3 is being used.

5.3.9 During the irradiation and subsequent throughput power measurements, the input coupling conditions and power levels shall not be changed.

5.3.10 Dose Rates and Attenuation Measurement Procedures

5.3.10.i Environmental Background Test

5.3.10.i.a Environmental background radiation effects, due to exposure to gamma radiation, shall be determined by subjecting the test sample to a dose rate of 0.20 Gy/h. The test sample shall be exposed to a total dose

of 1 Gy over 5 hours. Different dose rates and doses may be required by the Detailed Specification.

5.3.10.i.b Attenuation shall be measured at least immediately after the 1 Gy irradiation, and at other times and doses specified in the Detail Specification. Depending on System Stability (Section 3.13) and equipment availability, either of three types of measurements may be made

(1) a continuous measurement of system output power P_f may be made, allowing determination of attenuation via Section 6.0. This procedure requires that the System Stability criteria of Section 3.13 be maintained throughout the irradiation time. For extremely long times, this may not be possible.

(2) a two-point cutback attenuation measurement (analogous to the procedures specified in Section 5.3.4) may be made to determine the attenuation after irradiation times corresponding to selected total doses. In this case, the System Stability criteria of Section 3.13 need be satisfied only during the time required to accomplish the attenuation measurement. If sufficient fiber is available outside the irradiation volume, the irradiation may be continued to achieve additional dose on the fiber. To continue the irradiation, the procedure should return to Section 5.3.6 to reset the input power level to the level required in Section 3.2. However, the attenuation measured in the latest cut-back measurement should be used in place of A_f to scale the observed exit power to the input light level at Point A.

(3) an optical time-domain reflectometer may be used to document the fiber attenuation along its length. Use of the OTDR simplifies concerns with long-term source stability that would complicate measurements, especially if very small attenuations are being observed. The optical module of the OTDR must match the fiber type (single-mode or multimode) to be tested. The OTDR shall be used for measurements at selected times required in the Detail Specification. However, because of the time required for an OTDR measurement, it should not be used when the attenuation in the fiber is rapidly changing. The attenuation of the test sample measured by the OTDR prior to exposure shall be used in place of the preirradiation A_f specified in 5.3.6 to calculate the input light level at Point A.

When an attenuation measurement is required, the OTDR pulse shall be injected into the fiber. Since the OTDR measurement is performed only periodically and since there is usually no adjustment of the

average power injected into the fiber by the OTDR instrument, a means for maintaining 1 μW optical power (or as required by the Detail Specification) continuously injected into the test fiber length as measured at point A shall be established.

Accurate measurement of fiber loss can be obtained only over the fiber length where the attenuation remains within the dynamic range of the instrument. In addition, it is extremely important to establish an equilibrium-mode distribution in multimode fibers and to ensure that light is not propagating in the cladding. See Sections 3.4 and 3.7. The length of fiber to be irradiated should be preceded by at least 50 m of lead-in fiber, which serves as a self-reference and assists in removal of high-order lossy modes in multimode fibers. Preferably, this lead-in fiber should be an additional length of the test fiber, but a similar fiber fusion-spliced to the test fiber may be used.

5.3.10.ii Adverse Nuclear Environment Test

Adverse effects due to exposure to gamma radiation shall be determined by subjecting the test sample to one of the dose rate/total dose combinations specified in Table I or as specified in the Detail Specification.

Source Geometry shall be adjusted to maintain dose rates within $\pm 10\%$ of values of Table I or as specified in the Detail Specification.

TABLE I
TOTAL DOSE/DOSE RATE COMBINATIONS

Total Dose, Gy	Dose Rate, Gy/min
30	3
100	13
1000	13
10000	100

The output power from the test sample shall be recorded prior to (P_b) and for the duration of (P_l) the gamma irradiation cycle. The output power shall also be recorded for at least 1000 s after completion of the irradiation process or as specified in the Detail Specification. The power levels of the reference detector, if used, shall also be recorded before (P_b') and during (P_l') both the irradiation time and the recovery time

after completion of the irradiation. The output powers P_t and P_b (and P_t' and P_b') must be measured relative to a baseline of zero light; see Section 6.

5.3.10.iii Transient Test

A single pulse from the radiation source shall be directed onto the exposed length of optical fiber/cable, using one of the total absorbed doses (measured at the fiber) specified in Table II or as specified in the Detail Specification.

TABLE II: TOTAL DOSE

Total Dose, Gy
5
100

Source geometry shall have been adjusted to maintain doses within ±10% of values of Table II or as specified in the Detail Specification.

The output power from the test sample shall be recorded both prior to (P_b) the pulse of radiation and for the duration of the transient measurement (P_t) as specified in the Detail Specification. The power levels of the reference detector (P_b' and P_t', respectively), if used, shall also be recorded during the same time period. The output powers P_t and P_b (and P_t' and P_b') must be measured relative to a baseline of zero light; see Section 6. A typical recorder output is shown in Figure 2.

5.3.11 For an environmental background radiation test, unless otherwise specified in the Detail Specification, the radiation-induced change in attenuation ΔA_t should be reported at a time t = 5 h after a total dose of 1 Gy.

For an adverse nuclear-environment measurement, unless otherwise specified in the Detail Specification, ΔA_t should be reported at a time t corresponding to the total dose of the test level selected from Table I and at a time t = 1000 s after cessation of the radiation. See Section 6.

5.3.12 Steps 5.3.1 through 5.3.11 should be repeated for other required test temperatures, time regimes, and wavelengths. An unirradiated fiber/cable sample shall be used in each test unless otherwise specified in the Detail Specification.

6.0 CALCULATIONS

6.1 Measurements Without a Reference Detector

The radiation-induced change in ΔA_t at t shall be calculated from

$$\Delta A_t = -10 [\log (P_t/P_b)]/L \qquad \text{[in dB/km]} \qquad \text{(Eq. 6.1.A)}$$

where: P_t is the power output of the test sample at time t,
P_b is the power output of the test sample before irradiation, and
L is the length in km of irradiated test sample (excluding unirradiated fiber external to the irradiation environment.

P_t and P_b must be measured relative to a baseline of zero light. (Note the alternative equation in Section 6.2 if a reference detector is incorporated in the measurement procedure.)

Alternatively, for environmental background radiation tests, A_t at a time t may have been obtained from a two-point cutback technique, as discussed in Section 5.3.10.i.b.2. In this case, ΔA_t at time t is given by

$$\Delta A_t = A_t - A_1 \qquad \text{[in dB/km]} \qquad \text{(Eq. 6.1.B)}$$

where: A_1 is the attenuation of the test sample prior to exposure to gamma radiation, from Section 5.3.4.

6.2 Measurements with a Reference Detector

If a reference detector is used, the radiation-induced change in sample attenuation ΔA_t at time t should be calculated by modifying Eq. 6.1.A to:

$$\Delta A_t = -10 [\log(P_t/P_b) - \log (P_t'/P_b')]/L \qquad \text{[in dB/km]} \qquad \text{(Eq. 6.2.A)}$$

where: P_t' is the power measured by the reference detector at time t, and
P_b' is the power measured by the reference detector before irradiation.

P_t, P_b, P_t', and P_b' must be measured relative to a baseline of zero light.

7.0 REPORT

7.1 Report Data.

7.1.1 Date of Test

7.1.2 Title of test.
7.1.3 Length of test sample exposed to radiation.
7.1.4 Test wavelength.
7.1.5 Test temperature
7.1.6 Test reel diameter, composition, and geometry.
7.1.7 Change in attenuation ΔA_t,
7.1.7.i Environmental background steady state test: after t = 5 h and 1 Gy total dose.
7.1.7.ii Adverse environment steady state test: after time t corresponding to the specified total dose and t = 1000 s after cessation of irradiation.
7.1.7.iii Transient test: for times specified in the Detail Specification.
7.1.8 Reference detector characteristics, if used.
7.1.9 Method used to determine input power if different from Section 5.3.6.
7.1.10 Characteristics of test sample: fiber/cable type, dimensions, and composition.
7.1.11 Recorder output data.
7.1.12 Description of radiation source, including energy and type.
7.1.13 Test dose, dose rate (steady state), and time duration of test pulse (transient).
7.1.14 Description of dosimeters and dosimetry procedures.
7.1.15 Description of optical source.
7.1.16 Description of input and output optical filters or monochromators.
7.1.17 Description of cladding mode stripper.
7.1.18 Description of input launch simulator and launch conditions used.
7.1.19 Description of any optical splitter used.
7.1.20 Description of detection and recording system.
7.1.21 Documentation of detector/recorder system bandwidth. (Not required for steady state tests.)
7.1.22 System stability and background test data.
7.1.23 Description of characteristics of temperature chamber.
7.1.24 Date of calibration of test equipment.
7.1.25 Name and signature of Operator.

8.0 SPECIFYING INFORMATION

8.1 Detail Specification

8.1.1 Identification of fiber type and cable type
8.1.2 Request for type of test: environmental background steady state, adverse nuclear environment steady state, or transient. For transient tests, request for dose level and time range of measurement.
8.1.4 Other information pertinent to the tests for which the standard conditions of this Procedure do not match the intended system application of the optical fiber and/or optical cable.

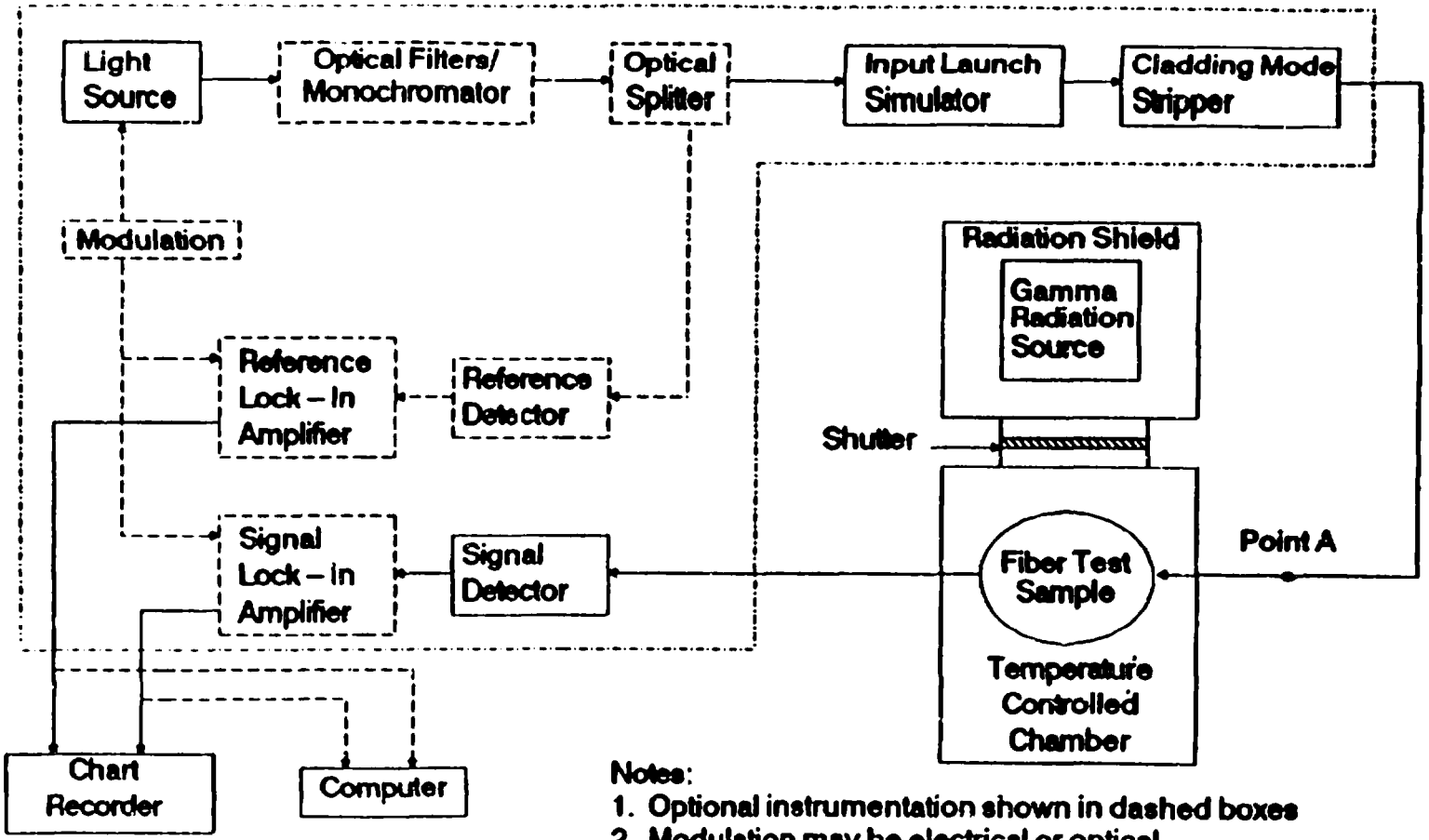

Notes:

1. Optional instrumentation shown in dashed boxes
2. Modulation may be electrical or optical
3. If an OTDR is used for the Environmental Test, it may be inserted in place of the instruments in the dashed box. See Sect. 5.3.10.I.b.3
4. A cladding mode stripper may not be needed. See Sect. 3.4

Figure 1a. Schematic Instrumentation Diagram – Steady State Tests

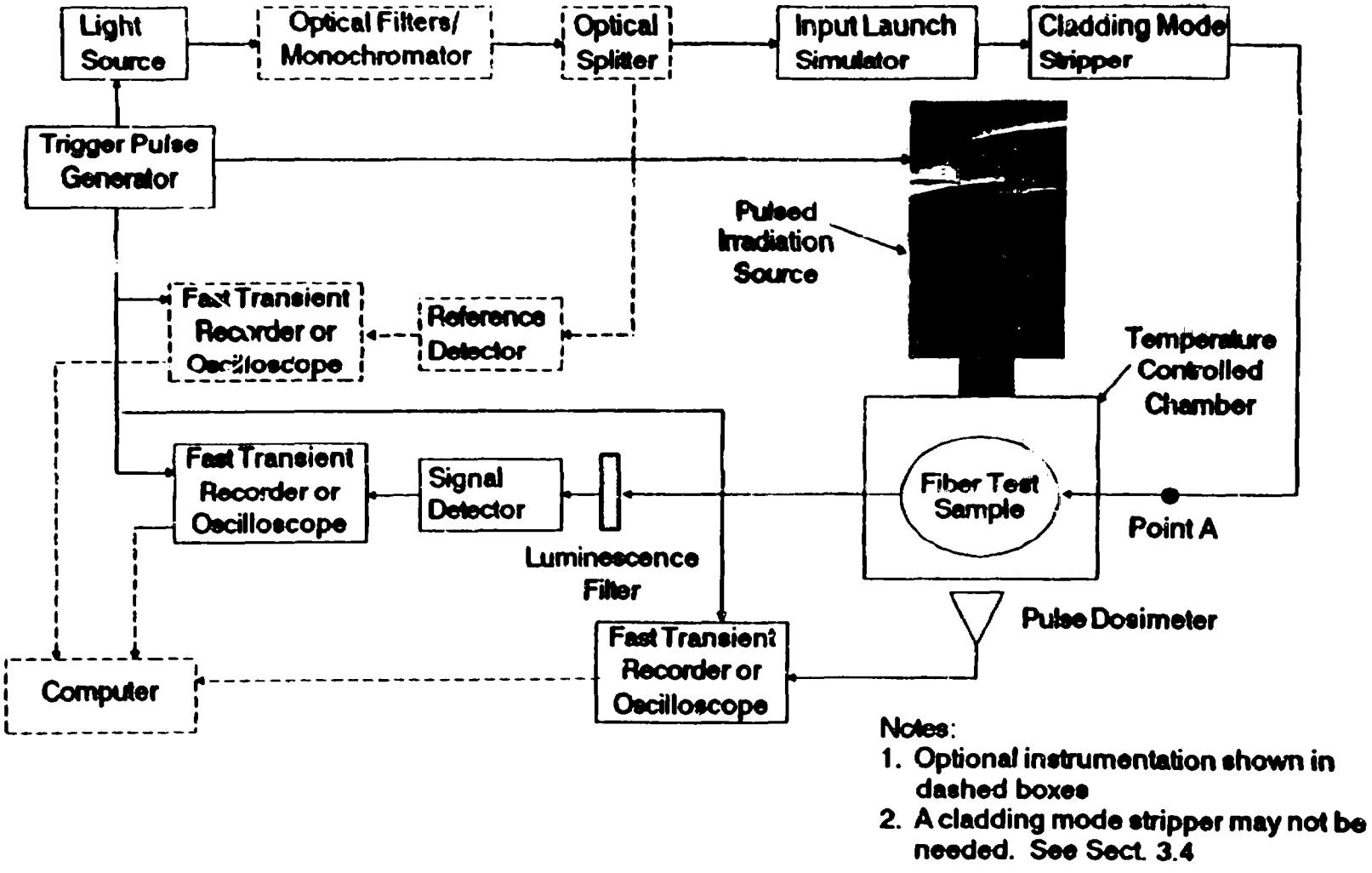

Figure 1b. Schematic Instrumentation Diagram – Transient Tests

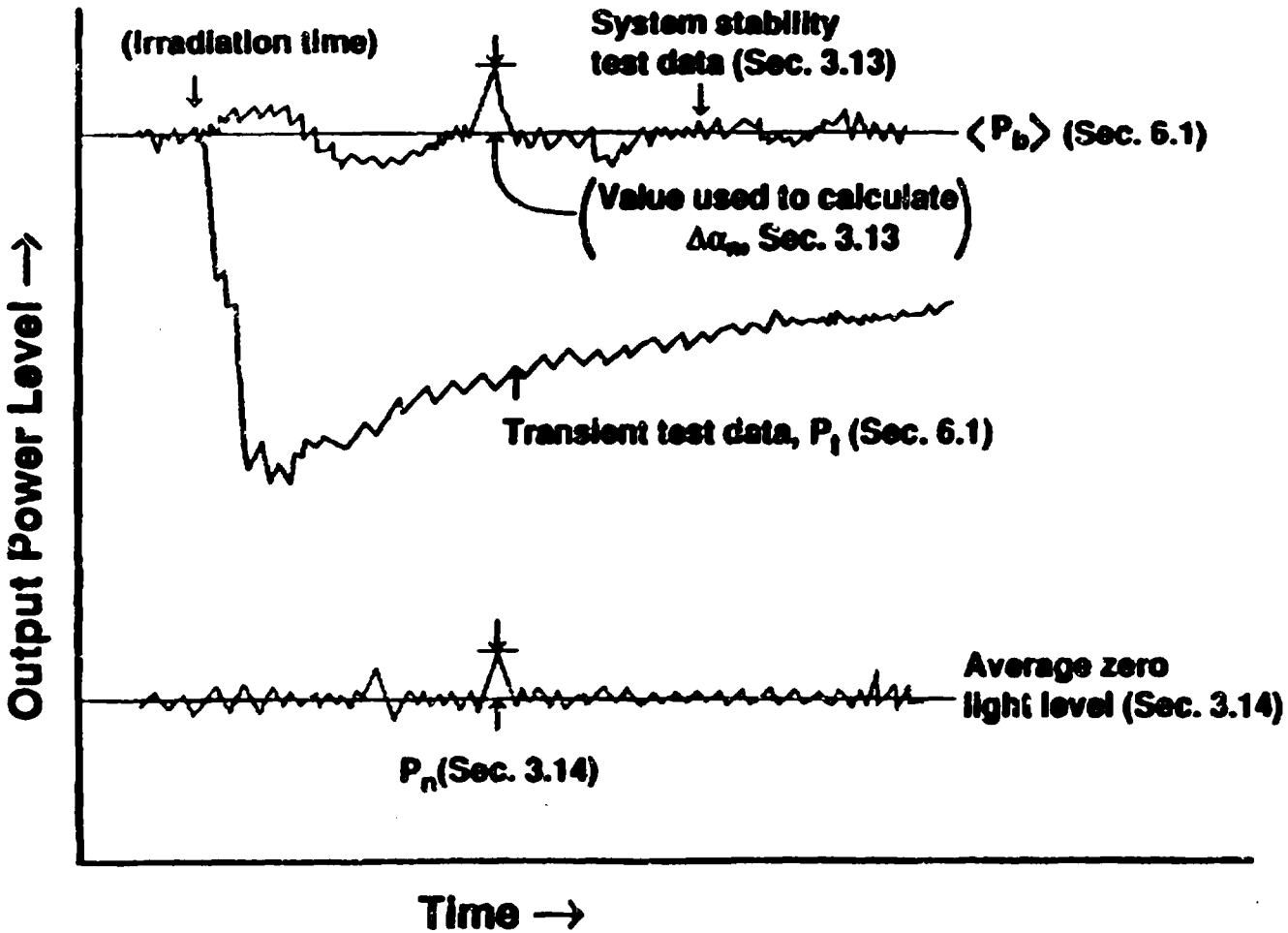

Figure 2. Typical Transient Data Traces